(U-Th)/He chronology: Part 1. Data, uncertainty, and reporting

R.M. Flowers[1,†], P.K. Zeitler[2], M. Danišík[3], P.W. Reiners[4], C. Gautheron[5], R.A. Ketcham[6], J.R. Metcalf[1], D.F. Stockli[6], E. Enkelmann[7], and R.W. Brown[8]

[1]*Department of Geological Sciences, University of Colorado Boulder, Boulder, Colorado 80309, USA*
[2]*Department of Earth and Environmental Sciences, Lehigh University, Pennsylvania 18015, USA*
[3]*John de Laeter Centre, Curtin University, Perth, Western Australia 6845, Australia*
[4]*Department of Geosciences, University of Arizona, Tucson, Arizona 85721, USA*
[5]*Université Paris-Saclay, CNRS, GEOPS, 91405 Orsay, France*
[6]*Department of Geological Sciences, Jackson School of Geosciences, University of Texas, Austin, Texas 78712, USA*
[7]*Geoscience Department, University of Calgary, Calgary, Alberta, Canada T2N 1N4*
[8]*School of Geographical and Earth Sciences, University of Glasgow, Glasgow G12 8QQ, UK*

ABSTRACT

The field of (U-Th)/He geochronology and thermochronology has grown enormously over the past ~25 years. The tool is applicable across much of geologic time, new (U-Th)/He chronometers are under continuous development, and the method is used in a diverse array of studies. Consequently, the technique has a rapidly expanding user base, and new labs are being established worldwide. This presents both opportunities and challenges. Currently there are no universally agreed-upon protocols for reporting measured (U-Th)/He data or data derivatives. Nor are there standardized practices for reporting He diffusion kinetic, ^{4}He/^{3}He, or continuous ramped heating data. Approaches for reporting uncertainties associated with all types of data also vary widely. Here, we address these issues. We review the fundamentals of the methods, the types of materials that can be dated, how data are acquired, the process and choices associated with data reduction, and make recommendations for data and uncertainty reporting. We advocate that both the primary measured and derived data be reported, along with statements of assumptions, appropriate references, and clear descriptions of the methods used to compute derived data from measured values. The adoption of more comprehensive and uniform approaches to data and uncertainty reporting will enable data to be re-reduced in the future with different interpretive contexts and data reduction methods, and will

facilitate inter-comparison of data sets generated by different laboratories. Together, this will enhance the value, cross-disciplinary use, reliability, and ongoing development of (U-Th)/He chronology.

1. INTRODUCTION

The (U-Th)/He dating method has tremendous temporal reach, ability to access a broad temperature range, applicability to numerous minerals, and a growing number and diversity of applications. It has been used to date materials as old as ca. 4.5 Ga (Min et al., 2003) and as young as ca. 2 ka (Marsden et al., 2021a). The technique can constrain thermal histories in a >300 °C to ~20 °C window depending on the mineral system, a range that is only partly accessible to other methods. Depending on the circumstance, it can be applied as a thermochronometer to decipher the thermal history of a rock or as a geochronometer to constrain mineral crystallization and the age of distinct geologic events (Fig. 1). Apatite and zircon are the minerals that have been dated most by (U-Th)/He, because these are common U-Th–bearing accessory minerals in many rock types and yield data that inform time-temperature (tT) paths at upper crustal and near-surface conditions of <220 °C. However, a much larger and diverse family of minerals is at least potentially dateable with (U-Th)/He, because most minerals do not incorporate initial He into the crystal structure such that any mineral containing even trace U-Th might be dated if it is retentive to He over a temperature range relevant to geological processes. Consequently, various minerals are still under development as (U-Th)/He geo- and thermochronometers, and this versatile method is used to address an array of Earth science problems from recent through

deep time. These studies now encompass not only landscape evolution, topographic development, and exhumation histories, but also weathering and fault zone processes, the evolution of sedimentary systems, the genesis of mineral deposits, the timing of ancient unconformity development, the age of volcanic eruptions, and extraterrestrial material investigations.

The (U-Th)/He technique was the first radiometric method used to date geologic materials (Rutherford, 1905; Strutt 1908a, 1908b, 1910a, 1910b, 1910c, 1910d). It was then applied only intermittently during the twentieth century (e.g., Damon and Kulp, 1957; Fanale and Kulp, 1962; Damon and Green, 1962; Turekian et al., 1970; Bender, 1973; Leventhal, 1975; Ferreira et al., 1975) owing to what was viewed as an unpredictable "He leakage" problem (Strutt, 1910b, 1910c; Holmes and Paneth, 1936; Hurley, 1954). The development of the field of thermochronology (e.g., Dodson, 1973) and the recognition that He leakage is predictable and governed by thermally activated volume diffusion led to a resurgence of the technique (e.g., Zeitler et al., 1987; Lippolt and Weigel, 1988; Wernicke and Lippolt, 1993, 1994a, 1994b; Lippolt et al., 1993, 1994; Farley et al., 1996; Warnock et al., 1997; Wolf et al., 1998; Reiners and Farley, 1999; Farley, 2000; Farley and Stockli, 2002; Reiners et al., 2002, 2004; Meesters and Dunai, 2002a, 2002b). Since then, the (U-Th)/He method has seen ongoing advances in understanding the controls on He diffusion in apatite and zircon (e.g., Shuster et al., 2006; Flowers et al., 2009; Gautheron et al., 2009; Guenthner et al., 2013; Mbongo Djimbi et al., 2015; Zeitler et al., 2017; Danišík et al., 2017a), development of other minerals as He chronometers (e.g., Farley, 2002; Farley and Stockli, 2002; Evans et al., 2005a; Copeland et al., 2007; Shuster et al., 2005a; Blackburn et al., 2007; Wolff et al., 2016;

R.M. Flowers ⬤ https://orcid.org/0000-0001-6563-1143
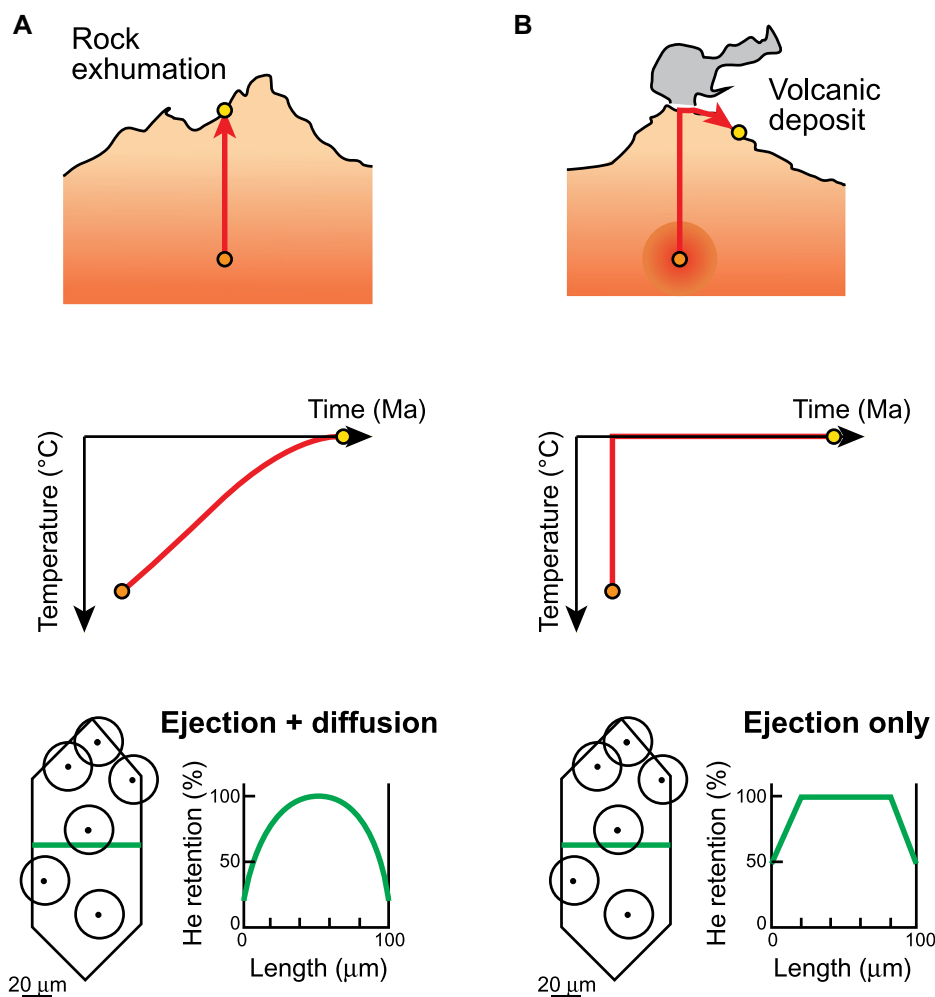†rebecca.flowers@colorado.edu

Figure 1. Two examples of geologic scenarios and tT path histories that can be constrained by (U-Th)/He dating are shown: (A) use of apatite or zircon as a thermochronometer to constrain rock exhumation and (B) use of apatite or zircon as a geochronometer to constrain the eruption age of volcanic deposits. Top panels schematically depict each sample's geologic history. Middle panels depict each sample's tT path. Bottom panels depict each sample's He distribution owing to alpha ejection and any partial diffusive He loss that occurred. In the mineral schematics, circles represent the average ejection distance that each alpha particle will travel through the crystal lattice after generation by radioactive decay, with distances that vary depending on the parent nuclide and mineral density. % He retention versus length plots (where the length corresponds to the green line in each mineral schematic) illustrate the distribution of He in the crystal owing to (A) alpha ejection and He diffusion, in the case of a mineral with a single diffusion domain and affected by partial diffusive loss during protracted transit through the He partial retention zone (HePRZ), and (B) alpha ejection only, in the case of a mineral with a single diffusion domain and rapid transit through the HePRZ.

especially when the data reduction choices made and the basis of the uncertainties presented are not always clear. Limited consensus on reporting formats has hindered the development and use of online databases for (U-Th)/He results, although such metadata archiving is an emerging requirement of journals and funding agencies to facilitate integration with other data sets and maximize the long-term impact and accessibility of data. Moreover, although He diffusion stepped-heating data comprise the foundation of the kinetic models that are used to interpret (U-Th)/He thermochronologic results, here again there are no universally adopted reporting approaches. ^{4}He/^{3}He results that can constrain the spatial distribution of ^{4}He in a crystal, and continuous ramped heating (CRH) data that can identify problematic samples, also lack uniform reporting practices.

Here we address these challenges by (1) offering an accessible resource for (U-Th)/He data producers, users, and reviewers on the generation and reduction of individual aliquot (U-Th)/He, kinetic, ^{4}He/^{3}He, and CRH data; (2) developing and recommending a set of practices for reporting data and uncertainties for conventional analyses on individual aliquots; and (3) developing and recommending data and uncertainty reporting practices for kinetic, ^{4}He/^{3}He, and CRH data. This contribution follows similar manuscripts for other geochronology communities (e.g., U-Pb laser ablation–inductively coupled plasma–mass spectrometry [LA-ICP-MS], Horstwood et al., 2016; ^{40}Ar/^{39}Ar, Schaen et al., 2020) that tangle with the difficult challenges associated with data reporting to enhance the quality, documentation, and scientific interpretation of geochronologic data.

In this contribution we place most emphasis on measurements of single crystals of apatite and zircon, the phases on which most (U-Th)/He work has been and is currently being done. Other minerals are now being analyzed more routinely and in some cases may have modified reporting needs (e.g., hematite and goethite). Laser ablation (U-Th)/He dating, in which one or more analyses are acquired in situ on a single crystal, is a valuable approach that is seeing wider adoption (Boyce et al., 2006, 2009; Vermeesch et al., 2012; Tripathy-Lang et al., 2013; Evans et al., 2015; Horne et al., 2016, 2019; Pickering et al., 2020), but such data also have differing reporting and interpretational considerations that are beyond the scope of this paper. We underscore that these other approaches are important and rapidly developing directions in the broad field of (U-Th)/He, but we are limited in how many topics we can cover comprehensively and hence focus our attention on those topics currently relevant for the majority of (U-Th)/He data users.

Cooperdock and Stockli, 2018; Robinson et al., 2019; Yakubovich et al., 2019), improvements in the modeling tools used to help interpret data (e.g., Ketcham, 2005; Gallagher, 2012; Braun et al., 2012; Gallagher and Ketcham, 2018), and a radical increase in the amount of data being reported and interpreted in the literature.

A current challenge to the field's progression is that despite the expanding number of data producers and consumers, there are no agreed-upon or standardized protocols for reporting data or uncertainties. Numerous published (U-Th)/He data sets lack sufficient information for measured data on individual aliquots to be re-reduced and data derivatives reproduced, for example, with newer interpretive contexts that may require modified data reduction methods. It also can be difficult to directly compare and appropriately interpret data produced by multiple laboratories that are reduced and presented in different ways,

We first review the fundamentals of the (U-Th)/He method (section 2), summarize the controls on He diffusion (section 3) and the types of materials that can be dated (section 4), and outline the steps associated with (U-Th)/He data acquisition (section 5). We then describe the process and choices when reducing individual aliquot (U-Th)/He data and make recommendations for associated data and uncertainty reporting (sections 6 and 7). We also review the basics of kinetic, ^{4}He/^{3}He, and CRH data, and similarly recommend reporting protocols (section 8). We conclude by describing future directions (section 9) and by summarizing the recommendations of this paper (section 10). The companion paper discusses considerations when evaluating and combining individual aliquot data from samples and for inputting such data into thermal history models (Flowers et al., 2022). Recent contributions provide more comprehensive reviews of the technique (Reiners et al., 2018) and summaries of its principles and applications (Ault et al., 2019; Tremblay et al., 2020, Elements volume). Here we build on that work with the goals of improving the consistency and rigor of (U-Th)/He data reporting to further promote developments in and applications of (U-Th)/He chronology.

2. FUNDAMENTALS OF THE (U-Th)/He METHOD: HE PRODUCTION, HE LOSS, AND SIGNIFICANCE OF (U-Th)/He DATES

2.1. Overview

(U-Th)/He chronology is based on the production of ^{4}He atoms by radioactive alpha decay in a crystal and the loss of those ^{4}He nuclides by thermally activated volume diffusion. At higher temperatures, the crystal is an open system such that the He atoms escape completely from the crystal, while at lower temperatures they may be retained (Fig. 2). The temperatures over which He is lost versus retained depends on the crystal's He diffusion characteristics. The total He measured in a crystal is the net result of He production and diffusion over the course of that mineral's history, minus any He expelled by alpha ejection. Thus, (U-Th)/He dates are quantities that represent this time-integrated thermal history. As such, they commonly represent neither the formation age of a rock nor the timing of a specific cooling event and therefore require additional context for their interpretation (e.g., Wolf et al., 1998; Gautheron and Zeitler, 2020).

Throughout this text, we follow the approach of Faure (1986, p. 41) and the U-Pb and ^{40}Ar/^{39}Ar geochronology communities (e.g., review papers by Schoene et al., 2013; Schaen
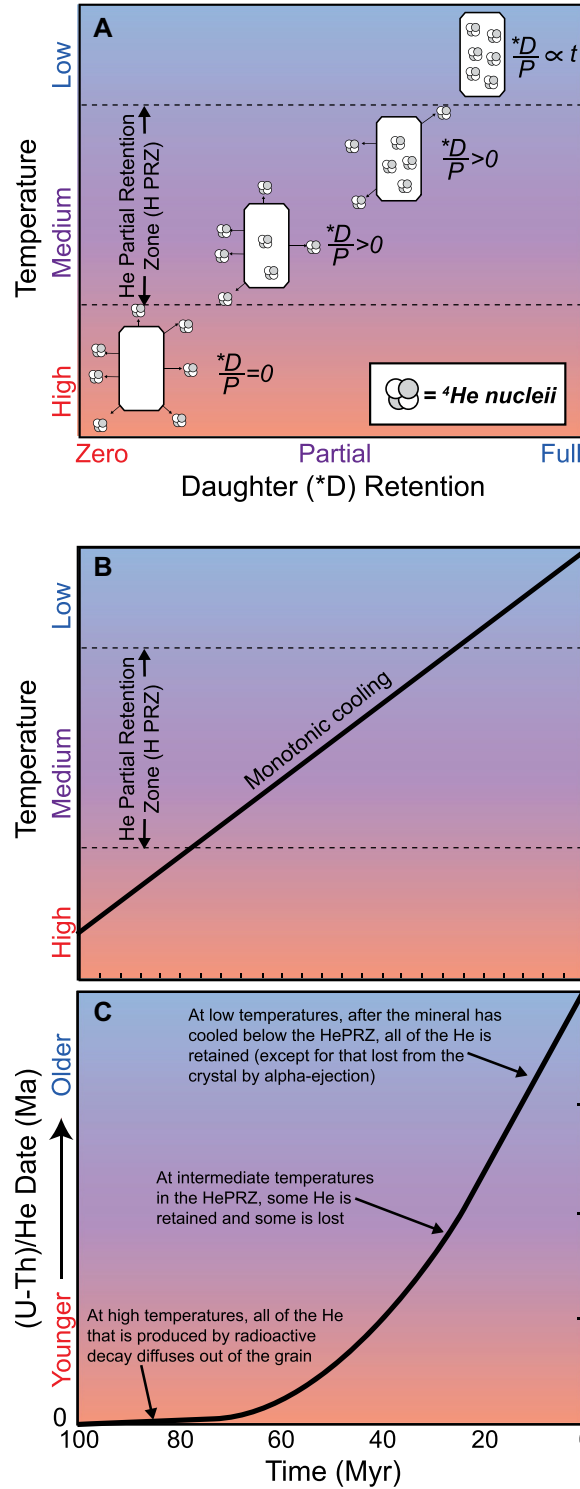

Figure 2. The transition between complete He loss to complete He retention during a thermal history characterized by monotonic cooling is illustrated. (A) Temperature versus radiogenic daughter (*D) retention (from zero to full retention). He is produced by radioactive decay of parent isotopes (U, Th, Sm) in the crystal lattice. At elevated temperatures, all He diffuses out of and is lost from the crystal, so the radiogenic daughter (D*) to P (parent) ratio is 0. At intermediate temperatures, He is retained partially (known as the He partial retention zone, HePRZ), and the D*/P ratio increases as He accumulates in the crystal lattice. At low temperatures, below the HePRZ temperature range, He is retained fully, and the D*/P ratio increases linearly with accumulation time. If a crystal has accumulated He and acquired a (U-Th)/He date, reheating the crystal to temperatures above the HePRZ will "reset" the crystal by causing the accumulated He to fully diffuse out, thus returning the D*/P ratio to 0. (B) Temperature versus time plot represents a 100-m.y.-long monotonic cooling history. (C) (U-Th)/He date versus time plot, where the curve represents the evolution of (U-Th)/He date for the thermal history in panel B.

et al., 2020) in differentiating between the terms "date" and "age." We use "date" or "apparent age" to refer to the number yielded by the decay equation (below, Equation 1; the uncorrected or raw date, see section 6.3.6) or the decay equation plus a correction for alpha ejection (the corrected date, see section 6.3.7). We use "age" when geo-logic meaning is inferred from that date, which requires additional interpretation.

2.2. He Production by Radioactive Decay

The radioactive decay of ^{238}U, ^{235}U, ^{232}Th, and ^{147}Sm generates ^{4}He atoms (i.e., alpha particles).

The technique has conventionally been referred to as (U-Th)/He rather than (U-Th-Sm)/He because of the low contribution of [147]Sm to total He production. In most of the text, we use U to signify total [238]U and [235]U, Th to refer to [232]Th, Sm to indicate [147]Sm, and He to signify [4]He, except in this subsection and in places where this usage may generate confusion (e.g., when discussing [4]He/[3]He thermochronology).

Over the decay chain of each parent isotope, 8, 7, 6, and 1 [4]He atoms are produced, respectively, which leads to this equation:

$$^4\text{He} = 8 * {}^{238}\text{U}(e^{\lambda_{238}t}-1) + 7 * {}^{235}\text{U}(e^{\lambda_{235}t}-1)$$
$$+ 6 * {}^{232}\text{Th}(e^{\lambda_{232}t}-1) + {}^{147}\text{Sm}(e^{\lambda_{147}t}-1) \quad (1)$$

where t is time, [4]He, [238]U, [235]U, [232]Th, and [147]Sm are the current number of atoms of each isotope in the mineral, and λ_{238}, λ_{235}, λ_{232}, and λ_{147} are the decay constants of the parent nuclides. This equation assumes secular equilibrium of daughters in all decay chains, which is reasonably appropriate for materials older than ca. 1 Ma. It also assumes no initial [4]He in the dated crystal, which is a reasonable assumption in most circumstances given the incompatibility of He in minerals (e.g., Baxter, 2003; Baxter et al., 2007; Zeitler et al., 2017). The (U-Th)/He system differs from most other geochronometers in that the same daughter isotope is generated by multiple isotopes of different elements.

The versatility of the (U-Th)/He method arises partly from the broad time span that it can access. Despite the long half-lives of the parent isotopes, the high productivity of He throughout the decay series means the (U-Th)/He technique can date materials even as young as historical time by accounting for the effects of secular disequilibrium on (U-Th)/He systematics (e.g., Farley et al., 2002; Schmitt et al., 2006, 2010, 2013, 2014; Danišík et al., 2012, 2017b, 2020; Ulusoy et al., 2019; Ito and Danišík, 2020). However, it is also possible to obtain dates as old as Archean and Hadean for materials with appropriate He retentivities and thermal histories (e.g., Min et al., 2003, 2013; Kelly et al., 2018).

It is important to note that [4]He production always generates damage to the crystal lattice (although this damage can be annealed at elevated temperature). During each decay event, the parent atom will be displaced a small distance (tens of nm for a single decay and up to hundreds of nm for the entire decay chain) opposite to the alpha particle and create recoil damage. The alpha particles are ejected from the parent nucleus, have high kinetic energy, and travel much farther than the parent (many μm), borrowing electrons during atomic elastic collisions to become [4]He atoms and displacing atoms in the mineral lat-

tice. The amount of damage created by parent element recoil is much greater than that generated by the alpha particle (~5000 versus 100 defect pairs; Nasdala et al., 2001; Devanathan et al., 2006; Farnan et al., 2007). This self-irradiation process during He production has direct relevance for understanding the evolution of He diffusivity in dated crystals (section 3).

2.3. He Loss and Redistribution by Alpha Ejection

When He nuclei are generated, these alpha particles have sufficient mean kinetic energy to travel a substantial distance through the crystal lattice (Figs. 1 and 3; Farley et al., 1996; Farley, 2002; Ketcham et al., 2011). Alpha-stopping distances depend both on the energy of alpha decay that is characteristic to the parent isotopes and

their intermediate daughters and on the mineral density. For most minerals, the average stopping distances are in the 14–22 μm range for [238]U, [235]U, and [232]Th and in the 4–6 μm range for [147]Sm, although the full range of stopping distances for the intermediate decay steps is greater (for example, in apatite and zircon, ~14–34 μm and ~12–29 μm, respectively, for the individual decay steps in the [238]U, [235]U, and [232]Th decay chain; Fig. 3; Farley et al., 1996). The average stopping distances in most minerals of interest to (U-Th)/He dating are relatively well known (typically to the 0.1 μm or 0.01 μm level).

The long alpha-particle stopping distances cause spatial separation of daughter and parent nuclei unrelated to diffusion, which introduces several complexities specific to the (U-Th)/He system. The relatively small size (10s–100s of μm) of most minerals dated by (U-Th)/He means
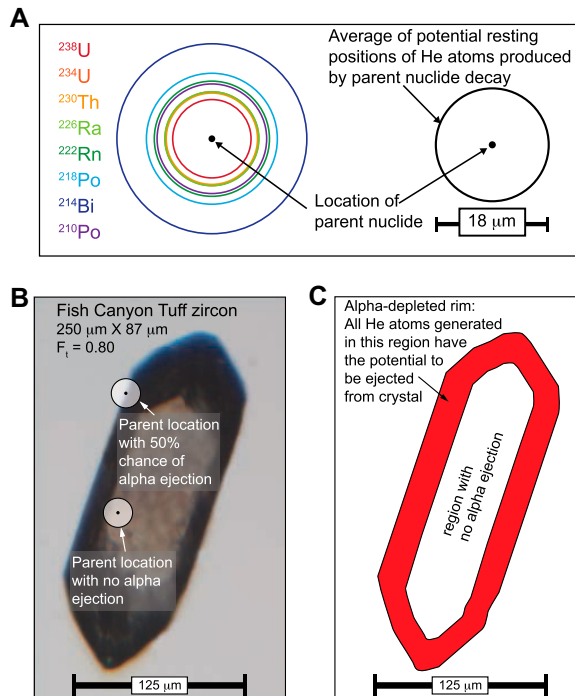

Figure 3. Illustration shows alpha ejection in zircon. (A) Circles on left represent the distances that alpha particles (which become [4]He atoms) will travel through the zircon crystal lattice after being produced by radioactive decay of [238]U and the intermediate daughters in this decay chain. Circle on right represents the average ~18 μm stopping distance of alpha-particles in the [238]U decay chain. (B) Microscopy image of a Fish Canyon Tuff zircon. For parent nuclides located near the grain edge, the portions of the circles that fall outside the grain represent positions where the He atoms can come to rest outside the crystal due to ejection, causing net He loss from the grain. For parent nuclides located in the grain interior, the He atoms are displaced from their site of generation, but this He is not ejected from the crystal. (C) Schematic of the Fish Canyon Tuff zircon in panel B, with the red area depicting the alpha-depleted outer portion of the grain. It is the He loss in this red region that is corrected for with the alpha-ejection correction (or F_T correction). This grain has a F_T correction of 0.80 assuming the idealized tetrahedral prism geometry of Ketcham et al. (2011) and no parent isotope zonation, which means that 20% of this crystal's He atoms are estimated to have been lost from the crystal due to ejection. This estimated amount of ejected He is included in the calculation of the corrected (U-Th)/He date. Zonation in parent nuclides introduces uncertainties into the F_T correction, because higher parent nuclide concentrations in the outer portion of the grain will lead to greater He ejection than is assumed in the unzoned case, with the opposite true for lower parent nuclide concentrations near the grain's exterior. Also note that the red region in (C) is susceptible to He injection or "He implantation" if high U-Th phases occur immediately adjacent to or coat the grain. This effect is generally insignificant in a high U-Th phase like zircon, but in some cases it may be important in minerals that are small and low in U-Th.

that an appreciable fraction of the alpha particles is ejected from the crystal. Most (U-Th)/He dates are therefore "corrected" for this ejected He based on the dated crystal's size and shape (see additional details in section 6.3.1). As the magnitude of this alpha-ejection correction (or F_T correction) increases for smaller grains due to their larger surface-area-to-volume ratio, this correction's accuracy becomes questionable. Grains with >50% of their alpha particles ejected (equivalent to a combined F_T value of <0.5) are generally considered to have unreasonably large corrections, such that crystals of this small size are not analyzed (Ehlers and Farley, 2003). The uncertainty of this correction also increases for crystals with morphologies that deviate substantially from the idealized geometry used to compute the F_T value (see also section 7.3.1). Abraded or fragmented crystals introduce additional uncertainty into the F_T correction if the timing of rounding or breakage is unknown (e.g., Rahl et al., 2003; Thomson et al., 2013; Brown et al., 2013), although this uncertainty is minimized for larger-sized grains. Parent isotope zonation can also introduce inaccuracy into F_T corrections (Meesters and Dunai, 2002a, 2002b; Hourigan et al., 2005; Danišík et al., 2017a). F_T values are typically computed assuming no zonation because it is not yet routine to measure parent nuclide distributions in dated grains. However, if zonation causes higher or lower parent nuclide concentrations in the outer shell of the grain affected by ejection, then this would mean more or less He was expelled than assumed in the unzoned case, causing some level of inaccuracy in the corrected (U-Th)/He date (e.g., Farley et al., 1996; Meesters and Dunai, 2002a, 2002b; Hourigan et al., 2005; Danišík et al., 2017a).

Alpha ejection has two other complicating effects. It modifies the shape of the He diffusion profile by depleting the He concentration at the crystal margin, therefore reducing the diffusional loss rate (Farley, 2000; Meesters and Dunai, 2002a, 2002b; Gautheron et al., 2012). Additionally, He can be implanted into the crystal if high U-Th phases coat or occur adjacent to the grain (Spiegel et al., 2009; Danišík et al., 2010). This injected "parentless He" causes erroneously old dates, with smaller and lower U-Th crystals most susceptible to this effect (e.g., Murray et al., 2014; see also companion paper, Flowers et al., 2022).

2.4. He Loss by Diffusion

He nuclei that are not ejected from the grain can reside in and/or diffuse through a crystal lattice. At low temperatures, He may be retained fully, while at higher temperatures, it can escape
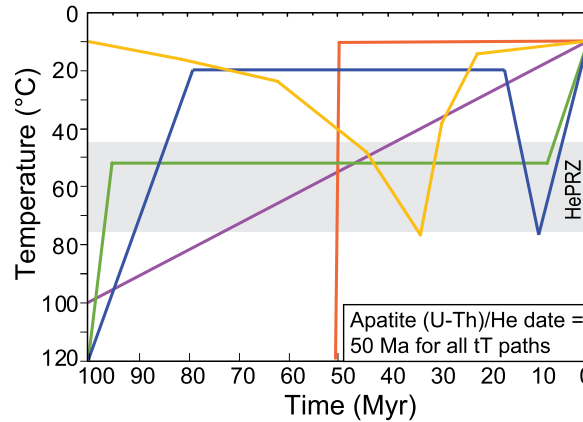

Figure 4. Temperature versus time plot shows different thermal trajectories that yield the same corrected apatite (U-Th)/He date of 50 Ma. The (U-Th)/He dates were modeled using the HeFTy software (Ketcham, 2005) for an apatite sphere with 50 μm radius with the apatite RDAAM model (Flowers et al., 2009). HePRZ—He partial retention zone.

completely via thermally controlled volume diffusion, and in an intermediate temperature range known as the He partial retention zone (HePRZ), it may be retained partially (Fig. 2; Wolf et al., 1998). The HePRZ is operationally defined as the temperature range where He dates occur between 90% and 10% of the isothermal holding time, so the HePRZ temperature range is time-dependent (Wolf et al., 1996).

A grain's He diffusivity and thus temperature range for He retention and associated temperature sensitivity as a (U-Th)/He thermochronometer is determined by the mineral structure. Even within a single mineral, the He loss rate by diffusion can be affected additionally by the crystal size (e.g., Farley, 2000), the accumulated radiation damage (e.g., Shuster et al., 2006; Flowers et al., 2009; Gautheron et al., 2009; Guenthner et al., 2013), the presence of imperfections of various types (Zeitler et al., 2017; Danišík et al., 2017a; Gautheron et al., 2020), the axial ratio if diffusion is anisotropic (e.g., Farley, 2007; Reich et al., 2007; Cherniak and Watson, 2011), and major element chemistry (Mbongo Djimbi et al., 2015) (additional discussion in section 3). Due to these effects, even for the same mineral from the same rock that underwent the same tT path, differences in crystal characteristics can cause variability in He diffusivity. In turn, these kinetic differences in He diffusion can cause variability in single crystal (U-Th)/He dates for thermal histories with sufficient time in the mineral's HePRZ to induce partial diffusive He loss from the crystals (Fig. 1A; see section 3).

2.5. Net He Retention and Significance of (U-Th)/He Dates

A key conceptual point for understanding the thermal history significance of (U-Th)/He data is that although the results are reported as dates, the date is a quantity that reflects the crystal's time-integrated history of He production from parent nuclide decay and He loss by diffusion, minus

the He ejected from the crystal, over the course of the tT path (Fig. 2; e.g., Wolf et al., 1998). Thus, a (U-Th)/He thermochronological date does not typically record the timing of a specific geologic event. A large variety of thermal histories can yield the same amount of accumulated He and thus the same (U-Th)/He date (Fig. 4). While a mineral that cooled rapidly through the HePRZ may yield a date that records the timing of a cooling event (e.g., a volcanic eruption; Fig. 1B), a mineral that cooled slowly through and/or resided in the HePRZ for an extended interval or one that repeatedly cooled through and re-entered the HePRZ will not. The dates in the latter cases reflect the total He retained in the crystal over the course of its more complex thermal history that includes partial He loss in the HePRZ.

Owing to this behavior, determining the geologic meaning of a (U-Th)/He date is not always straightforward. Diverse strategies are used to reduce ambiguity in possible tT paths that can explain the data. These include sampling strategies to harness geologic constraints or to capitalize on date-elevation relationships (see section 5.2); acquiring data for multiple geo-/thermochronometers with different temperature sensitivities either by dating different minerals or crystals of the same mineral with variable kinetics; using stepped-heating methods like ^{4}He/^{3}He to examine ^{4}He concentration distributions because in some cases different styles of thermal history that yield the same date have different ^{4}He diffusion profiles (Shuster and Farley, 2004); and employing forward thermal history modeling to acquire a conceptual understanding of which portions of tT paths the data do or do not constrain. Any or all of these may then be combined with inverse thermal history modeling that is deliberately designed to test geologically plausible hypotheses for the data and determine the full swath of tT paths that honor both the data and the sample's geologic context (e.g., Braun, 2003; Ketcham, 2005; Gallagher, 2012; Braun

et al., 2012; Gallagher and Ketcham, 2018; companion paper, Flowers et al., 2022).

The "closure temperature" (T_C) concept refers specifically to monotonic (i.e., constant cooling) mineral systems and not to more complex types of tT paths. Closure temperature is strictly defined as the temperature of a monotonically cooling mineral system at the time of its measured date and can be calculated using an equation that includes a mineral's diffusion parameters, the effective diffusion dimension, a diffusion-geometry term, and the cooling rate (Dodson, 1973). Closure temperature also serves as a convenient means for comparing the temperature sensitivities of different minerals, as we do below. When reporting and assessing closure temperatures, the assumed grain size and cooling rate should be specified. However, because closure temperature is defined based on a monotonic cooling-only thermal history and samples commonly undergo tT paths more complex than that, in many cases it is incorrect to consider a (U-Th)/He date from a natural sample as representing the timing of cooling through a specific closure temperature. Such logic is appropriate only in the limited circumstances where the geologic setting and constraints suggest a history characterized by simple and relatively rapid cooling without significant residence or reheating within the HePRZ. More typically, especially as (U-Th)/He dating is applied to deconvolve thermal histories over longer timescales, monotonic cooling assumptions are overly simplistic and inappropriate.

3. CONTROLS ON DIFFUSIONAL LOSS OF HE

3.1. Overview

A mineral's He diffusion kinetics determine its temperature sensitivity range and thus its utility for addressing different geologic problems. High-resolution interpretation of (U-Th)/He thermochronologic data depends on an accurate understanding of how He mobility varies as a function of temperature and other factors in the minerals dated. It also relies, to a large degree, on the observation that the fundamental control on the migration and loss of He through and from crystals follows thermally activated volume diffusion, where He atoms can be treated as interstitial impurities within a crystal lattice. He atoms located at various sites can randomly access neighboring sites at a rate that depends on the energy needed to jump between sites. The energy needed for jumping is determined by the nature of the mineral lattice. The different types of sites within a specific mineral grain (e.g., interstitial sites, vacancy sites, fine-scale crystal defects as well as larger imperfections,

and damage created by alpha recoil decay or spontaneous fission) will require different jump energies. Consequently, radiation damage, other defects, and chemical substitutions will modify the bulk diffusion characteristics of natural crystals relative to a perfect crystal lattice (e.g., Shuster et al., 2006; Mbongo Djimbi et al., 2015; Danišík et al., 2017a; Zeitler et al., 2017). What we generally imagine as smooth bulk diffusion is in reality an emergent process that follows from an ensemble of many completely random walks in 3-D. Moreover, He escape at grain boundaries after crossing the grain radius is actually the net result of a very lengthy random walk (meters in length) through the crystal (e.g., Zeitler et al., 2017). If the crystal is a single diffusion domain and if temperatures are appropriate for partial He loss, then a He diffusion profile will develop defined by concentrations that are higher in the grain interior and decline toward the grain edge (Fig. 1A). If, instead, the crystal is a polycrystalline aggregate consisting of multiple diffusion domains and undergoes partial He loss, then rounded He diffusion profiles will develop within the individual crystallite domains rather than at the scale of the entire crystal.

He diffusion can be characterized by the Arrhenius law in which diffusion has an exponential temperature dependence. Arrhenius diffusion is described by activation energy (E_a) and a pre-exponential frequency factor (D_0) or its equivalent normalized by a diffusion domain size squared (D_0/a^2) (e.g., McDougall and Harrison, 1999). E_a represents the exponential temperature dependence of diffusion, whereas D_0 or D_0/a^2 can be thought of as the rate of diffusion at infinite temperature. Both of these kinetic parameters may be anisotropic within minerals. For example, for typical zircon and rutile compositions without substantial radiation damage, He diffusion is anisotropic (e.g., Reich et al., 2007; Farley, 2007; Cherniak et al., 2009; Cherniak and Watson, 2011; Guenthner et al., 2013; Anderson et al., 2020). In contrast, in apatite and titanite, He diffusion is isotropic (e.g., Reiners and Farley, 1999; Farley, 2000; Cherniak and Watson, 2011).

Here, we briefly describe the factors that influence diffusional loss of He and how they can contribute to date variation. How He diffusion kinetics are measured, and associated considerations for reporting those data and their uncertainties, are described in section 8.

3.2. Crystal Size

The diffusion of He from a mineral depends not just on temperature but also on the size of the diffusion domain. In larger domains, the average He atom has a longer path from its site

of generation in the domain interior to where it is lost at the domain edge than in smaller diffusion domains. In all minerals studied to date, including apatite (Farley, 2000), zircon (Reiners et al., 2002), and titanite (Reiners and Farley, 1999), the He diffusion domain corresponds to the size of the crystal or crystallite, or in the case of anisotropic zircon, at least the length scale of the c-axis-parallel dimension (Ginster, 2018). Thus, for mineral crystals that are identical except for dimension, larger crystals have a lower bulk diffusivity (higher closure temperature) than smaller crystals. This grain size effect can cause closure temperatures to vary by ~10 °C for typical crystal kinetics, dimensions, and cooling rates, and thus can induce positive correlations between the size and (U-Th)/He date of single mineral crystals from the same sample, particularly when samples have resided in the HePRZ for extended periods of time (Fig. 5; e.g., Farley, 2000; Reiners and Farley, 2001). Conveniently, a sample's grain size can be well represented by the radius of a sphere with either an equivalent surface-area-to-volume ratio (R_{SV}) or an equivalent F_T-correction (R_{FT}) as the analyzed grain, although for zircon this is probably better represented as the half-length of the c-axis parallel dimension, at least up to a certain extent of radiation damage. R_{SV} or R_{FT} is a standard parameter reported in (U-Th)/He data sets (see section 6.3.2 for how calculated), and is required for diffusion modeling. For anisotropic diffusion, an "active radius" that incorporates anisotropy and crystal length can also be used (Gautheron and Tassan-Got, 2010).

For materials analyzed that are polycrystalline aggregates, consisting of crystallites with variable sizes, no correlation between the size of the analyzed aggregate and date will occur. Such aggregates are characterized by multiple diffusion domain (or poly-crystalline domain) behavior, which yields diagnostic He release patterns during He diffusion experiments (e.g., Farley, 2018). Hematite is an example of a mineral that commonly forms as a polycrystalline aggregate and displays this type of He diffusion behavior (Farley and Flowers, 2012). However, when individual hematite crystallites are isolated from the aggregate and dated, positive correlations between the size and (U-Th)/He date of single crystallites can occur (Jensen et al., 2018).

3.3. Radiation Damage

The bulk He diffusivity of a mineral can be strongly affected by the amount of accumulated radiation damage due to self-irradiation of the crystal from decay of the parent isotopes. Consequently, the mineral diffusivity will change over its history owing to the accumulation and
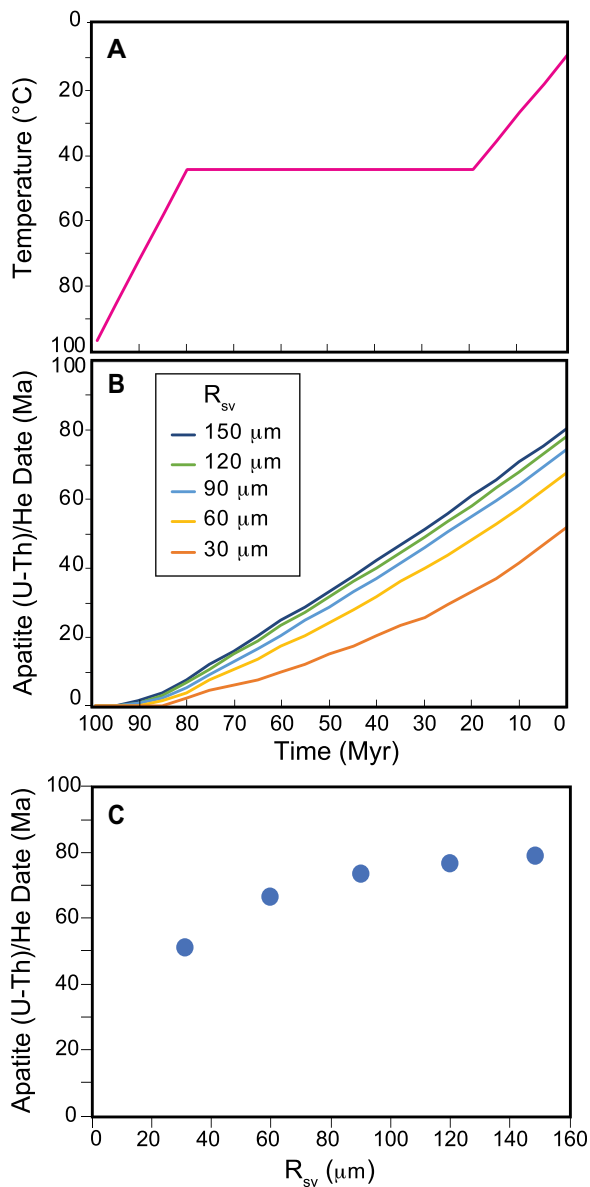
Figure 5. Influence of crystal size on (U-Th)/He date is shown. (A) Temperature versus time plot, where pink line represents a 100-m.y.-long cooling path that includes extended residence in the He partial retention zone (HePRZ). (B) Apatite (U-Th)/He date versus time plot, where the curves represent the evolution of (U-Th)/He date for apatite grains of differing equivalent spherical radius (R_{SV}) but with the same eU value of 28 ppm for the thermal history in panel A. (C) Apatite (U-Th)/He date vs R_{SV} for the thermal history in panel A. The dates plotted correspond to those in panel B at 0 m.y. (present day) for apatite grains with different R_{sv} values after the (U-Th)/He dates have evolved for 100 m.y. from the thermal history in panel A. The (U-Th)/He dates were modeled using the HeFTy software (Ketcham, 2005) with the apatite RDAAM model (Flowers et al., 2009).

Gautheron et al., 2009; Guenthner et al., 2013; Gerin et al., 2017; Willett et al., 2017; Guenthner, 2021). These assume that He is impeded by damage mostly created during parent isotope recoil, but they make different assumptions regarding annealing kinetics. Fission-track annealing kinetics are employed to track damage annealing in the more commonly used models (Flowers et al., 2009; Gautheron et al., 2009; Guenthner et al., 2013), but there is active investigation underway about whether the annealing kinetics of other types of damage are different and should be used instead (e.g., Willett et al., 2017; Ginster et al., 2019). Chemical composition may also modify the annealing rates of radiation damage (e.g., Flowers et al., 2009; Gautheron et al., 2013).

The total radiation damage due to alpha decay in a crystal (also referred to as alpha dose) is a function of both effective U concentration (eU, which weights the parent isotopes for their alpha productivity; see section 6.3.5) and damage accumulation and annealing durations. Crystals of the same mineral from a single sample can be characterized by closure temperatures that can vary by 10s °C (apatite) to >100 °C (zircon and titanite) owing to differences in eU. This is because higher-eU crystals have greater damage production rates than lower-eU crystals and therefore accumulate more damage over the same thermal history. eU is a useful proxy for relative damage for samples with a shared tT path where damage accumulation duration is the same for all crystals dated (although eU is an imperfect proxy, owing to the potential for heterogeneous damage annealing). For some types of thermal histories, the radiation damage effect can cause positive (at lower damage levels) or negative (at higher damage levels) correlations between date and eU for grains that underwent the same tT path (Fig. 6; e.g., Shuster et al., 2006; Flowers et al., 2007; Guenthner et al., 2013).

3.4. Major Element Chemistry

Theoretical models suggest that chemical substitutions should affect He diffusion to some degree by modifying the mineral lattice structure and thus changing the energy required for He to move between sites (e.g., Mbongo Djimbi et al., 2015; Gautheron et al., 2020), although observational evidence for this effect has been generalized and inconsistent. In addition, chemical composition may influence He diffusivity in some minerals like apatite by modifying the annealing kinetics of radiation damage (e.g., Carlson et al., 1999; Flowers et al., 2009; Gautheron et al., 2013; McDannell and Issler, 2021). For minerals with larger

annealing of radiation damage. Diffusion experiments and patterns of data variation document that radiation damage influences He diffusion in apatite (e.g., Shuster et al., 2006; Flowers et al., 2007; Gautheron et al., 2009), zircon (e.g., Hurley, 1954; Guenthner et al., 2013), titanite (e.g., Hurley, 1954; Baughman et al., 2017), and possibly rutile (Robinson et al., 2019). Quantum calculations and intra-grain He distribution mapping provide additional support for this phenomenon (e.g., Danišík et al., 2017a; Gerin et al., 2017; Gautheron et al., 2020). At lower levels, damage-induced defects may act to impede He diffusion (e.g., inferred for apatite; Shuster et al., 2006) or to block faster pathway channels (e.g., inferred for zircon; Guenthner et al., 2013; Ketcham et al., 2013), thus lowering the bulk crystal He diffusivity. At higher lev-

els, the defects may interconnect and accelerate He loss, thus increasing the bulk crystal He diffusivity (e.g., Guenthner et al., 2013; Ketcham et al., 2013).

Parent isotope recoil during alpha decay, alpha-particle damage, and spontaneous fission events create different types of damage in the crystal structure. How these different damage types affect the mineral He diffusivity as a function of the damage volume fraction in the crystal lattice, and what governs the elimination of that damage by annealing, are key topics of study (Shuster et al., 2006; Flowers et al., 2009; Shuster and Farley, 2009; Guenthner et al., 2013; Ketcham et al., 2013; Willett et al., 2017; Ginster et al., 2019). Different models of damage accumulation and annealing exist for apatite and zircon (Shuster et al., 2006; Flowers et al., 2009;
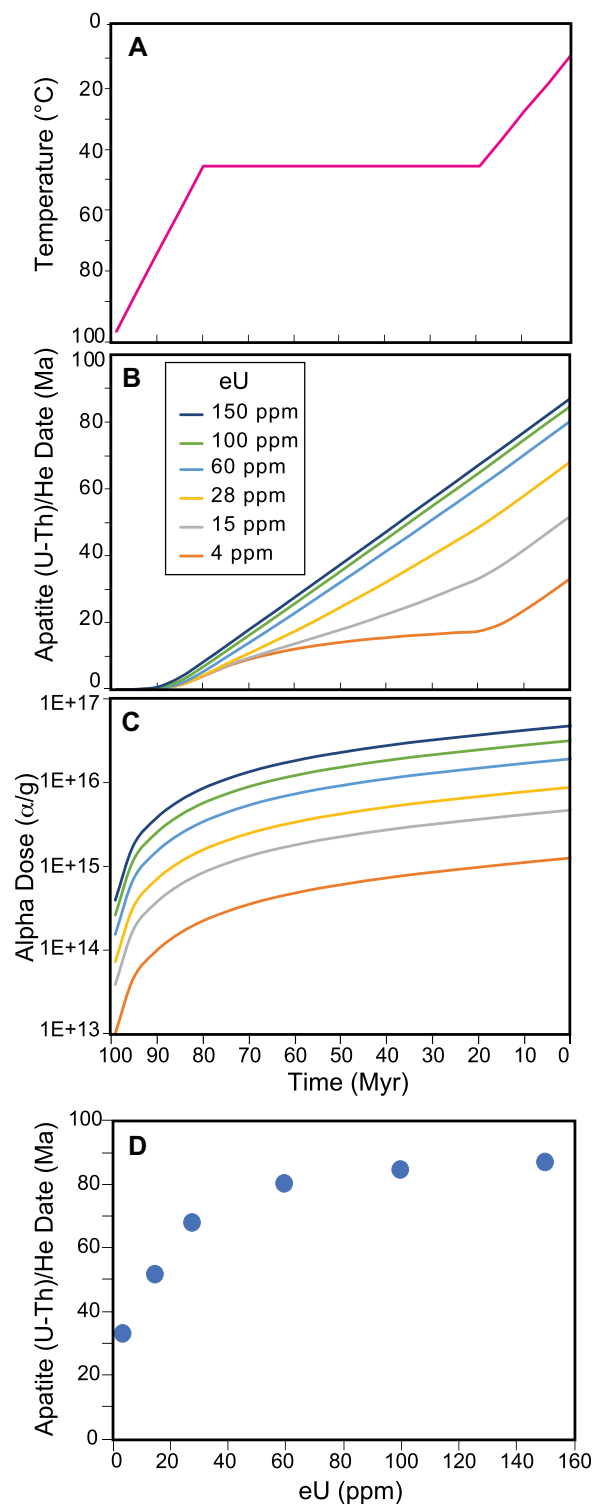
Figure 6. Influence of radiation damage on apatite (U-Th)/He date is shown. (A) Temperature versus time plot, where pink line represents a 100-m.y.-long cooling path that includes extended residence in the He partial retention zone (HePRZ). (B) Apatite (U-Th)/He date versus time plot, where the curves represent the evolution of (U-Th)/He date for apatite grains of differing eU but with the same R_{sv} value of 60 μm for the thermal history in panel A. (C) Plot shows the same as in panel B, but for alpha dose, which is the total radiation damage due to alpha decay in a crystal. (D) Apatite (U-Th)/He date versus eU for the thermal history in panel A. The dates plotted correspond to those in panel B at 0 m.y. (present day) for apatite grains with different eU values after the (U-Th)/He dates have evolved for 100 m.y. during the thermal history in panel A. The (U-Th)/He dates were modeled using the HeFTy software (Ketcham, 2005) with the apatite RDAAM model (Flowers et al., 2009).

3.5. Coarser Defects

Beyond finer-scaled defects such as those related to chemistry and radiation damage, larger crystal imperfections should also have the potential to modify the He diffusivity or He diffusion behavior of a mineral. These include microvoids such as fluid inclusions, microstructural defects induced by strain, or other vacancies. Depending on their size and nature, these defects could serve to impede movement of He through a crystal (like radiation damage) or actually serve as reversible sinks during both geological and laboratory diffusion (e.g., Gerin et al., 2017; Zeitler et al., 2017; Danišík et al., 2017a; McDannell et al., 2018; Guo et al., 2021). Active research into these features is attempting to determine whether, like radiation damage, they alter kinetics in a way that can be used to gain additional information about the thermal history or if they represent artifacts and complications that should be identified and either corrected for or avoided.

4. MINERALS SUITABLE FOR (U-Th)/He ANALYSIS

4.1. Overview

Most (U-Th)/He development and application studies have focused on apatite and zircon because these minerals are abundant in crustal rocks, contain reasonable eU values (10s–1000s of ppm), commonly are 10s to >100 μm in size, and have closure temperatures <220 °C that are relevant for constraining upper crustal and near-surface thermal histories. Consequently, this paper is focused primarily on apatite and zircon data acquisition and reporting practices. However, in addition, a growing number of other (U-Th)/He chronometers is available with sensitivities to temperatures from >300 °C to ~20 °C. The development and calibration of new He chronometers are largely motivated by the desire to resolve more detailed tT paths, to date processes and events that are otherwise difficult to constrain (e.g., weathering), and to expand thermal history reconstructions to igneous, metamorphic, and sedimentary lithologies (e.g., ultramafic or carbonate rocks) that do not contain minerals traditionally used for thermochronology. Factors that bear on the feasibility and utility of a phase as a (U-Th)/He chronometer include mineral abundance, eU, crystal size (grains less than a few 10s of μm have unreasonably large F_T corrections, section 2.3), He retentivity at Earth surface conditions, and closed-system behavior, for example, of the parent isotopes (e.g., dissolution-precipitation processes can be a concern for phases like goethite and calcite).

compositional variability than apatite and zircon, the influence of chemical substitutions may be accordingly greater. For example, in natural fluorites, He diffusivity appears to decrease with REE + Y substitutions owing to vacancy reduction and constriction of key diffusion pathways (Wolff et al., 2016). ³He diffusion study of synthetic monazite structure and zircon structure phosphates with endmember compositions demonstrates that He diffusivity changes systematically with chemical composition in a given structure as expected based on how the chemical substitutions modify diffusion paths (Farley, 2007).

Here, we first briefly describe the apatite and zircon (U-Th)/He chronometers (section 4.2). We then summarize the work done and current state of knowledge of the diffusion kinetics of other mineral phases (section 4.3). We place the discussion of mineral temperature sensitivities in the context of mineral T_C values (section 2.5) to make this information conceptually more accessible to the non-expert than if described in the context of the kinetic parameters (Ea, D_0; section 3.1) that are, in reality, used to characterize He diffusion behavior in minerals. The Tc values reported from the studies below generally assume typical grain sizes for the mineral investigated and a 10 °C/m.y. cooling rate. For greater detail, the reader is referred to Chapter 11 of Reiners et al. (2018), which provides an in-depth discussion of He diffusion kinetic parameters for different minerals and explains how this understanding has evolved over the last several decades.

4.2. Most Commonly Dated Minerals: Apatite and Zircon

For the reasons described above, He diffusion in apatite and zircon has received greater attention and application than in other minerals. Models for He loss from these phases must account, at least empirically, for the effects of radiation damage (section 3.3). In apatite, for commonly encountered alpha doses, damage addition can cause the Tc values to increase from ~40 °C to ~115 °C (Shuster et al., 2006; Flowers et al., 2009; Gautheron et al., 2009; Mbongo Djimbi et al., 2015), with a possible decrease in He retentivity at higher damage levels (e.g., Recanati et al., 2017). The Durango apatite standard (Mc-Dowell et al., 2005) provides a useful reference point for He diffusion in moderately damaged apatite, with [3]He and [4]He stepped-heating experiments pointing to T_C values of 67–69 °C for a domain size of 75 μm and assuming a cooling rate of 10 °C/m.y. (Shuster et al., 2004). This increase in apatite He retentivity with damage has been modeled as local traps that accumulate with time at low temperature and impede the migration of He atoms through an otherwise defect-free apatite lattice (Shuster et al., 2006; Flowers et al., 2009). The radiation damage that affects He diffusion also anneals as a function of time and temperature, which must be accounted for by models that describe the evolution of He diffusivity during the thermal history of an apatite crystal. A now widely used model parameterizes the abundance of radiation damage traps as a function of damage extent, or equivalent spontaneous fission-track density, and treats annealing kinetics as those of etchable fission tracks, although specific parameters within the model

can be adjusted for sample-specific annealing kinetics (e.g., Flowers et al., 2009). Additional models are available that use different parameterizations between accumulated damage and trap abundance, and/or assume different annealing kinetics (Gautheron et al., 2009; Gerin et al., 2017; Willett et al., 2017).

Helium diffusion in zircon is similar to that in apatite in some ways but is more complex due to anisotropic diffusion and greater radiation damage accumulation. In zircon, damage accumulation induces a T_C increase from values of ~140 °C to ~220 °C, followed by a decrease to <50 °C after a damage percolation threshold is crossed (Guenthner et al., 2013; Ketcham et al., 2013). For low damage crystals, experimental evidence (Farley, 2007; Cherniak et al., 2009) and computational models (Reich et al., 2007; Bentson et al., 2012) show that c-axis–parallel diffusion is ~100 times faster than c-axis perpendicular diffusion rates. However, anisotropic diffusion differences decrease dramatically as radiation damage increases (Guenthner et al., 2013; Ginster, 2018). The threshold behavior where He mobility increases with additional damage has been modeled as the effect of percolation of an increasing fraction of highly damaged/amorphous crystal domains that represent fast paths for He escape (Guenthner et al., 2013; Ketcham et al., 2013). Although there is debate about the extent of damage at the percolation threshold (e.g., Anderson et al., 2017; Gautheron et al., 2020), [3]He and [4]He stepped-heating experiments on crystallographically oriented slabs of gem-quality zircon with effective alpha doses measured by Raman spectroscopy suggest a "rollover" at ~1.3–1.6 × 10^{18} a/g (Guenthner et al., 2013; Ginster, 2018). As with apatite, the radiation damage that affects He diffusion also anneals with time and temperature. Some models (e.g., Guenthner et al., 2013) assume this annealing follows that of etchable fission tracks. New work (Ginster et al., 2019) shows that alpha-recoil damage, at least as measured by Raman spectroscopic characteristics, requires considerably higher temperatures and/or longer durations than etchable fission tracks to achieve the same extent of annealing, and also follows more complex, multi-kinetic laws. The high damage end of the zircon kinetic model is the least well-calibrated portion of its alpha-dose range (Guenthner et al., 2013), and in some cases the model fails to reproduce (U-Th)/He dates for zircon with a high alpha dose (e.g., Johnson et al., 2017). This suggests that interpreting dates for high alpha-dose zircon with current kinetic models should be done only with caution.

Despite the complexity of full radiation damage accumulation and annealing models (RDAAM) that involve multiple parameters and

relationships among kinetics, damage extent, time, and temperature, in practice they are relatively straightforward to incorporate in numerical models (see section 8.2.1 and companion paper, Flowers et al., 2022) that relate He content (and therefore date) to a crystal with given eU, size, and tT path. These computational frameworks allow relationships between He date, eU, and grain size to be exploited and inverted to constrain permissible thermal histories.

4.3. Other Dated Minerals

4.3.1. U- and Th-Bearing Accessory Minerals

U- and Th-bearing accessory minerals besides apatite and zircon have been an important emphasis of (U-Th)/He investigation. These include titanite, monazite, xenotime, rutile, baddeleyite, and perovskite.

Titanite ($CaTiSiO_5$) is a relatively common accessory phase in igneous and metamorphic rocks and was a focus of early (U-Th)/He dating studies (e.g., Strutt, 1910c; Hurley, 1954). A T_C value of ~190–220 °C for low-damage titanite is documented by [4]He diffusion and (U-Th)/He data (Reiners and Farley, 1999; Stockli and Farley, 2004), as well as by [4]He/[3]He diffusion experiments (Shuster et al., 2003) and He ion implantation data that additionally demonstrate that titanite He diffusion is isotropic (Cherniak and Watson, 2011). In more damaged titanite crystals, radiation damage can decrease the titanite T_C to <50 °C (Baughman et al., 2017; see section 3.3). Although titanite grains commonly occur as fragments, which introduces uncertainty into the F_T correction (section 2.3), titanite fragments are generally large in size such that the magnitude of the F_T correction and its influence on the corrected (U-Th)/He date are minimized (e.g., Baughman et al., 2017). Titanite (U-Th)/He has been used to date felsic-intermediate volcanic rocks (e.g., House et al., 2000; Tincher and Stockli, 2009), impact structures (van Soest et al., 2011; Biren et al., 2014), and kimberlite emplacement (Blackburn et al., 2008), as well as to reconstruct thermal histories (e.g., Reiners et al., 2000; Pik et al., 2003; Flowers and Schoene, 2010; Grabowski et al., 2013; Weisberg et al., 2018; Baughman and Flowers, 2020). Moving forward, titanite has the potential to become a more routinely used thermochronometer owing to its common occurrence, moderate eU (10–200 ppm), and relatively large crystal sizes (commonly 100s of μm).

Monazite (($Ce,La,Th)PO_4$) and xenotime (YPO_4) are phosphate accessory minerals that can occur in igneous and metamorphic rocks and are typified by extremely high U and Th concentrations (100s of ppm to wt% levels). He diffusion studies on the same monazite standard yield

T_C estimates of 206–291 °C (Farley and Stockli, 2002; Boyce et al., 2005; Peterman et al., 2014). He implantation study of natural monazite (Cherniak and Watson, 2013) and ^{3}He diffusion investigation of synthetic monazite (Farley, 2007) also imply T_c values in this range and suggest that He diffusion is predominantly isotropic. The high parent isotope concentrations of monazite made it an attractive target for early laser ablation (U-Th)/He development work (Boyce et al., 2006, 2009). Xenotime has received less attention, with diffusion experiments suggesting T_C values of ~110 °C (Farley and Stockli, 2002) and ~75 °C (Anderson et al., 2019). ^{3}He diffusion study on synthetic phosphates documented pronounced diffusional anisotropy in synthetic xenotime and other zircon structure phosphates (Farley, 2007). Despite the high eU in monazite and xenotime, their typically small size (10s of μm) and potential to be characterized by extreme U-Th zonation means that they have seen few applications.

Rutile (TiO_2) is a common accessory mineral in high-pressure metamorphic rocks and lower crustal granulites. Experimental and empirical constraints from He diffusion studies suggest rutile T_C values of ~155–199 °C with a possible increase in T_C to much higher values with increasing radiation damage (Robinson et al., 2019). Earlier He diffusion study implied T_C values of ~220–235 °C (Stockli et al., 2007), while He implantation investigation of synthetic rutile inferred T_c values of ~150–225 °C (Cherniak and Watson; 2011). Both the implantation studies and diffusion experiments show that rutile He diffusion is highly anisotropic (Cherniak and Watson, 2011; Robinson et al., 2019). Few studies have applied rutile (U-Th)/He dating (Stockli et al., 2007; Robinson et al., 2019). This might be attributable to erroneous dates in pilot studies due to parent isotope loss from some rutile crystals during laser heating (Robinson et al., 2019) and/or to the potential of rutile in metamorphic assemblages to react and form titanite, resulting in a polymineralic material. However, with appropriate characterization and analytical care, rutile is a promising target for (U-Th)/He work in metamorphic rocks due to its abundance in these lithologies, eU that is typically in the 10s of ppm, and reasonable grain sizes (commonly >100 μm).

Perovskite ($CaTiO_3$) and baddeleyite (ZrO_2) are other U- and Th-bearing accessory minerals that have received limited attention. Perovskite is a common phase in kimberlites. Previous (U-Th)/He dating and He diffusion study showed the utility of perovskite (U-Th)/He dates to determine kimberlite emplacement ages and suggest a perovskite T_C value of >300 °C (Stanley and Flowers, 2016). Baddeleyite can occur in mafic rocks that are too low in silica to crystallize zircon. Empirical constraints suggest a baddeleyite T_C value higher than that of zircon or titanite, and thus it is likely >200 °C (Baughman and Flowers, 2018). More restrictive constraints on baddeleyite diffusion kinetics through laboratory stepped-heating experiments have been hindered by the difficulty of extracting He from this retentive mineral (Metcalf and Flowers, 2013). Despite the commonly small size (1–10s of μm) of perovskite and baddeleyite crystals, their reasonably high eU values (in the 10s–100s of ppm) and occurrence in mafic lithologies that may lack alternative minerals as chronologic targets means that these phases may continue to see applications in the future.

4.3.2. Metallic Oxide and (Oxy)hydroxide Dating

Metallic oxide and hydroxide dating are an increasing focus of (U-Th)/He studies. These phases include hematite (Fe_2O_3), goethite (FeO.OH), magnetite (Fe_3O_4), and spinel ((Mg,Fe)($Al,Cr)_2O_4$). Early investigations focused on dating ore deposit mineralization (e.g., Fanale and Kulp, 1962; Lippolt et al., 1993; Wernicke and Lippolt, 1993, 1994a, 1994b), while more recent (U-Th)/He work exploits the metallic oxides for numerous diverse geologic applications (e.g., Cooperdock and Ault, 2020).

The Fe-oxides have been studied most. Hematite diffusion studies document multiple diffusion domain behavior owing to the polycrystalline aggregate character of most materials analyzed (Farley and Flowers, 2012; Balout et al., 2017; Farley, 2018). ^{3}He diffusion experiments suggest a He T_C value of ~250 °C and ~70 °C for hematite crystallites with radii of ~1 mm and 20 nm, respectively (Farley, 2018). Hematite ^{4}He/^{3}He thermochronology has the potential to constrain thermal histories between ~250 °C and surface conditions depending on the crystallite size distribution (Farley and Flowers, 2012). Goethite also shows multiple diffusion domain behavior that is possibly due to a polycrystalline aggregate structure, but goethite is far less retentive of He than hematite (Shuster et al., 2005a). A significant analytical concern for the Fe-oxides has been the volatilization and loss of U during laser heating (e.g., Vasconcelos et al., 2013; Danišík et al., 2013), which is attributable to Fe reduction during a phase change from hematite to magnetite (Hofmann et al., 2020). This analytically induced loss of U can lead to erroneous results, although approaches have now been developed to circumvent this issue (Hofmann et al., 2020). Hematite (U-Th)/He dating has been used to date fault surfaces and paleo-earthquakes (e.g., Evenson et al., 2014; Ault et al., 2015; Jensen et al., 2018; Ault, 2020; Calzolari et al., 2020), weathering (e.g., Pidgeon et al., 2004; Reiners et al., 2014; Cooper et al., 2016; Wells et al., 2019; dos Santos Albuquerque et al., 2020), ore deposit formation (e.g., Danišík et al., 2013), and hydrothermal alteration (e.g., Farley and McKeon, 2015; Wu et al., 2019). Goethite (U-Th)/He dating has constrained the timing of lateritic weathering in several settings (e.g., Shuster et al., 2005a; Monteiro et al., 2014, 2018; Allard et al., 2018; Wells et al., 2019; dos Santos Albuquerque et al., 2020). It is clear that the Fe-oxides will continue to be an important focus of (U-Th)/He investigations owing to reasonable eU concentrations in many materials (up to 100 ppm) and the potential to apply them in weathering-related geochronology and to constrain other difficult-to-date processes.

Magnetite and spinel are also promising (U-Th)/He dating targets. Magnetite He diffusion data suggest a T_C value of ~250 °C (Blackburn et al., 2007). Magnetite (U-Th)/He has been applied to date basalts and kimberlites (Blackburn et al., 2007, 2008) as well as to constrain the timing of serpentinization (Cooperdock and Stockli, 2016) and ophiolite exhumation (Schwartz et al., 2020). (U-Th)/He dating of spinel from ultramafic rocks from different geodynamic environments suggests that this mineral can be used to resolve peridotite cooling and exhumation histories (Cooperdock and Stockli, 2018). However, the low eU of typical magnetite and spinel crystals (commonly ~50–300 ppb) makes analysis of these phases analytically difficult.

4.3.3. Other Mineral Phases

(U-Th)/He dating has also been applied to a limited number of other phases. Of these, He diffusion in fluorite (CaF_2) is best constrained and has been applied most (Evans et al., 2005a; Pi et al., 2005; Siebel et al., 2010; Wolff et al., 2015), with a range of T_C values between ~45 °C and 170 °C (Evans et al., 2005a; Wolff et al., 2016) that appear to depend on composition (Wolff et al., 2016). Fluorite (U-Th)/He dating will likely see more applications due to the reasonable eU of many crystals (1–10s of ppm), the common occurrence of fluorite in low-temperature hydrothermal veins and ore deposits, and the applicability of the results for dating ore deposit formation.

Garnet (($Ca,Mg,Fe,Mn)_3(Al,Fe,Cr)_2(SiO_4)_3$), calcite ($CaCO_3$), conodont bioapatite ($Ca_5(PO_4)_3$), and allanite (($Ce,Ca,Y,La)_2(Al,Fe)_3(SiO_4)_3(OH)$) have also received some attention. Garnet (U-Th)/He dating has been attempted on volcanic rocks, but its T_C value remains controversial and poorly constrained (e.g., Dunai and Roselieb, 1996; Aciego et al., 2003; Blackburn and Stockli, 2006). Calcite (U-Th)/He dating and associated He diffusion studies have yielded variable date reproducibility and He diffusion

kinetics results, which are attributed to excess He, dissolution/reprecipitation processes, and/or multiple diffusion domain behavior (Copeland et al., 2007; Cros et al., 2014). He implantation study of calcite, dolomite, magnesite, and aragonite provides evidence that typical carbonate materials have minimal He retentivity at Earth surface conditions (Cherniak et al., 2015). He diffusion study of conodont bioapatite suggests a He retentivity similar to that of magmatic apatite (Peppe and Reiners, 2007), but conodont (U-Th)/He dating has yielded results of variable reproducibility, likely due to late-stage parent isotope loss and diagenetic processes (Peppe and Reiners, 2007; Landman et al., 2016; Bidgoli et al., 2018; Powell et al., 2018). Allanite with high Th content has been used to date Quaternary volcanic rocks in eastern California (Cox et al., 2012). Additional study on all of these phases is required to evaluate the viability of their more routine use as He chronometers.

5. (U-Th)/He DATING: SAMPLING, MEASUREMENT, AND ASSOCIATED SAMPLE AND METHOD REPORTING

5.1. Overview

(U-Th)/He dating is a multistep process. Unlike most other geochronology methods, current (U-Th)/He techniques require measurement of daughter and parent nuclides on different instruments owing to their contrasting chemical behaviors (i.e., He is a gas whereas U, Th, and Sm are not). Today most conventional (U-Th)/He analyses consist of single mineral crystals, except in cases of extremely low parent or daughter amounts, or of mineral aggregates (e.g., Fe-oxides) where separation of single mineral crystals is not possible (e.g., Shuster et al., 2005a). Multigrain analyses consisting of multiple single crystals were more common during the early developmental era of the method (e.g., Wolf et al., 1996). Importantly, both parent and daughter are measured on the same crystal, eliminating the requirement for delicate weighing, which removes this uncertain step from date determinations.

Below, we provide a brief summary of common sampling strategies followed by a description of the laboratory steps associated with conventional (U-Th)/He analyses, with a particular emphasis on apatite and zircon. Figure 7 illustrates the workflow and approximate time for each step. As described further below, these include: (1) sampling (variable time) and mineral separation (1–2 weeks); (2) grain selection, crystal dimension measurement, possible additional grain characterization, and grain packing into metal packets (0.25–2 h/grain); (3) heating, He degassing, and He measurement on a noble gas mass spectrometer (~1 h/grain); (4) retrieval of the mineral-bearing metal packets, crystal dissolution, and U-Th (and sometimes Sm, Ca, Zr, and/or trace elements) measurement, typically by inductively coupled plasma–mass spectrometry (ICP-MS, hours to days/grain); and (5) data reduction and interpretation (variable time). We then summarize the key sample information and methods that should be reported or referenced for (U-Th)/He analyses (Table 1, section 5.7).

5.2. Sampling Strategies and Mineral Separation

Sampling is done strategically to restrict the viable tT paths that can explain the data to be acquired and answer the geologic question being addressed (see also section 2.5). The range of feasible thermal histories can be narrowed by capitalizing on geologic and chronologic constraints such as sample crystallization or depositional ages, emplacement depth estimates, the age of an unconformity that constrains when the sample was at the surface, or the age of a faulted unit. Sample suites from elevation transects, drill cores, or large paleodepth ranges are commonly used because the thermal histories must be internally consistent across all samples. For some studies of landscape evolution, it is important to sample at different spatial wavelengths (<10 km and >100 km) to address the way that topography alters the shallow thermal field (e.g., Braun, 2002). Combining multiple geo- and thermochronometers with different temperature sensitivities on the same samples increases the tT range that can be constrained, which can further reduce ambiguity in thermal history interpretation.

Additional sampling considerations include lithology, degree of alteration, sample age, the probability that the rock contains the minerals of interest, and grain size. For example, younger igneous samples that are apatite- and

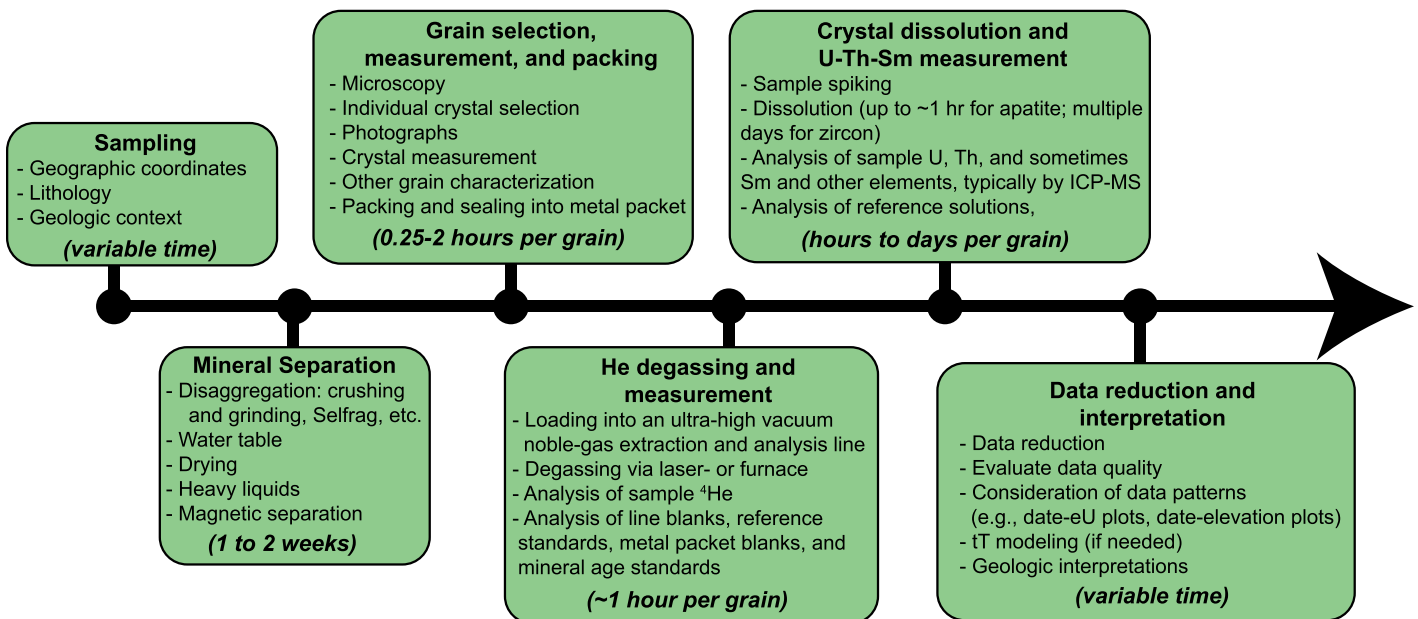## Workflow and time for conventional individual aliquot (U-Th)/He data acquisition

Figure 7. Summary of steps and approximate time to acquire conventional individual aliquot (U-Th)/He data.

TABLE 1. CHECKLIST OF NEEDED (OR REFERENCED) SAMPLE INFORMATION AND METHODS TO REPORT FOR (U-Th)/He ANALYSES

Sample Information
- ☐ Geographic coordinates in a specified geodetic datum: Latitude, longitude, elevation
- ☐ Lithology
- ☐ Type of sample collected: In situ sample, loose rock, river sand
- ☐ Geologic context
- ☐ Any additional geochronologic or thermochronologic data available for the sample

Methods (Either describe or cite an appropriate reference)
- ☐ Mineral separation procedures: type of rock disaggregation (e.g., standard crushing and grinding, SelFrag), water table, heavy liquids, drying temperature, and magnetic separation, as well as any pre-concentration techniques for detrital samples or chemical cleaning procedures.
- ☐ Mineral selection procedures: microscopy, magnification used, and any additional tools.
- ☐ Criteria used for grain selection: size, morphology, clarity, color, lack of mineral and fluid inclusions, etc.
- ☐ Methods for He measurements: instrumentation used, laser or furnace heating, type of He analysis (e.g., isotope dilution or external calibration).
- ☐ Methods for mineral dissolution and U, Th, Sm measurements: dissolution protocol, instrumentation used, type of analysis (e.g., isotope dilution).
- ☐ Secondary mineral standards used for quality control (e.g., Durango apatite, Fish Canyon Tuff zircon).
- ☐ Name(s) of lab(s) where data were acquired.

zircon-bearing tend to contain higher quality euhedral crystals that record relatively short and simple thermal histories, detrital samples may have rounded grains with disparate pre-depositional histories, and ancient rocks may have more complex thermal histories that are more challenging to interpret. For apatite, intermediate composition igneous rocks generally provide the best yield, with immature clastic sedimentary rocks (sand size and larger) also sometimes yielding reasonable material. For zircon, a wider range of felsic to intermediate igneous rocks, and many clastic sedimentary lithologies, are good targets. In metamorphic rocks, secondary overgrowths on primary zircon can be problematic owing to parent isotope zonation effects on the corrected (U-Th)/He date if the typical no zonation assumption is adopted (section 2.3). Highly altered samples due to hydrothermal fluid circulation or intense weathering are best avoided if the aim to is decipher the pre-alteration thermal history, because alteration may cause open-system behavior and interfere with accessing the older history of interest. In all cases, medium- to coarse-grained rock types are preferred so that crystals of sufficient size (with F_T value of >0.5, section 2.3) are obtained for analysis. A sample of 1–3 kg is typically collected to ensure enough material is obtained that is suitable for dating. For sedimentary rocks and unconsolidated detrital material (e.g., medium-grained river sand), the mineral yield is often lower, and larger samples (>5 kg) are generally collected.

Target minerals are separated from samples using a variety of techniques. These generally include rock disaggregation via standard crushing and grinding or high-voltage disaggregation methods (the latter include SelFrag methods, which can help keep minerals like apatite intact that are otherwise prone to breakage), followed by sieving, water table, drying, heavy liquids, and magnetic separation techniques. Pre-concentration methods are sometimes used for unconsolidated detrital materials during sample collection (i.e., panning). Chemical cleaning procedures are also used routinely in some labs.

5.3. Grain Selection, Crystal Dimension Measurement, and Packing for Analysis

Like sampling, the selection of grains for analysis is done strategically to acquire the data needed to address the geologic question of interest. Considerations include the choice of mineral(s), numbers of crystals, and potentially other characteristics such as radiation damage or size that affect the mineral He retentivity. Typically, 3–10 single crystals are selected from each sample for separate analyses. More grains may be analyzed in settings with protracted thermal histories where the dates may vary in potentially interpretable ways with factors such as eU or grain size (e.g., cratonic basement studies, burial studies of basin strata), in detrital investigations when characterization of the distribution of "unreset" grain dates is the objective (e.g., provenance studies, catchment erosion studies), or in circumstances where high precision is desired (e.g., dating of volcanic eruptions).

Analysis of high-quality grains is essential for high-quality data. Selection of quality crystals or other types of aliquots for analysis is typically accomplished by hand-picking from mineral separates using a binocular microscope at 100–240× magnification with transmitted and/or polarized light; some labs have used picking under various liquids to try to improve optical clarity. Crystals are chosen based on size and morphology as well as additional criteria that may include a lack of inclusions and overall crystal clarity. Larger crystals yield smaller F_T corrections and generally contain more parent and daughter atoms for measurement, which leads to smaller analytical uncertainties, but larger grains also have a higher probability of containing inclusions due to their larger volumes. Euhedral crystals with a morphology that can be approximated with standard geometries such as hexagonal or orthorhombic prisms are preferred, because these are the most straightforward to convert into accurate surface areas and volumes for F_T parameters, equivalent spherical radius, mass, and isotopic concentrations (see section 7.3). For apatite, mineral inclusions are generally avoided, because refrac-

tory U-Th rich inclusions such as zircon, which cannot be distinguished from inclusions that lack U-Th under the microscope, may yield erroneously old (U-Th)/He dates. This potential bias is caused by "parentless" [4]He, because [4]He produced by U-Th in the zircon inclusion will be measured, but the unrecovered parent will not be owing to incomplete zircon dissolution using the typical apatite HNO_3 dissolution procedure (e.g., Farley, 2002). For all minerals, crystals that lack fluid inclusions are preferred, because these inclusions may either contain initial He or act as He traps and yield anomalously old results (e.g., Zeitler et al., 2017; Danišík et al., 2017a; McDannell et al., 2018). Grains containing internal fractures are generally avoided, because pre-existing fractures may change the diffusion domain size by allowing fast pathways for diffusion. Grains with surficial discoloration are also best excluded from analysis, because this characteristic may indicate the former presence of a U-Th rich grain boundary phase that implanted He into the grain, biasing results to be erroneously old (e.g., Murray et al., 2014; see also Flowers et al., 2022). Crystal clarity and color may be factors in selecting minerals such as zircon because zircon opacity increases with greater radiation damage (e.g., Garver and Kamp, 2002; Ault et al., 2018; unfortunately, unlike zircon, color/opacity can't be used as a measure of radiation damage for typical apatite crystals). It can be advantageous to select a zircon suite with a wide range of radiation damage to obtain additional thermal history information from a zircon (U-Th)/He data set, although it may be problematic to interpret very high-damage zircon data with current kinetic models (sections 3.3 and 4.2).

In some cases, additional tools are used to assist with selecting the optimal material for analysis. Besides petrographic microscopy, these may include examination by cathodoluminescence and backscatter images or fission-track maps (e.g., Danišík et al., 2010; Johnson et al., 2017; Barham et al., 2019), LA-ICP-MS constraints on parent-isotope zonation (e.g., Hourigan et al., 2005; Farley et al., 2011; Johnstone et al., 2013; Danišík et al., 2017a), as well as Raman spec-

troscopy spot analyses or maps bearing on the magnitude and/or heterogeneity of intracrystalline radiation damage (e.g., Hardie et al., 2017; Danišík et al., 2017a; Anderson et al., 2020).

After selection, each grain is photographed, the crystal dimensions are measured, and the shape is characterized. Grains are typically measured using 2-D microscopy images and associated information is recorded, including the mineral length, width, number of terminations, grain geometry, and whether the grain is a whole crystal or a fragment. It is best to capture more than one 2-D image in order to measure not just grain length but also both minor axes, since assuming symmetry can lead to inaccuracies—for example, apatite grains may be somewhat flattened in shape. More comprehensive approaches for 3-D characterization of grain shape, such as via X-ray micro-computed tomography, are also sometimes used (section 7.3; e.g., Herman et al., 2007; Evans et al., 2008; Glotzbach et al., 2019; Cooperdock et al., 2019). The crystal dimension information comprises key measured data that are used for computation of the F_T correction and other derived parameters (see section 6.3). Each selected crystal is then packed and sealed in a small metal packet, typically Pt or Nb, prior to He analysis.

5.4. He Measurement

The next step in the data acquisition process is to determine the absolute amount of the daughter (^{4}He) in the crystal. The most common ^{4}He analysis protocol is for each selected crystal in its metal packet to be loaded into an ultra-high vacuum noble gas extraction and analysis line and degassed via heating by laser or furnace. The metal packet creates an evenly heated "microfurnace" during lasing and reduces parent nuclide volatilization that can occur during direct crystal heating (House et al., 2000). The sample is heated sufficiently to outgas all ^{4}He within several minutes, taking care not to reach extreme temperatures that can cause volatilization of parent nuclides. Typical temperatures may be $\sim$1000 °C for apatite and as much as $\sim$1350 °C for zircon, which can be quite retentive of some gas. ^{4}He quantities in the crystals are typically determined by isotope dilution using known amounts of ^{4}He reference gas standards and ^{3}He spike, or by peak height comparison to the ^{4}He reference gas standards measured before and after analysis. The ^{4}He and ^{3}He reference aliquots are, directly or indirectly, calibrated against absolute pressure and volume measurements made on standard purified gases using techniques such as capacitance manometry. Most labs monitor results by dating aliquots of a mineral standard (e.g., Durango apatite; see section 7.4) to be sure

that tank depletion calculations and original volume determinations are correct. Gases evolved from samples are purified using alloy-metal getters and/or a temperature-cycled cryogenic cold trap and then measured using either a quadrupole or magnetic-sector noble gas mass spectrometer. Typically, this process is repeated at least twice for each crystal to ensure complete gas extraction, and the second and additional treatments are usually referred to as "re-extracts." Line blanks, ^{4}He/^{3}He and/or ^{4}He reference standards, metal packet blanks (a.k.a. "hot blanks"), and secondary mineral age standards are typically analyzed with each batch of unknowns. The hot blanks are used for background correction of the measured He signal.

5.5. Crystal Dissolution and U-Th-Sm Measurement

The final step of data acquisition is to determine the absolute amount of the parent (U, Th, and in some cases Sm) in the crystal. This is commonly done by isotope dilution (e.g., Evans et al., 2005b). The degassed samples are removed from the ultra-high vacuum line, spiked with artificially isotopically enriched U and Th (e.g., ^{233}U, ^{235}U, or ^{236}U, ^{229}Th, or ^{230}Th) and potentially other isotopic tracers (e.g., ^{145}Nd, ^{42}Ca, and ^{90}Zr), and dissolved in acid (typically while still in the metal packets). Apatite crystals are dissolved with diluted HNO_3 at temperatures of <100 °C for several minutes to hours. Refractory minerals such as zircon and titanite require more aggressive, multi-day, acid-vapor dissolution techniques involving sequential HF and HCl dissolution steps in high-pressure vessels at temperatures >180 °C. The dissolved unknown and standard mineral solutions, reference solutions of known U and Th concentrations, and blanks are then measured for U-Th by quadrupole or sector-field ICP-MS. Sm is also analyzed in Sm-bearing minerals such as apatite and titanite. The amount of parent in each sample is determined by isotope dilution, and the blanks are used to correct for the background level of all measured isotopes in the samples. Typically, the amount of ^{235}U in the sample is calculated from the measured ^{238}U assuming the ^{238}U/^{235}U value of 137.818 (Hiess et al., 2012). Ca or Zr may additionally be analyzed in apatite or zircon either by Ca or Zr isotope dilution or by standard peak height calibrations to enable stoichiometric estimates of the crystal mass (Guenthner et al., 2016).

5.6. Data Reduction and Interpretation

After data acquisition, data reduction occurs as outlined in the next section. Analyses are

generally screened to ensure that all grains are of sufficient size (typically >0.5 F_T value) and have measured daughter and parent amounts high enough above blank values to be considered reliable (which depends on the stability and characterization of the lab's blank values). These steps are typically followed by the construction of data plots, development of first-order interpretations based on data patterns and geologic context, thermal history modeling, and geologic interpretation (see companion paper, Flowers et al., 2022).

5.7. Sample Information and Method Reporting (Checklist in Table 1)

Basic sample information, along with essential methods, should be referenced appropriately or reported in the main text, supplementary materials, or data tables.

Sample information includes the geographic coordinates in a specified geodetic datum (latitude, longitude, elevation, borehole depth), lithology, type of sample (e.g., in situ sample, loose rock, or river sand), geologic context, formation name/stratigraphy, and any additional geochronologic and thermochronologic data available for the sample.

Methods include those associated with each step of the process following sample collection. Methods either should be described or an appropriate reference cited. Mineral separation procedures include the type of rock disaggregation (e.g., standard crushing and grinding, SelFrag), water table, heavy liquids, drying temperature, and magnetic separation, as well as any pre-concentration techniques for detrital samples or chemical cleaning procedures. Mineral selection procedures include the method (microscopy and magnification used, any additional tools) and the criteria used for crystal selection (e.g., size, morphology, clarity, color, lack of mineral and fluid inclusions, etc.). Analytical procedures include the methods for He measurements (e.g., instrumentation, laser or furnace heating, type of He analysis), the methods for crystal dissolution and U, Th, and Sm measurements (e.g., dissolution protocol, instrumentation used, type of analysis), the mineral standards used for quality control, as well as the lab(s) where the data were acquired.

6. INDIVIDUAL ALIQUOT (U-Th)/He DATING: DATA AND REPORTING

6.1. Overview

(U-Th)/He results consist of primary measured data as well as a set of data derivatives

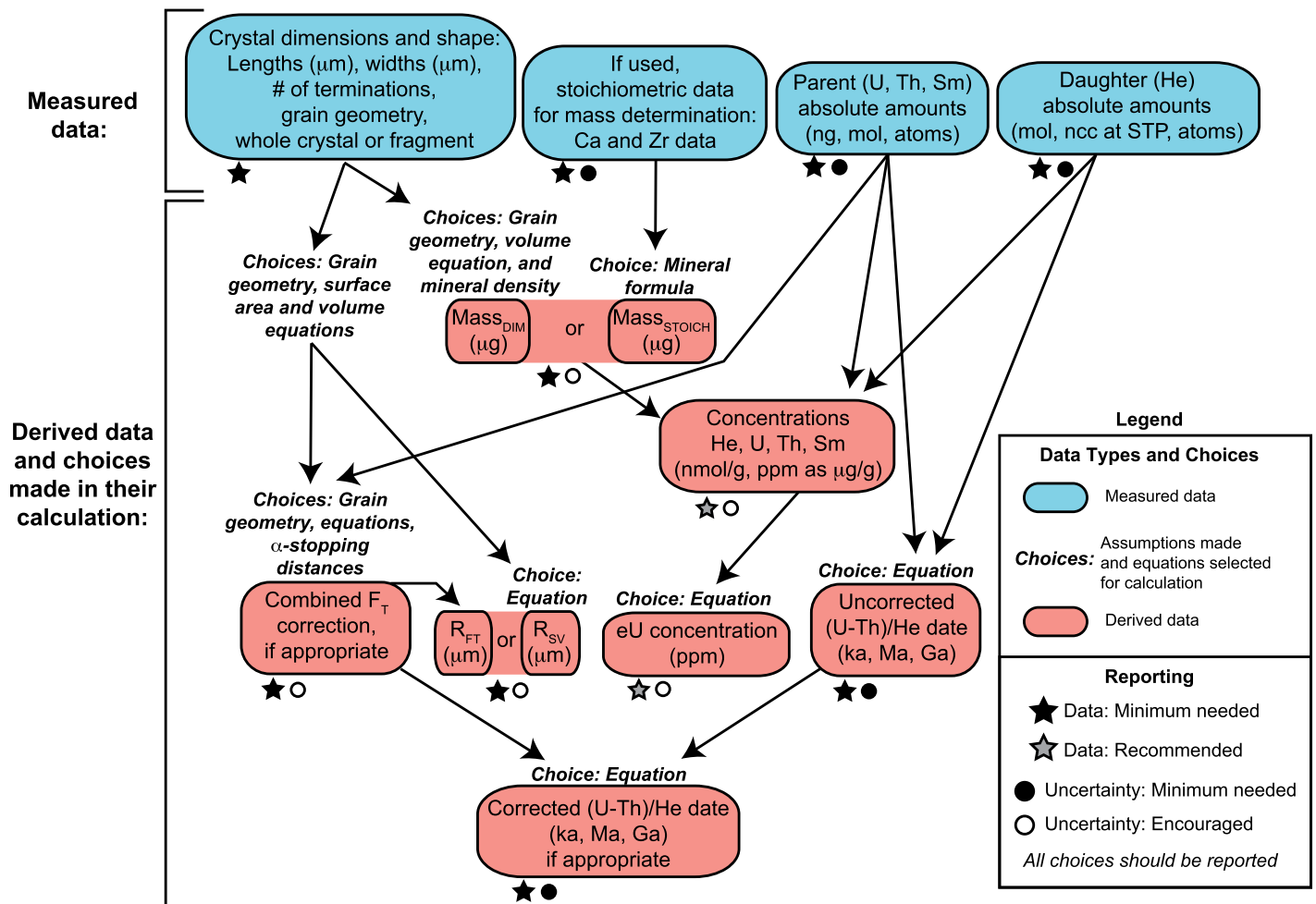## Data reduction and reporting for individual aliquot (U-Th)/He data

Figure 8. Flow chart for individual conventional (U-Th)/He analyses illustrates the path from measured data (blue) to derived data (pink) and the associated choices made during the data reduction (black italics). The minimum needed, recommended, and encouraged reporting for data and uncertainties are marked as noted in legend. For all derived data that are reported, assumptions and methods associated with their calculation should be noted or references cited. For all uncertainties, report them in same unit as data, state what factors are included in uncertainty calculation, and if given at 1σ or 2σ. Sample information and experimental methods also are minimum needed data that should be reported or references given. See reporting table checklists in Tables 1–2 for complete details. See Table 3 for an example of a reporting table that includes all minimum needed and recommended information. Mass$_{DIM}$—mass calculated from measured grain dimensions. Mass$_{STOICH}$—mass calculated using stoichiometric approach.

calculated from the measured data that require various choices (e.g., equation used) and/or assumptions (e.g., assumed grain geometry). Figure 8 depicts the data reduction path, from the measured data (blue labels) to the derived data (red labels), with the choices required for derived data computation (black italicized text). We first summarize the key measured data (section 6.2) and then explain the seven main types of derived data and how they are calculated (section 6.3). We conclude with a set of recommendations for reporting information and data associated with individual (U-Th)/He analyses (Tables 2–3; section 6.4).

Uncertainty reporting for individual aliquots is discussed in section 7.

6.2. Primary Measured Data

The primary measured data consist of the (1) crystal dimension and, in some cases, stoichiometric data; (2) daughter (He) absolute amounts; and (3) parent (U, Th, and in some cases Sm) absolute amounts. These data are generated by the three main laboratory steps associated with conventional (U-Th)/He analyses described in the previous section.

The crystal dimension information includes the length, widths (if both widths are measured, with the second termed either the "second width" or the "height"), number of terminations, grain geometry (e.g., hexagonal prism, tetrahedral prism, ellipsoid), and whether the grain is a whole crystal or a fragment. This information is used to calculate the F_T correction, the equivalent spherical radius, and the crystal mass, which in turn are used to compute parent and daughter concentrations, eU concentration, and the corrected (U-Th)/He date. If crystal mass is estimated stoichiometrically from Ca and Zr data rather than from the crystal dimension information, the

TABLE 2. CHECKLIST OF DATA, UNCERTAINTIES, AND ASSOCIATED INFORMATION TO REPORT FOR INDIVIDUAL (U-Th)/He ANALYSES

Minimum Needed Reporting
<u>Crystal dimensions and shape if 2-D microscopy measurements were used</u>
- ☐ Crystal length and width(s) (typically in μm)
- ☐ Number of grain terminations
- ☐ Grain geometry (e.g., hexagonal prism, tetrahedral prism, ellipsoid)
- ☐ Whole crystal or fragment

<u>Daughter and parent absolute amounts</u>
- ☐ He absolute amount (mol, ncc at standard temperature and pressure, or atoms; mol is preferred as an SI unit).
- ☐ U and Th absolute amounts (ng, mol, or atoms). Sm absolute amount (ng, mol, or atoms) for minerals with sufficient Sm to affect the date, typically apatite and titanite, but not zircon.

<u>Derived data</u>
- ☐ Combined F_T value in cases considered appropriate to use an F_T correction.
  - - If reported, explain assumptions and methods associated with its calculation (or provide reference), including assumed grain geometry, equations used, isotope-specific alpha-stopping distances, assumptions regarding parent isotope zonation (or lack thereof).
  - - For broken or abraded crystals, state any assumptions made regarding ejection across broken or rounded surfaces.
  - - If not reported, explain why an F_T correction is considered inappropriate. For example, no F_T value should be reported for fragments without an ejection-depleted rim.
- ☐ Equivalent spherical radius (μm), whether SV-equivalent sphere (R_{SV}) or F_T-equivalent sphere (R_{FT}), and equations used.
- ☐ Crystal mass (μg) and how calculated.
  - - For dimensional mass approach, report grain geometry, volume equations used, mineral density assumptions, and any additional corrections made.
  - - For stoichiometric approach, report assumed chemical formula (e.g., for apatite, $Ca_5(PO_4)_3(OH)$, $Ca_5(PO_4)_3F$, or $Ca_5(PO_4)_3Cl$) and associated Ca and Zr data.
- ☐ Uncorrected (U-Th)/He date (in most appropriate unit, e.g., ka, Ma, Ga) and method used.
- ☐ Corrected (U-Th)/He date in cases considered appropriate to use an F_T correction. If reported, give method used. No corrected (U-Th)/He date should be reported for fragments without an ejection-depleted rim.

<u>Uncertainties*</u>
- ☐ Uncertainties in daughter and parent absolute amounts, what factors are included in the uncertainty calculation (e.g., propagated precision from repeat measurements of the sample, blanks, spikes, and reference standards), and if reported as the standard error or standard deviation.
- ☐ Total analytical uncertainty[†] on uncorrected (U-Th)/He date.
- ☐ Total analytical uncertainty[†] on corrected (U-Th)/He date in cases considered appropriate to use an F_T correction and report a corrected date.

Recommended Reporting
<u>Concentrations</u>
- ☐ Daughter (He) concentration (nmol/g).
- ☐ U and Th concentrations (ppm calculated as μg/g)[§]. Sm concentration if Sm absolute amount is reported (see above).
- ☐ eU concentration (ppm calculated as μg/g)[§] and equation used.

<u>Uncertainties*</u>
- ☐ Second level of uncertainty on the corrected (U-Th)/He date that includes both the total analytical uncertainty and an estimated uncertainty associated with the F_T correction; explain how the uncertainty on the FT correction is estimated (e.g., by propagating an estimated uncertainty on the F_T value, or approximating the uncertainty based on the reproducibility of alpha-ejected mineral standards).

<u>Secondary mineral standards</u>
- ☐ Secondary mineral standard averages (e.g., Durango apatite, FCT zircon) over a time frame appropriate for the analyzed samples, number of analyses included in the average, their reproducibility, and how the reproducibility is reported (e.g., standard error or standard deviation, 1σ or 2σ).
  - - Reporting the full details of the individual mineral standard analyses in a manner consistent with reporting of the individual sample analyses is encouraged.

Encouraged Reporting (especially as the methods to quantify these improve)
<u>Uncertainties*</u>
- ☐ Uncertainty on the combined F_T and/or isotope-specific F_T values, what factors are included in uncertainty calculation, and how determined.
- ☐ Uncertainty on equivalent spherical radius, what factors are included in uncertainty calculation, and how determined.
- ☐ Uncertainty on mass, what factors are included in uncertainty calculation, and how determined.
- ☐ Uncertainties on daughter and parent concentrations, what factors are included in uncertainty calculation, and how determined.
- ☐ Uncertainty on eU concentration, what factors are included in uncertainty calculation, and how determined.

*For all uncertainties, report in same unit as data and state if given at 1σ or 2σ.
[†]Total analytical uncertainty: includes the propagated uncertainties on the parent and daughter absolute amounts.
[§]Reporting as μg/g is recommended for SI units (Thompson and Taylor, 2008), because it is less ambiguous than ppm in clearly referring to a mass ratio (rather than an atomic or other ratio).

relevant Ca and Zr isotopic data also comprise primary measured data.

The absolute amount of daughter (He) is required to calculate He concentrations as well as uncorrected and corrected dates. The absolute amounts of parent (U, Th, and in some cases Sm) are required to calculate the F_T factor, parent and eU concentrations, and uncorrected and corrected (U-Th)/He dates. Sm is measured for minerals with sufficient Sm to affect the date (typically apatite and titanite, but not zircon).

6.3. Derived Data and How They Are Calculated

The seven main types of derived data are: (1) F_T values, (2) equivalent spherical radius, (3) mass, (4) daughter and parent concentrations, (5) eU concentration, (6) uncorrected (U-Th)/He date, and (7) corrected (U-Th)/He date (corrected for F_T).

6.3.1. F_T Values

F_T is the proportion of He retained after loss due to ejection from a grain or crystal, such that higher F_T values indicate smaller corrections (section 2.3). For example, an F_T value of 1.00 would indicate that no He had been ejected, whereas a value of 0.75 indicates 25% loss by ejection. Because alpha-stopping distances differ depending on the parent isotope, isotope-specific F_T values are computed. These calculations require: (1) surface area and volume estimates of the grain analyzed, (2) selection of grain geometry and associated F_T equations, (3) mean ^{4}He atom-stopping distances specific to the mineral dated and each parent isotope, (4) assumption/knowledge of parent isotope distribution, and (5) for broken or abraded crystals, assumption/knowledge regarding the timing of breakage or rounding. Computation of a combined F_T value additionally requires the ratio of parent isotopes.

Calculations of crystal surface area and volume use the crystal geometric information, which include the length, widths, and number of terminations of the analyzed grain, as well as a choice regarding the geometry that best approximates the crystal analyzed. For example, a hexagonal prism for apatite and a tetrahedral prism for zircon are commonly used. Surface area and

TABLE 3. EXAMPLE OF A REPORTING TABLE FOR INDIVIDUAL ALIQUOT (U-Th)/He RESULTS THAT INCLUDES ALL "MINIMUM NEEDED" AND "RECOMMENDED" DATA, UNCERTAINTIES, AND ASSOCIATED INFORMATION

Sample name and aliquot[a]	length 1 (µm)[b]	width 1 (µm)[b]	length 2 (µm)[c]	width 2 (µm)[c]	Geo-metry[d]	Np[e]	^{4}He (fmol)[f]	±[g]	U (ng)[i]	±[g]	Th (ng)[i]	±[g]	^{147}Sm (ng)[j]	±[g]	^{4}He (nmol/g)[m]	Mass (µg)[l]	Rs (µm)[k]	U (ppm)[m]	±[n]	Th (ppm)[m]	±[n]	Sm (ppm)[m]	±[n]	eU (ppm)[o]	±[p]	Uncorr date (Ma)[q]	±[p]	Uncorr date analytical ±(Ma) 2σ[r]	F_T comb[s]	Corrected date (Ma)[t]	±TAU (Ma) 2σ[u]	±F_T (Ma) 2σ[v]	±TAU +F_T (Ma) 2σ[v,w]
Sample A																																	
a01	197	133	210	117	4	4	4.92	0.05	0.037	0.002	0.024	0.002	0.038	0.002	1.15	4.3	63	8.7	0.5	5.5	0.5	59	3	10.1	1.5	21.1	1.1	1.1	0.77	27.3	1.5	1.5	1.9
a02	185	132	140	125	4	2	3.24	0.03	0.024	0.001	0.019	0.001	0.049	0.003	1.05	3.1	59	7.8	0.4	6.1	0.8	59	3	9.4	1.4	20.7	1.0	1.0	0.75	27.3	1.4	1.4	1.8
a03	231	125	234	93	4	2	5.83	0.12	0.039	0.001	0.033	0.001	0.056	0.003	1.52	3.8	56	10.3	0.2	8.6	0.8	98	2	12.4	1.9	22.7	0.7	0.7	0.74	30.5	0.9	0.9	1.5
a04	164	151	150	91	4	2	4.29	0.09	0.024	0.001	0.026	0.001	0.072	0.002	2.04	2.1	49	11.3	0.4	12.3	1.2	228	5	14	1.2	26.1	0.9	0.9	0.71	36.7	1.3	1.3	2.0
a05	140	107	112	103	4	1	4.24	0.13	0.020	0.001	0.022	0.001	0.020	0.002	1.83	2.3	51	8.7	0.3	9.4	0.8	163	5	11.1	1.7	30.4	1.3	1.3	0.72	42.1	1.8	1.8	2.4

Notes: This table is an example of the types of information that should be reported. However, the methods used for calculations, and the manner in which uncertainties are represented, need not follow exactly those used here. Reporting additional uncertainties is encouraged, as listed in Table 2 and described in the text. Additional sample information and methods should be reported in the paper, as listed in Table 1 and described in the text. In some cases it may be simpler to divide this table into two separate tables: one that contains derived data for the main text and one that contains primary measured data for the supplement. All significant figures reported in this table follow the recommendations of Taylor (1997). This table uses the common practice of expressing uncertainties as σ because σ is a statistical term with broad recognition. However, the use of s is strictly more appropriate than σ because s refers to the sample standard deviation while σ refers to the total population (which was not fully sampled here; e.g., Horstwood et al., 2016).

a—Sample and mineral being analyzed; a is apatite.
b—Length is measured parallel to the c-axis and includes pyramidal terminations. It is measured twice on two perpendicular sides.
c—Width 1 is measured perpendicular to the c-axis. Width 2 is measured perpendicular to both the c-axis and width 1.
d—Geometry is defined as described in Figure 3 of Ketcham et al. (2011). 1 is ellipsoid, 2 is cylinder, 3 is tetrahedral prism, and 4 is hexagonal prism. f is noted if the analyzed grain is a fragment, otherwise the analyzed grain is a whole crystal.
e—Np denotes the number of pyramidal terminations of the grain.
f—Blank-corrected ^{4}He.
g—Uncertainties on ^{4}He, U, Th, and Sm are reported as the 2σ standard error and include the propagated uncertainties on the measurements of the sample, blank, spike, and standard.
h—Total blank-corrected ng of ^{238}U and ^{236}U. Total ^{238}U is measured, and ^{235}U is calculated assuming ^{235}U = ^{238}U/137.818 after Hiess et al. (2012).
i—Total blank-corrected ng of ^{232}Th.
j—Total blank-corrected ng of ^{147}Sm. In some cases Sm may not be measured, for example in minerals like zircon with negligible Sm.
k—Rs is the radius of a sphere with an equivalent alpha-ejection correction as the grain, calculated using equation A6 in Cooperdock et al. (2019).
l—Mass is the mass of the crystal. Determined from the measured grain dimensions, the volume assuming the reported grain geometry, and the volume equations and mineral densities in Ketcham et al. (2011).
m—Concentration of each element (He, U, Th, and Sm) computed from the absolute amount of the measured isotopes (where ^{147}Sm is 0.15 of the total Sm reported here) and the estimated dimensional mass. In some cases, Sm may not be measured, for example in minerals like zircon with negligible Sm.
n—Uncertainties on U, Th, Sm, and He concentrations are reported at 2σ and include the propagated total analytical uncertainties (TAU).
o—eU is effective uranium concentration. Calculated as U + 0.238*Th + 0.0012*Sm after equation 9 in this paper and Appendix A of Cooperdock et al. (2019).
p—Uncertainty on eU is estimated at 15% of the eU value.
q—Uncorrected (U-Th)/He date is calculated iteratively using the ^{4}He production equation defined as equation 1 in Wolf et al. (1998) modified to include He produced from Sm decay and assuming secular equilibrium.
r—Uncertainty on the uncorrected (U-Th)/He date is reported at 2σ and includes the propagated total analytical uncertainties (TAU) on the U, Th, Sm, and He measurements.
s—The combined alpha-ejection correction for the crystal calculated from the parent isotope-specific F_T corrections, the proportion of U and Th contributing to ^{4}He production, and assuming homogeneous parent isotope distributions using equation A4 in Cooperdock et al. (2019). The parent isotope-specific alpha-ejection corrections were computed assuming the reported grain geometry in this table and the equations and alpha-stopping distances in Ketcham et al. (2011).
t—The corrected (U-Th)/He date is calculated iteratively using the absolute values of He, U, Th, and Sm, the isotope specific F_T corrections, and equation 34 in Ketcham et al. (2011) assuming secular equilibrium.
u—Uncertainty on the corrected (U-Th)/He date is reported at 2σ and includes the propagated total analytical uncertainties (TAU) on the U, Th, Sm, and He measurements. Uncertainty propagation done using HeCalc (Martin, 2021).
v—Uncertainty on the corrected (U-Th)/He date reported at 2σ and includes the propagated total analytical uncertainties (TAU) on the U, Th, Sm, and He measurements as well as an estimated uncertainty on the F_T correction that is estimated to be 5%. Uncertainty propagation done using HeCalc (Martin, 2021). The 5% uncertainty on the F_T value is a conservative estimate and may be lower for grains with shapes highly similar to the hexagonal prism geometry assumed in determination of the F_T correction here (Cooperdock et al., 2019; Zeigler et al., 2021).
w—Durango apatite fragments run in conjunction with these analyses yield an unweighted mean and 2σ standard error of 31.1 ± 0.6 Ma (n = 9). Durango is dated at 31.44 ± 0.18 Ma (2σ) based on ^{40}Ar/^{39}Ar analysis of associated ignimbrites (McDowell et al., 2005).

volume equations for a suite of common geometries are in Ketcham et al. (2011).

Isotope-specific F_T parameters are calculated from the mean He atom-stopping distances for each isotope decay chain for the mineral dated and equations based on grain geometry that use the crystal volume and surface area estimates. A combined F_T value for the crystal can then be determined from the isotope-specific F_T values and the proportion of each parent contributing to He production. The initial treatment of F_T corrections was presented in Farley et al. (1996) and followed by refinements in a series of papers (e.g., Farley, 2002; Farley and Stockli, 2002; Hourigan et al., 2005; Herman et al., 2007; Gautheron and Tassan-Got, 2010; Cooperdock et al., 2019). Ketcham et al. (2011) presents the most generalized approach, with polynomial corrections that incorporate the stopping distances explicitly in the formula for a variety of crystal morphologies. Alternatively, 3-D data from X-ray micro-computed tomography can be used to calculate F_T corrections using Monte Carlo methods (Herman et al., 2007; Cooperdock et al., 2019; Glotzbach et al., 2019).

Unless noted differently, F_T values are typically computed assuming a homogeneous parent isotope distribution (i.e., no zonation). F_T values also generally assume that the modern grain geometry existed for the entire life of the crystal, unless different assumptions are made for detrital grains that were abraded during transport (see companion paper, Flowers et al., 2022). Grains that were mounted and polished to enable other analyses prior to (U-Th)/He dating are typically assumed to have been ground halfway through, in which case the F_T correction is the same as for their unmounted counterparts (Reiners et al., 2007, 2018; Marsden et al., 2021b), although different polishing depths would yield somewhat different F_T values owing to the removal of differing proportions of the alpha-depleted grain exterior.

6.3.2. Equivalent Spherical Radius

The equivalent spherical radius is a standard geometric parameter used in diffusion modeling and thermal history inversions of (U-Th)/He data. A spherical geometry is more efficient for He diffusion modeling than other more realistic grain geometries, and it has been demonstrated to closely approximate He diffusion in a variety of shapes (e.g., Meesters and Dunai, 2002a, 2002b; Ketcham, 2005; Dunai, 2005).

The equivalent spherical radius is typically computed in one of two ways. It has been most commonly reported as the radius of a sphere with a surface-area-to-volume ratio equivalent to that of the grain analyzed, referred to here as the SV-equivalent sphere or R_{SV} (also referred

to in the literature as RS or ESR). However, an alternative and arguably better approach is to report the radius of a sphere with an equivalent F_T-correction as the analyzed grain, referred to here as the F_T-equivalent sphere or R_{FT} (Ketcham et al., 2011; equation A6 in Cooperdock et al., 2019). For some grain geometries, R_{SV} and R_{FT} values are not identical, and the use of the latter in diffusion modeling yields solutions closer to those using the real 3-D grain shapes (Ketcham et al., 2011).

6.3.3. Mass

Crystal mass is typically derived from the geometric data by using the estimated volume and an assumed mineral density. The assumed mineral density is important, because in the case of zircon the density is not constant but drops by up to 16% with increasing radiation damage (e.g., Holland and Gottfried, 1955), which can affect the eU concentration estimated for zircon crystals (section 6.3.5). An alternative or complementary approach is to determine the abundance of a stoichiometric element in the mineral (e.g., Ca for apatite and Zr for zircon) by either isotope dilution or external calibration and then assume the mineral's stoichiometry to convert that abundance to grain mass (Guenthner et al., 2016). This method circumvents the need to assume a mineral density. Using both the dimensional and stoichiometric approaches allows one to compare the estimated masses and diagnose potential problems with the aliquot (e.g., the analyzed grain was not apatite).

6.3.4. Daughter (He) and Parent (U, Th, and in Some Cases Sm) Concentrations

Daughter (He) and parent (U, Th, and in some cases Sm) concentrations are calculated from the daughter and parent absolute amounts and the grain or aliquot mass estimate. Concentrations are not required for the calculation of conventional individual aliquot (U-Th)/He dates because parent and daughter measurements are usually made on the same aliquot. However, concentrations can be useful because anomalous values may indicate other potential complications (e.g., inclusions). In addition, because of the effect of radiation damage on apatite and zircon He retentivity, parent isotope concentrations are standard parameters required for He diffusion modeling and for calculation of eU (see next section).

6.3.5. eU Concentration

eU concentration is a parameter that weights the decay of the parent isotopes for their ^{4}He productivity and is computed from the parent concentrations. eU is commonly plotted versus (U-Th)/He date because eU is a useful proxy for radiation damage in a mineral suite that underwent the same thermal history (see section 3.3 for caveats). This assumes that the damage associated with alpha decay exerts a primary control on He retentivity, rather than only damage from fission of uranium (because Th does not generate fission tracks). The concept of parent isotope ^{4}He productivity was used by Wernicke and Lippolt (1993) in the generation of isochron plots, where it was calculated as U (ppm) + 0.23 * Th (ppm). Effective U concentration (eU) was later introduced in the context of apatite (U-Th)/He dating by Shuster et al. (2006), where the fraction of ^{4}He produced by Th was defined as 0.235.

Here we suggest a slightly refined eU equation, the same as that in Appendix A of Cooperdock et al. (2019). We first calculate the modern productivity of each isotope (α_{238}, α_{235}, α_{232}, and α_{147}) in alphas per year per gram of element:

$$\alpha_{238} = \frac{8 * \lambda_{238} * A * (0.9928)}{238.029} \tag{2}$$

$$\alpha_{235} = \frac{7 * \lambda_{235} * A * (0.0072)}{238.029} \tag{3}$$

$$\alpha_{232} = \frac{6 * \lambda_{232} * A}{232.039} \tag{4}$$

$$\alpha_{147} = \frac{\lambda_{147} * A * (0.1499)}{150.360} \tag{5}$$

where λ_{238}, λ_{235}, λ_{232}, and λ_{147} are the decay constants of the parent nuclides and A is Avogadro's number. We compute the productivity in grams rather than moles, because eU is a concentration, which here is based on mass. We can then calculate the fraction of ^{4}He generated by Th relative to that generated by U as:

$$f_{Th} = \frac{\alpha_{232}}{\alpha_{238+}\alpha_{235}} = 0.238 \tag{6}$$

We can similarly calculate the fraction of ^{4}He generated by Sm relative to U as:

$$f_{Sm} = \frac{\alpha_{147}}{\alpha_{238+}\alpha_{235}} = 0.0012 \tag{7}$$

Using the modern productivity of the parent isotopes as described above yields the following equation for eU:

$$eU = U + (0.238 * Th) + (0.0012 * Sm) \tag{8}$$

where U, Th, and Sm are the concentration of each element in ppm (presuming total Sm; if ^{147}Sm is used, then the 0.1499 in Equation (5) is omitted, and the 0.0012 factor in Equation (9) becomes 0.0083). In many cases, the contribution of Sm to eU is negligible and can be reasonably neglected owing both to its low He productivity and its low abundance in most minerals dated by the (U-Th)/He technique. In reality, the fractional contribution of each isotope to the total alpha productivity is time-dependent, and thus eU is time-dependent, mostly because of the changing abundance of ^{235}U over long timescales. However, it is reasonable to employ the modern productivity approximation for computing eU, especially when the primary function of eU is as a general radiation damage proxy.

6.3.6. Uncorrected (U-Th)/He Date

The uncorrected or raw (U-Th)/He date is calculated from the absolute parent and daughter amounts without accounting for ^{4}He potentially lost from the crystal owing to α-ejection. The most rigorous approach is to calculate the date iteratively using the age equation (Equation 1), which assumes secular equilibrium (appropriate for dates >1 Ma; equations that accommodate secular disequilibrium must be used for younger materials; Farley et al., 2002; Schmitt et al., 2006, 2010). A noniterative analytical approach using a crystal's weighted mean He production rate was proposed by Meesters and Dunai (2005). This approximation is reasonable for dates as old as a few hundred million years but deviates increasingly from the iterative solution with older age. The main advantage of this algorithm is improved computational efficiency for use in 3-D, thermo-kinematic, landscape evolution modeling.

6.3.7. Corrected (U-Th)/He Date

The corrected (U-Th)/He date accounts for the ^{4}He lost from the crystal by ejection. The F_T parameters are used in this calculation. Two approximations have been proposed for calculating the corrected date: simply dividing the uncorrected date by the combined F_T (Farley et al., 1996) or dividing the measured ^{4}He by the combined F_T and using the corrected ^{4}He in the age equation (Min et al., 2003). Over long timescales, however, these approximations underestimate the corrected date to varying degrees (Ketcham et al., 2011).

The most rigorous approach is to incorporate the parent isotope-specific F_T corrections into the age equation and calculate the corrected date iteratively, as in Ketcham et al. (2011):

$$\begin{aligned}
^4\text{He} = &\ 8 * F_{T,238} *^{238}\text{U}(e^{\lambda_{238}t} - 1) \\
&+ 7 * F_{T,235} *^{235}\text{U}(e^{\lambda_{235}t} - 1) \\
&+ 6 * F_{T,232} *^{232}\text{Th}(e^{\lambda_{232}t} - 1) \\
&+ F_{T,147} *^{147}\text{Sm}(e^{\lambda_{147}t} - 1)
\end{aligned} \tag{9}$$

For fragments that lack an ejection-depleted rim, no F_T correction should be applied, and therefore no corrected date should be reported.

6.4. Summary of Data Reporting for Individual Aliquots (Checklist in Table 2; Example Reporting in Table 3)

This section summarizes good practices for reporting key primary measured and derived data and how derived data were calculated. The overarching goal is that sufficient information be reported so that one can move vertically (both up and down) through the data reduction path in Figure 8 and reproduce all values. Table 2 is a reporting checklist that summarizes these recommendations. Table 3 is an example table that accomplishes the reporting recommendations, although the methods used for the calculations, and the manner in which uncertainties are represented, need not follow exactly those used there. The checklist divides the data reporting into "minimum needed" and "recommended" categories. Given the amount of information, in some cases it may be effective to include the key derived data in a table in the main text and additional data in a separate supplementary data table.

How to appropriately report uncertainties for individual analyses is an important topic discussed separately in the next section. Considerations for when it is appropriate to combine multiple individual analyses from a single sample into a mean sample date is covered in the companion paper (Flowers et al., 2022).

6.4.1. Minimum Needed Reporting

Minimum needed data include the primary measured results that are needed to reproduce derived values. The core objective of reporting the measured data is to allow them to be reduced again in the future, which is important for the longer-term development of the technique as new discoveries about systematics are made and new statistical treatments are developed. The data measured thus also constitute the basic information necessary for inclusion in any database of (U-Th)/He data.

In addition, as described more fully below, five main types of derived data should be reported (combined F_T value, equivalent spherical radius, crystal mass, uncorrected date, and corrected date if considered appropriate). The various choices (e.g., grain geometry calculation methods) made to compute the derived from the measured data should also be described. The rationale for reporting the derived data is that they are in a user-friendly format that is accessible to the broader Earth science community, are most readily used for data interpretation and thermal history modeling, and allow others to reproduce data plots and tT simulations efficiently without risk of mistake during data re-recalculation.

Crystal dimension and stoichiometric (if acquired) data. Reported crystal dimension data should include the length and width(s) (typically in μm), the number of terminations, grain shape (e.g., hexagonal prism, tetrahedral prism, ellipsoid), and whether the grain is a whole crystal or a fragment. The goal is to report all of the measurement data needed for volume and surface area estimates and therefore for calculation of F_T values, equivalent spherical radius, mass, concentrations, and corrected (U-Th)/He date. If crystal mass is estimated stoichiometrically from Ca and Zr data rather than from the crystal dimensions, then these isotopic data should also be reported.

Daughter (He) absolute amount. For each aliquot, the absolute amount of ^{4}He should be reported, generally in nmol, ncc at standard temperature and pressure (STP), or atoms.

Parent (U, Th, and in some cases Sm) absolute amounts. For each aliquot, the absolute amounts of U (^{238}U + ^{235}U), ^{232}Th, and ^{147}Sm (if enough Sm is present in the mineral to merit measurement) should be reported, typically in ng, mol, or atoms.

F_T values. In cases considered appropriate to use an F_T correction, report the combined F_T value, and report or provide references for the assumptions and methodology associated with its calculation. The latter include the assumed grain geometry and equations used, the isotope-specific α-stopping distances, assumptions regarding parent isotope zonation (or lack thereof), and for broken or abraded crystals, any assumptions made regarding ejection across broken or rounded surfaces. If no F_T value is reported, explain why an F_T correction is considered inappropriate. For example, for fragments without an ejection-depleted rim, no F_T value should be reported.

Equivalent spherical radius. Report an equivalent spherical radius (typically in μm), specify whether it is R_{SV} or R_{FT}, and state equations used. We favor R_{FT} because it better approximates the true grain geometry in diffusion modeling.

Mass. Report the crystal mass (typically in μg) and how it was calculated. For the dimensional mass approach, report the grain geometry, equations used, mineral density assumptions, and any additional corrections made (in some cases the calculated dimensional mass substantially overestimates the actual mass; see section 7.3.2). For the stoichiometric approach, report the assumed chemical formula (e.g., for apatite, $Ca_5(PO_4)_3(OH)$ or $Ca_5(PO_4)_3F$ or $Ca_5(PO_4)_3Cl$).

Uncorrected (U-Th)/He date. Report the uncorrected date in the most appropriate unit (e.g., ka, Ma, or Ga) and the method used in its computation. We favor use of the more rigorous iterative calculation.

Corrected (U-Th)/He date. In cases considered appropriate for reporting a corrected date, report the corrected date in the most appropriate unit (e.g., ka, Ma, or Ga) along with details of the calculation method. We favor use of Equation 9, the more rigorous iterative calculation that includes the parent isotope-specific F_T values. For fragments that lack an ejection-depleted rim, no ejection-corrected date should be reported.

6.4.2. Recommended Reporting

Concentrations. We recommend reporting daughter (He), parent (U, Th, and in some cases Sm), and eU concentrations, and the equation used to calculate eU. Concentrations are not used in the date calculation. However, eU values are important for thermal history modeling and for constructing date-eU plots that enable evaluation of the potential influence of radiation damage-induced differences in He retentivity on the data (see companion paper, Flowers et al., 2022). He concentrations are typically reported in nmol/g. Parent and eU concentrations are best reported as ppm calculated as μg/g, in accordance with SI unit recommendations (Thompson and Taylor, 2008).

7. INDIVIDUAL ALIQUOT (U-Th)/He DATING: UNCERTAINTIES AND REPORTING

7.1. Overview

There is currently no universally adopted approach for estimating, propagating, and reporting uncertainties associated with individual aliquot (U-Th)/He data. Some labs report uncertainties in (U-Th)/He dates that propagate the analytical uncertainties on the parent and daughter measurements. A few additionally propagate an estimated uncertainty on the F_T correction. Still others report a uniform uncertainty of the individual dates (commonly 10%) based on the reproducibility of standards such as Fish Canyon Tuff zircon, which is considered to be representative of unknowns. Many early published data sets lacked any reported uncertainty, owing to the challenges of thoroughly characterizing uncertainty contributions to the results.

More comprehensively quantifying and propagating uncertainties associated with (U-Th)/He data, and establishing more uniform protocols for uncertainty reporting, will facilitate comparison of different data sets and increase confidence that interpreted similarities and differences in data are real. In turn, this will contribute to improved scientific interpretations. Here we focus on the sources of uncertainty associated with individual aliquot data. The additional complexity of when and how to integrate and report the

date and uncertainty for multiple aliquots from the same sample is discussed in the companion paper (Flowers et al., 2022).

We use the terms "uncertainty" and "error" in the context of precision and accuracy, respectively. The latter terms are used in the conventional sense, where precision refers to the reproducibility of repeat measurements (e.g., of repeated sample He measurements) and accuracy refers to the closeness to the true value (e.g., of the measured He amount to the true He amount). Thus, in the context of precision, the "uncertainty" represents a confidence interval around the measured value such that any repeat measurement will yield a result within this interval. In the context of accuracy, the "error" refers to the deviation between the measured value and the "true" value. This terminology follows that in the International Vocabulary of Metrology (JCGM, 2012).

Sources of uncertainty on individual aliquot data can be subdivided into three main types: (1) analytical uncertainties, (2) geometric uncertainties, and (3) unquantifiable or unmeasured uncertainties. In general, analytical uncertainties are well quantified (we know exactly how well we know this number). Geometric uncertainties are currently less well quantified (we do not know how well we know this number), but there are paths forward to quantify these uncertainties better. Sources of uncertainty that are not regularly quantified or are difficult or impossible to quantify, such as parent isotope zonation and He implantation (see companion paper, Flowers et al., 2022), are not included in the propagated uncertainties on (U-Th)/He data. Uncertainties on decay constants are generally ignored because their contribution relative to other factors is trivial.

Here, we first discuss uncertainties associated with analytical and geometric measurements (sections 7.2 and 7.3) and then describe the most commonly used natural mineral standards that are analyzed with each batch of unknowns (Tables 2–3; section 7.4). We conclude with recommendations for uncertainty reporting on individual aliquots (section 7.5).

7.2. Analytical Uncertainties on Daughter and Parent Absolute Amounts

The analytical uncertainties on the daughter and parent absolute amounts can be relatively well quantified. These include the reproducibility of repeated measurements on blanks, He reference standards, U-Th(-Sm) reference solutions, and the sample. Estimated analytical precisions for representative single-grain apatite and zircon analyses typically are 1%–3% for He measurements and 1%–2% for U, Th, and Sm

measurements (1σ), although they can be much higher for materials with very low amounts of daughter or parent (Reiners et al., 2018). When the uncertainties on these measured data are propagated, they typically contribute a few % to the uncertainty of the data derived from them (Fig. 8). For example, the analytical precision on (U-Th)/He dates not corrected for F_T for representative single-grain apatite and zircon analyses is typically <2%–6% (2σ) (Reiners et al., 2018). As discussed in the companion paper, however, this uncertainty is far lower than the intra-sample variation in dates observed for apatite and zircon from most samples (Flowers et al., 2022).

The absolute accuracy of the ^{4}He amount in the sample depends on accurate knowledge of the pipette volume that delivers the ^{4}He reference aliquot or the ^{3}He spike, and of the initial pressure and volume of the reference ^{4}He tank or ^{3}He spike tank, depending on the method. Similarly, the absolute accuracy of U, Th, and Sm depends on the accuracy of the reference standard solutions. The accuracy of both daughter and parent is additionally determined by appropriate corrections for isobars and outliers in mass spectra (if present) and matrix matching/similar behavior of samples, reference standards, and blanks.

7.3. Geometric Uncertainties

The uncertainties on the crystal geometric information are less well quantified because they are far more challenging to estimate than the analytical uncertainties. It may be possible to reasonably estimate the precision of absolute length and width measurements. However, conversion of these values to derived data requires a subjective evaluation of crystal shape compared to an idealized crystal geometry. It is difficult to quantify the uncertainty in how much the morphology of each dated grain deviates from that assumed, because this difference may vary substantially between grains depending on the analyzed and assumed geometries or surface roughness, and this uncertainty increases for crystals of small size (see also section 2.3). Dated grains are rarely characterized by idealized euhedral shapes owing to natural crystal irregularities, chipping, breakage, or rounding by abrasion during transport. This poorly constrained geometric uncertainty contributes to uncertainty in volume and surface area estimates, which are used to calculate the isotope-specific and combined F_T values, R_{SV} or R_{FT}, and the dimensional mass. F_T values are then used to compute the corrected (U-Th)/He date. Dimensional mass is typically used to calculate concentrations (Fig. 8).

7.3.1. F_T Value Uncertainty

The uncertainty and possible systematic error associated with F_T values are important because they contribute to uncertainty and possible inaccuracy in the corrected (U-Th)/He date. Several studies have estimated the uncertainty associated with F_T values, with most of the focus on apatite. For example, an early estimate of F_T uncertainty as a function of apatite crystal width for ideal hexagonal crystals suggested 2σ uncertainties of $\pm 2\%$ to $\pm 25\%$ for grain cross-sections of 125 μm to 50 μm, respectively (Ehlers and Farley, 2003). However, the degree to which these uncertainties are applicable to crystals with imperfect morphologies is unclear.

X-ray micro-computed tomography (CT) has been used in several studies to characterize the uncertainty and improve the accuracy of F_T factors. This tool measures X-ray attenuation, and thus density, of objects in 3-D, from which crystal volumes and surface areas can be determined. This technique was first used in a (U-Th)/He study to constrain F_T factors for detrital grains of irregular shape not easily approximated by idealized geometries (Herman et al., 2007). The first quantitative comparison of F_T values derived from 3-D CT data versus those from 2-D microscopy measurements concluded that, in the worst case, these differed by ~5% for apatite and zircon crystals >100 μm in width, with greater inconsistency for smaller grains (Evans et al., 2008). A similar comparison by Glotzbach et al. (2019) for apatite inferred 1%–7% differences between 3-D and 2-D results. This work also proposed an improved microscopy approach for estimating grain volumes, surface areas, and related information using a protocol involving a series of photomicrographs taken parallel and perpendicular to the c-axis to better reconstruct the 3-D grain shape than possible using only one or two 2-D grain images. This "3-D He approach" reduced the deviation from CT results to ~2.5%. A recent, comprehensive comparison of 3-D CT and 2-D microscopy data for high-quality apatite grains (N > 100) from two granitic samples concluded that the F_T values differed by ~2 $\pm$ 2% (~1.3% standard deviation for apatite with F_T >0.8 and 2.4%–2.7% deviation for smaller grains), which in turn introduced a deviation of 2 $\pm$ 2% to the corrected dates (Cooperdock et al., 2019). The better accuracy and precision of 2-D F_T values in this work than inferred by prior study may be due to the selection of grains with nearly ideal shapes for the comparative analysis.

Moving forward, there are several possible paths for improving the accuracy and precision of F_T values, and thereby better quantifying the uncertainties of the corrected (U-Th)/He dates derived from them. First, 3-D CT data could be

used to systematically characterize the accuracy and precision of 2-D microscopy F_T values as a function of size for apatite crystals that encompass the full range of routinely analyzed morphologies (Zeigler et al., 2021). These rule-of-thumb values could then be applied to correct 2-D microscopy F_T values for systematic bias, and the associated uncertainty could be propagated into the uncertainties on the derived parameters, without acquiring 3-D CT data for every grain dated (Zeigler et al., 2021). For example, for euhedral apatite crystals, the errors of Cooperdock et al. (2019) could be applied to correct for the ∼2% overestimate of 2-D F_T values, and the 1.3%–2.7% uncertainty on that correction (depending on crystal size) could be propagated. However, these values are inappropriate for apatite crystals with non-ideal shapes and for other minerals such as zircon that are characterized by different morphologies. Additional rule-of-thumb values should be determined for a wider range of shapes before this approach is applied broadly.

Alternatively, the accuracy and precision of F_T values could be improved directly by applying the 3-D He approach (Glotzbach et al., 2019) or CT study (e.g., Cooperdock et al., 2019) to all dated crystals. The 3-D He protocol can be implemented with the same microscope used for standard 2-D measurements, and while requiring more time, it does not involve additional analytical expense or access to more equipment. In contrast, the CT approach requires specialized instrumentation and greater analytical cost. While CT access is improving and bench-top systems are now available, whether the CT measurements can be accomplished with the right mix of resolution and scan speed to sufficiently improve F_T corrections to be worthwhile and affordable for routine (U-Th)/He analysis requires more exploration. In both the 3-D He and CT approaches, uncertainties on the F_T estimates still remain. In addition, unless U-Th zonation is characterized and accounted for in the F_T value, this will remain a source of uncertainty and error for F_T corrections (see also companion paper, Flowers et al., 2022).

7.3.2. Equivalent Spherical Radius, Mass, and Concentration Uncertainties

More limited work has been aimed at constraining the uncertainty and accuracy of equivalent spherical radius, mass, and concentration values. None of these parameters are used to derive the uncorrected or corrected (U-Th)/He date, so they do not affect the uncertainty or accuracy of the date. However, equivalent spherical radius and eU bear on the diffusional characteristics of the grain and therefore affect the certainty of thermal histories that are interpreted using these parameters.

One CT study addressed the uncertainty and accuracy of these values for high-quality apatite crystals (Cooperdock et al., 2019). This work estimated that 3-D CT versus 2-D microscopy values for equivalent spherical radius (both R_{SV} and R_{FT}) differed by ∼5 ± 5% for this apatite suite. It also found that the 2-D microscopy approach overestimated volumes and surface areas for apatite crystals with high-quality shapes by ∼20%, leading to an overestimate of mass by 23 ± 16% and an underestimate of eU by 31 ± 20% (Cooperdock et al., 2019). The authors attributed the higher uncertainties on mass and concentration values, relative to those on F_T and equivalent spherical radius, to the former relying on volume alone, whereas the latter use the surface area/volume ratio such that the volume and surface area overestimates cancel.

A similar magnitude of uncertainty on eU was estimated in a comparison of stoichiometric-derived and dimensional-derived parameters. This study suggested average percent differences of 15% and 25% between the two methods for apatite and zircon, respectively (Guenthner et al., 2016). In this work, the 2-D image approach both over- and under-estimated eU for apatite and systematically underestimated eU for zircon. In the case of zircon, an additional uncertainty is a decline in density by up to 16% with increasing radiation damage (Holland and Gottfried, 1955). The stoichiometric approach provides an alternative to the dimensional approach for volume estimates and thus can circumvent the uncertainties associated with crystal geometries and mineral density for the derived mass and concentration values (Guenthner et al., 2016). However, because the stoichiometric method does not constrain surface area, it alone cannot be used to derive F_T parameters and equivalent spherical radius values.

As is the case for F_T, there are several ways to improve the accuracy and precision of equivalent spherical radius, mass, and concentration estimates in the future. First, a CT study (like that described above for F_T) could systematically determine the accuracy and precision of 2-D values for grains with the full range of routinely analyzed shapes and sizes (Zeigler et al., 2021) as well as for morphologically different minerals like zircon. These values could then be used to routinely correct 2-D estimates for systematic error and to assign appropriate uncertainties without 3-D CT data acquisition, although mineral density will remain a lesser source of uncertainty for mass and therefore concentration values. Alternatively, the stoichiometric approach could be used for mass estimation. In this case, analytical uncertainties on the Ca and Zr measurements still exist, and the accuracy depends on the assumed stoichiometry of apatite

and zircon, which may vary owing to elemental substitutions.

7.4. Secondary Mineral Standard Reproducibility and Accuracy

Natural mineral standards are analyzed with each batch of samples as a quality check to verify a lab's reproducibility and accuracy on natural reference materials. Mineral standards with rapid cooling histories are preferred because fast cooling minimizes the date variation that can be introduced during slower cooling through diffusive loss of He or development of variable diffusion kinetics. Durango and Fish Canyon Tuff (FCT) are the most widely used apatite (e.g., Zeitler et al., 1987; Farley, 2000) and zircon (e.g., Dobson et al., 2008; Gleadow et al., 2015) standards, respectively. These materials are well understood and easily available.

Durango apatite is from a volcanic deposit in Mexico, is generally inclusion-free, and has limited zonation (e.g., Boyce and Hodges, 2005; Chew et al., 2016). It is dated at 31.44 ± 0.18 Ma (2σ) based on sanidine-anorthoclase $^{40}Ar/^{39}Ar$ dates on associated ignimbrites (e.g., McDowell et al., 2005). Centimeter-scale crystals of Durango apatite are available, such that fragments from the crystal interior are typically analyzed, which eliminates the need for an F_T correction. The primary shortcomings of Durango as a standard are its unusual composition and high Th/U ratio relative to most apatite crystals dated by (U-Th)/He. The reproducibility of Durango apatite, even without an F_T correction, is typically ∼6% (2σ) (e.g., Reiners et al., 2018).

The Fish Canyon Tuff (FCT) from the San Juan volcanic field in Colorado, USA, has been intensively studied and dated because it is also used as a standard in the U-Pb, $^{40}Ar/^{39}Ar$, and fission-track communities. FCT has been the subject of a series of high-precision $^{40}Ar/^{39}Ar$ and U-Pb dating studies, with a date of 28.201 ± 0.046 Ma yielded by $^{40}Ar/^{39}Ar$ sanidine analysis and astronomical tuning (Kuiper et al., 2008). Typical zircon crystals are <250 µm long and <150 µm wide, such that F_T corrections of up to 30% are required (e.g., Dobson et al., 2008). Compilations of zircon (U-Th)/He results for FCT yield combined values with 2σ population standard deviations of 28.3 ± 3.1 Ma (n = 127 from multiple labs; Dobson et al., 2008) and 28.16 ± 3.07 Ma (n = 165 from a single lab; Horne et al., 2016). The observed 10.9%–11.0% of dispersion in these compilations is at least partly attributable to the effects of variable U-Th zonation on the F_T correction (Dobson et al., 2008).

Some labs use or have proposed additional standards for apatite, zircon, titanite, and other

phases. These include zircon megacrysts from Penglai, Hainan Island, China (Li et al., 2017; Yu et al., 2020), Miocene apatite and titanite from the Limberg t3 tuff in Germany (Kraml et al., 2006), and quickly cooled Cretaceous titanite from Mount Dromedary, Australia (Reiners and Farley, 1999). Other standards have been used for monazite (Boyce et al., 2005), hematite (Lippolt et al., 1995; Wu et al., 2019), and fluorite (Evans et al., 2005a). There remains a strong need for more reference materials of differing age, type, and mineral phase that are well described and widely accessible (section 9).

7.5. Summary of Uncertainty Reporting for Individual Aliquots (Checklist in Table 2)

Good practices for uncertainty reporting are subdivided into "minimum needed," "recommended," and "encouraged" categories. For the last category, reporting these uncertainties is especially encouraged as the methods to estimate them improve. For all uncertainties, the units are typically the same as those for the relevant associated data. What factors are included in the uncertainty calculation and whether uncertainties are reported at 1σ or 2σ should be stated. The Table 2 checklist notes the uncertainties that should be reported, and Table 3 is an example data table that includes the minimum needed and recommended uncertainties.

7.5.1. Minimum Needed Reporting

Uncertainties on daughter (He) and parent (U, Th, and Sm) absolute amounts. Uncertainties should be reported along with the factors included in the uncertainty calculation (e.g., propagated precision on repeat measurements of the sample, blanks, spikes, and reference standards). For uncertainties on measured data, note whether they are reported as the standard deviation or standard error.

Total analytical uncertainty on uncorrected (U-Th)/He date. An uncertainty should be reported that includes the propagated uncertainties on the absolute amounts of daughter and parent.

Total analytical uncertainty on corrected (U-Th)/He date. An uncertainty should be reported that includes the propagated uncertainties on the absolute amounts of parent and daughter.

7.5.2. Recommended Reporting

Second level of uncertainty on corrected (U-Th)/He date. We recommend reporting a second level of uncertainty that includes both the total analytical uncertainty and an estimated uncertainty associated with the F_T correction and how it was calculated as our estimates of crystal geometric uncertainties improve. This approach of reporting multiple levels of uncertainty is analo-

gous to the recommended practice in both the high-precision isotope dilution–thermal ionization mass spectrometry U-Pb community (e.g., Schoene et al., 2006) and the LA-ICP-MS U-Pb community (e.g., Horstwood et al., 2016).

Secondary mineral standard results (e.g., Durango apatite and FCT zircon). We recommend reporting secondary mineral standard averages over a time frame appropriate for the analyzed samples (run in conjunction with or bracketing the sample analyses). The number of analyses included in the average, their reproducibility, and how the reproducibility is reported (e.g., standard error or standard deviation, 1σ or 2σ) should be stated. Additional analytical details of secondary mineral standard measurements are encouraged.

7.5.3. Encouraged Reporting (Especially as Methods to Quantify These Improve)

As the uncertainties on F_T values, equivalent spherical radius, mass, and concentrations are better quantified, we encourage that these uncertainties be reported along with statements of what factors are included in the uncertainty calculation and how they were calculated. The uncertainties on these parameters are influenced by uncertainties on the crystal geometric information, which are not well quantified at present (section 7.3). In some cases, the standard 2-D microscopy approach for estimating volumes and surface areas may yield systematic errors in the parameters derived from them (e.g., up to a $31 \pm 20\%$ overestimate in apatite eU based on Cooperdock et al., 2019). Active work is underway to better quantify geometric uncertainties and systematic error and to improve the accuracy and precision of the associated derived parameters. Methodologies include the 3-D He approach (Glotzbach et al., 2019), the direct CT measurement approach (Cooperdock et al., 2019), the size and morphology approach (Zeigler et al., 2021), and the stoichiometric approach (which can be used only for mass, not FT; Guenthner et al., 2016).

8. KINETICS, ^{4}He/^{3}He, AND CONTINUOUS RAMPED HEATING (CRH): FUNDAMENTALS, DATA, UNCERTAINTIES, AND REPORTING

8.1. Overview

Interpretation of (U-Th)/He data acquired via the whole-crystal methods of analysis discussed above depends on knowledge of diffusion kinetics and diffusion behavior in the materials of interest. There are also other analytical methods that can shed light on the diffusion process that are likely to see increased use in the near future.

Here, we first describe how He diffusion kinetic data are obtained and the types of Arrhenius relationships that are observed for minerals with single diffusion domain behavior (section 8.2). Such data are typically acquired by laboratory diffusion experiments using either natural ^{4}He or proton-spallation–induced ^{3}He, although the CRH method also yields data from which kinetic parameters can be derived. We then discuss the ^{4}He/^{3}He method, which can not only be used to constrain kinetics (section 8.3), but also can be applied to infer the spatial distribution of ^{4}He in a crystal and thus the character of a mineral's ^{4}He diffusion profile; this can better constrain a sample's thermal history (e.g., Shuster et al., 2005b; Schildgen et al., 2010; Valla et al., 2011; Flowers and Farley, 2012; Christeleit et al., 2017). We also summarize the fundamentals of the CRH method and its use to screen crystals for anomalous He release behavior (section 8.4). In each case, we provide an overview of the methods and primary data that are involved as well as recommend reporting practices (Table 4).

8.2. Kinetics

8.2.1. Fundamentals and Measurement Methods

Determining thermal histories is the goal of most (U-Th)/He mineral analyses, and given the significant mobility of He, even in geochronological applications it is important to assess whether the mineral has behaved as a closed system. As such, accurate knowledge of He diffusion kinetics is an essential underpinning of (U-Th)/He dating. As discussed in section 3.1, the Arrhenius parameters D_0 and E_a are key values that must be known when interpreting results from a mineral analysis.

D_0 (or D_0/a^2) and E_a are most commonly determined using fractional degassing of He during laboratory stepped-heating diffusion experiments. Figure 9 illustrates the path from measured data to derived kinetic data for such experiments, and they are the focus of our reporting recommendations (Fig. 10; Table 4). These experiments subject samples under vacuum to heating increments of precisely known duration and temperature followed by measurement of the amount of He released by each step. Note that the heating schedule does not require progressive heating or constant heating durations, and more complex cycled heating with retrograde steps can be useful in exploring diffusion systematics (e.g., Farley, 2018). Measured He can be natural ^{4}He measured on either a quadrupole or magnetic sector noble gas mass spectrometer (e.g., Zeitler et al., 1987; Farley, 2000) and/or proton-spallation induced ^{3}He that is typically measured on a magnetic sector instrument ow-

TABLE 4. CHECKLIST OF DATA, UNCERTAINTIES, AND ASSOCIATED INFORMATION TO REPORT
FOR KINETIC, ^{4}He/^{3}He, AND CONTINUOUS RAMPED HEATING ANALYSES

Kinetics

Minimum Needed Reporting
- ☐ Information about sample: origin, age, geological history, assumed starting helium concentration profile(s).
- ☐ Temperature and uncertainty of each heating step (°C) and how uncertainty in temperature was assessed.
- ☐ Duration (s, m, or h) of each heating step.
- ☐ ^{4}He and/or ^{3}He beam values or amounts for each step (A, nmol, ncc at standard temperature and pressure [STP], or atoms), uncertainties, and what factors are included in the uncertainty calculation (e.g., propagated precision from repeat measurements of sample, blanks, and reference standards).
- ☐ Derived Arrhenius data:
  - Values and uncertainties for 10,000/K and ln(D/a^2) along with what factors are included in the uncertainty calculation (e.g., uncertainties on temperature, gas amount).
  - Diffusion geometry assumed and reference to equations used to calculate diffusivities.
- ☐ Derived kinetic data:
  - Values and uncertainties for D_0/a^2 and Ea determined by regression through data.
  - Criteria used in selecting data for regression; nature of regression algorithm and whether uncertainties reflect analytical uncertainties or just scatter in data.

Recommended Reporting
- ☐ Values of cumulative fractional loss, f, to allow data to be used more directly.

^{4}He/^{3}He Data

Minimum Needed Reporting
- ☐ Bulk sample information: All information needed for individual aliquot (U-Th)/He data reporting (see Tables 1–3).
- ☐ Information about where the sample was irradiated and under what conditions.
- ☐ Temperature and uncertainty of each heating step (°C) and how uncertainty in temperature was assessed.
- ☐ Duration (s, m, or h) of each heating step.
- ☐ Values and uncertainties for either ^{3}He absolute amount (nmol, ncc at STP, or atoms) and ^{4}He/^{3}He ratio or ^{4}He and ^{3}He absolute amounts (nmol, ncc at STP, or atoms). What factors are included in the uncertainty calculation (e.g., propagated precision from repeat measurements of sample, blanks, and reference standards) should be stated.
- ☐ If data are used to derive kinetic parameters, then the additional data, uncertainties, and information noted above for calculating diffusivities, D_0/a^2, and E_a should be reported.

Recommended Reporting
- ☐ Values of cumulative fractional loss, f, to allow data to be used more directly.

CRH Data

Minimum Needed Reporting
- ☐ Bulk sample information: All information needed for individual aliquot (U-Th)/He data reporting (see Tables 1-3).
- ☐ Information about how blanks were assessed and removed from reported data.
- ☐ Information about which active gases were monitored and gettered during heating.
- ☐ Heating ramp rate(s) (°C/m) or heating schedule.
- ☐ Cumulative He beam values or amounts (A, nmol, ncc at STP, or atoms).
- ☐ Start time of each He analytical block and temperature at that time (s or m; °C).
- ☐ Uncertainties on temperature and He beam values or amounts and how they were assessed across range of values reported.
- ☐ Information on procedures for determining total He release from sample.
- ☐ If data are used to derive kinetic parameters, then the additional data, uncertainties, and information noted above for calculating diffusivities, D_0/a^2, and E_a should be reported.

Recommended Reporting
- ☐ Values of cumulative fractional loss, f, to allow data to be used more directly.

*For all uncertainties, report in same unit as data and state if given at 1σ or 2σ. For uncertainties on measured data, indicate if reported as standard error or standard deviation.

---

ing to the small ^{3}He abundances generated during proton irradiation (e.g., Shuster and Farley, 2004). Important assumptions embedded in this approach are that the mineral under study remains stable during vacuum heating and that the portion of the gas release used to obtain kinetic information is representative of diffusion processes in nature (that occur at lower temperature and over far longer time scales). Data reduction is much easier if the measured isotope has a uniform distribution at the start of the experiment (without diffusion gradients, alpha-ejection profiles, or variations due to parent isotope zoning). The amount of He released at each step relative to the total amount of He in the sample yields fractional degassing information that can be converted to diffusivities using a set of simple equations (Fig. 9; e.g., Fechtig and Kalbitzer, 1966; or McDougall and Harrison, 1999). These diffusivities are then plotted as ln(D/a^2) versus 1/T on an Arrhenius diagram, and these data are linearly regressed to calculate D_0 and E_a (Figs. 9 and 10D; see next subsection). Diffusivity data

are obtained using an assumed diffusion geometry (e.g., sphere, infinite slab, infinite cylinder), so it is critical that all subsequent calculations use this same assumed geometry.

Several alternative experimental approaches are available for determining D_0 and E_a. One strategy is to implant ^{4}He or ^{3}He in the outer hundreds of nanometers of crystals to induce He concentration profiles followed by ion beam experiments to characterize the profiles, which can be fit with D_0 and E_a (Ouchani et al., 1998; Miro et al., 2006; Cherniak et al., 2009; Gerin et al., 2017). Another method is to heat crystals with uniform ^{4}He concentrations to various temperatures and durations followed by characterization of ^{4}He concentration profiles by laser ablation–noble gas mass spectrometry (van Soest et al., 2011). Theoretical first-principles models that describe atomic level He diffusion behavior are also growing in use and predictive ability (e.g., Reich et al., 2007; Mbongo Djimbi et al., 2015; Balout et al., 2017; Gautheron et al., 2020). Differences between bulk-grain and microsampling

approaches are common and yield important insight into the factors that modify volume-diffusion behavior.

Experimentally determined D_0 and E_a parameters for a mineral are incorporated into He diffusion kinetic models that describe He diffusivity as a function of temperature, time, and potentially other factors that change through time such as radiation damage. The kinetic models are then applied to perform thermal history modeling of the data assuming the kinetic parameters derived for a fairly limited set of natural samples apply generally to all instances of that mineral. A great advantage of the ^{4}He/^{3}He method is that ^{3}He-based diffusion kinetics can be obtained as a by-product of stepped-heating analysis for a specific sample, providing there is good temperature control for the experiment (section 8.2.4). The recently developed CRH approach (Idleman et al., 2018) generates data that can be treated the same as stepped-heating analysis in obtaining kinetic parameters. Natural, empirical calibration experiments, in which (U-Th)/He dates

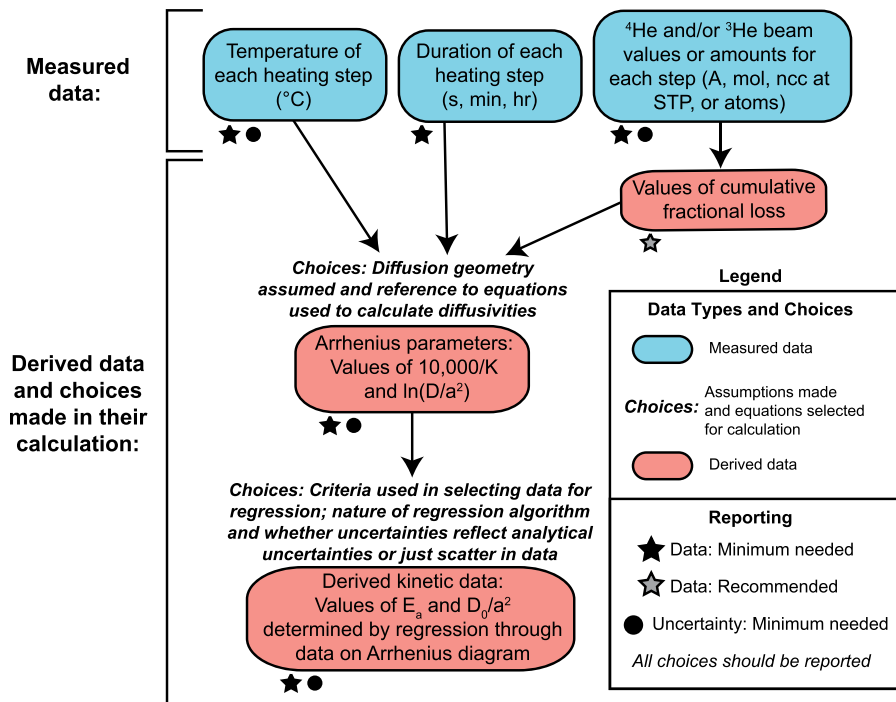## Data reduction and reporting for stepped-heating kinetic data

Measured data:

Temperature of each heating step (°C) ★ ●

Duration of each heating step (s, min, hr) ★

⁴He and/or ³He beam values or amounts for each step (A, mol, ncc at STP, or atoms) ★ ●

Values of cumulative fractional loss ☆

Derived data and choices made in their calculation:

Choices: Diffusion geometry assumed and reference to equations used to calculate diffusivities

Arrhenius parameters: Values of 10,000/K and ln(D/a²) ★ ●

Choices: Criteria used in selecting data for regression; nature of regression algorithm and whether uncertainties reflect analytical uncertainties or just scatter in data

Derived kinetic data: Values of E_a and D_0/a^2 determined by regression through data on Arrhenius diagram ★ ●

Legend

Data Types and Choices

○ Measured data

Choices: Assumptions made and equations selected for calculation

○ Derived data

Reporting

★ Data: Minimum needed

☆ Data: Recommended

● Uncertainty: Minimum needed

All choices should be reported

Figure 9. Flow chart for stepped-heating kinetic data illustrates the path from measured data (blue) to derived data (pink) and the associated choices made during data reduction (black italics). Minimum needed and recommended reporting for data and uncertainties are marked as noted in legend. For all derived data that are reported, assumptions and methods associated with their calculations should be noted or references cited. For all uncertainties, report in same units as data, state what factors are included in uncertainty calculation, and if given at 1σ or 2σ. Sample information and experimental methods also are minimum needed data that should be reported or references given. See reporting table checklist in Table 4 for complete details.

for different minerals from the same rock sample are compared, are also important for evaluating the overall validity of diffusion kinetics inferred from experimental studies.

The number of kinetics studies is relatively few, and there has been no community agreement to use a particular primary kinetic calibration. As such, no formal database has been established for noble gas kinetic data. Current practice is to make use of primary kinetic information embedded into current versions of thermal history modeling software, which generally use more evolved kinetic models that incorporate the primary data, and this represents a de facto consensus by the thermochronological community. To give a concrete example, the RDAAM model for apatite published by Flowers et al. (2009) accounts for not only core diffusion kinetics but also the impacts of temperature-sensitive radiation damage; RDAAM is calibrated against published studies of He diffusion in various apatite crystals (e.g., Shuster et al., 2006). In turn, the RDAAM model is incorporated as one of several options

in thermal history modeling software packages like HeFTy (Ketcham, 2005) and QTQt (Gallagher, 2012) (see companion paper, Flowers et al., 2022). In addition, other radiation damage models for apatite by Gautheron et al. (2009) and Gerin et al. (2017) are incorporated in QTQt.

An issue that arises is that this approach treats all grains as identical in their kinetics, with radiation damage effects and grain size being the only control. Fits of more evolved kinetic models such as RDAAM to the primary kinetic observations (Flowers et al., 2009) leave considerable scatter in the kinetic data unexplained, which could be attributable to grain specifics like chemistry or the presence of defects. Thus, while the use of de facto community models provides some consistency, these may be inaccurate for specific grains. In many cases, this will not be a major problem, but it should be kept in mind. More widespread use of ⁴He/³He and possible CRH analysis will likely change the landscape as these approaches can provide grain-specific kinetics and other parameters. In any case, ad-

ditional studies of He diffusion kinetics by more laboratories would be helpful.

8.2.2. Nature of Arrhenius Relationship for Commonly Dated Minerals

Simple volume diffusion should yield a linear array in Arrhenius space defined by coordinates of $\ln(D/a^2)$ and $1/T$; the slope of this array is proportional to the activation energy, and the intercept is D_0/a^2 (Fig. 10D). During laboratory heating, changes in diffusion behavior can occur at higher temperatures, as in the rollover often seen in apatite results at temperatures above 300 °C (e.g., Farley, 2000). Common practice is to derive kinetics from the earliest gas release obtained at low temperatures, which generally yields a linear array of data, and to assume that this best represents He diffusion behavior in nature. However, it is important to keep in mind that this linear data array often represents only a few percent of the gas released in total, with the lowest-temperature steps yielding very small amounts of gas.

Arrhenius plots are also subject to artifacts as follows. If proton-induced ³He is used for kinetic analysis, determining an Arrhenius relationship is fairly straightforward because it is a reasonable expectation that the initial distribution of ³He is uniform, a key assumption made in the equations for obtaining values of D from fractional loss (Fig. 10A). However, if ⁴He is used, then for whole crystals the Arrhenius data may be complicated by non-uniform concentration profiles caused by some combination of alpha ejection, diffusional rounding, and intracrystalline zonation in U-Th (Fig. 10A; e.g., Goldsmith et al., 2020). Both alpha-ejection and diffusional rounding deplete ⁴He in the outer portion of the crystal. This produces a ⁴He concentration profile that generates an Arrhenius array that is concave-up early in release and that only slowly approaches the expected linear array; the degree to which this occurs depends on the degree of rounding of the starting concentration profile relative to the flat profile that diffusion calculations expect (e.g., Goldsmith et al., 2020). In addition, when modeling low-temperature Arrhenius data, both analytical infinite-series equations as well as finite-difference code have difficulty with accurately predicting very small fractional losses, requiring either a very large number of terms or very fine grid spacings to yield accurate results. Consequently, use of ⁴He for recording diffusion kinetics is best for internal shards of large, minimally zoned samples (e.g., the Durango apatite standard). However, apatite and zircon crystals with these characteristics are rare, proton-irradiation to generate ³He is expensive, and many (U-Th)/He labs lack the magnetic sector noble gas mass spectrometer instrumentation needed
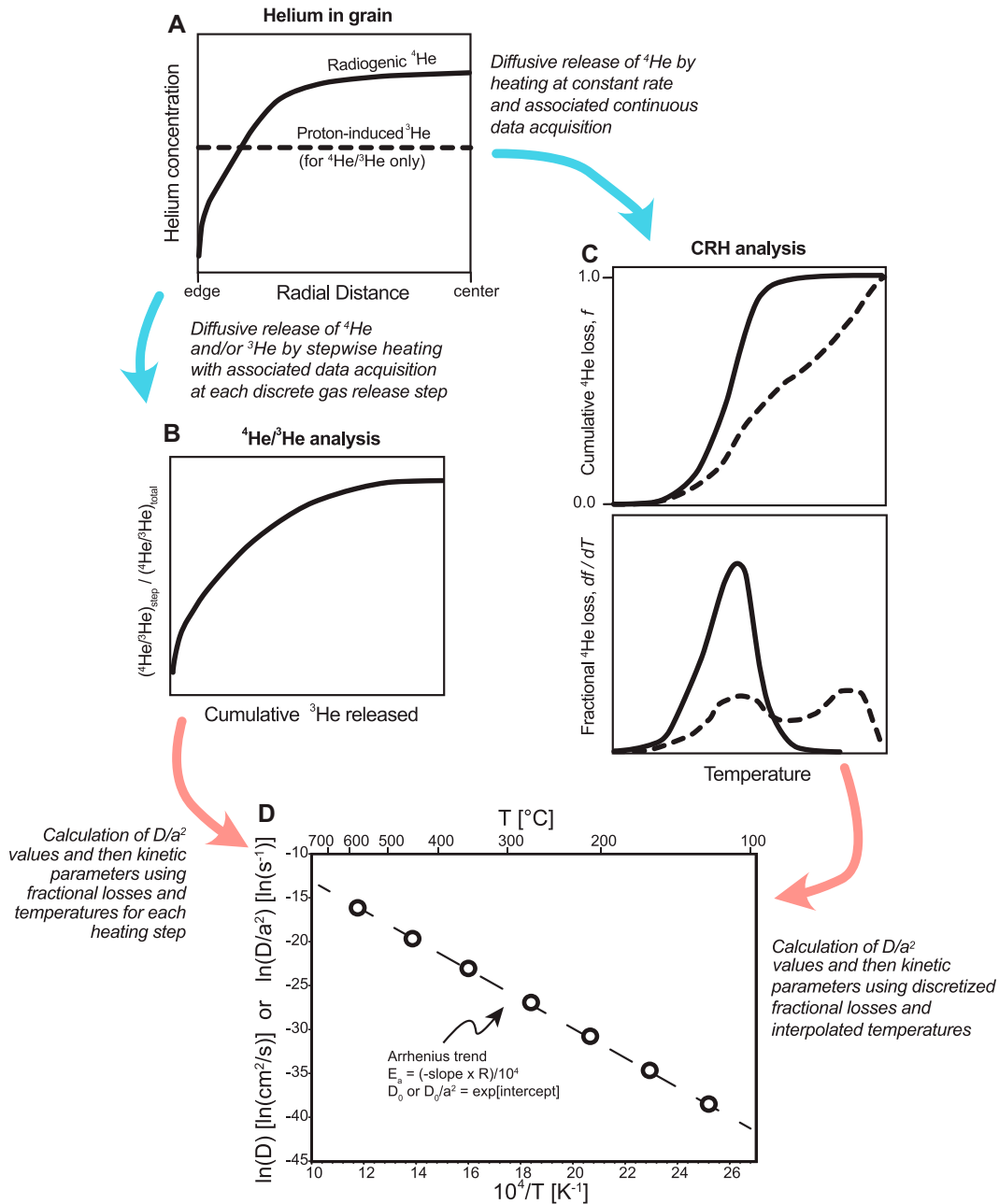
Figure 10. Illustration shows approaches for acquiring He diffusion kinetic data and related information. (A) He concentration as a function of radial distance from the crystal edge. The concentration of radiogenic ^{4}He (solid line) is likely to be non-uniform owing to alpha ejection, diffusional rounding, and possibly other effects. For ^{4}He/^{3}He analysis, proton-spallation is used to generate a uniform distribution of ^{3}He in the crystal (dashed line). Stepped-heating experiments involve stepwise heating and associated data acquisition at each discrete gas release step and can use either ^{4}He or ^{3}He for kinetic analysis, but the uniform distribution of ^{3}He makes such data more straightforward to interpret. Continuous ramped heating (CRH) experiments involve continuous heating and continuous ^{4}He data acquisition. (B) ^{4}He/^{3}He stepped-heating data plotted as ^{4}He/^{3}He ratio of each step normalized to the bulk crystal ^{4}He/^{3}He ratio versus cumulative fraction of ^{3}He released. ^{4}He/^{3}He data can be used to simultaneously derive kinetic parameters from the ^{3}He data and to constrain the spatial distribution of ^{4}He in the crystal (solid line in panel A). (C) CRH ^{4}He data plotted as cumulative ^{4}He fractional loss (*f*) versus temperature (top plot) and fractional ^{4}He loss (*df/dT*) versus temperature (bottom plot) for a sample characterized by simple volume diffusion (solid line) and a sample with a more complex diffusive release pattern (dashed line). The sample with the complex pattern is more likely to yield an anomalous or biased date and may be excluded from additional analysis (e.g., parent isotope measurement) and interpretation. CRH ^{4}He data may also be used to obtain kinetic information. (D) Arrhenius diagram shows hypothetical He diffusion experiment data (using either ^{4}He or ^{3}He). Each point represents the amount of He released from a crystal under vacuum during a heating step of precisely known duration and temperature. The *x*-axis is the inverse temperature of the heating step. The *y*-axis is the diffusivity for each point calculated from the fractional degassing information (including the fraction of He released and the duration of each temperature step). For crystals from which He loss is dominated by volume diffusion, the slope of the data points on an Arrhenius array can be used to determine E_a, and the y-intercept yielded by linear regression through the data represents D_0 (or D_0/a^2).

for ^{3}He analyses, so for practical reasons many diffusion experiments are conducted with ^{4}He on typical minerals while keeping data interpretation caveats in mind.

Several other considerations also exist. Reversible trapping of He in imperfections (e.g., Zeitler et al., 2017; Guo et al., 2021) and radiation damage annealing during stepped-heating (e.g., Farley, 2000) can introduce complications for interpreting both ^{4}He and ^{3}He stepped-heating data. In addition, while the subject is beyond the scope of this paper, some minerals (e.g., Fe

oxides; see section 4.3.2) display multiple diffusion domain behavior that results in complex Arrhenius plots (e.g., Farley and Flowers, 2012; Farley and McKeon, 2015).

8.2.3. Kinetic Data and Reporting (Checklist in Table 4)

Table 4 is a reporting checklist that includes "minimum needed" and "recommended" reporting for kinetic data, uncertainties, and associated information. The core measured data that should be documented for kinetic experiments are simple: temperature and duration of each step or interval and the amount of gas released for each temperature step or interval. The minimum needed derived data are: values of 10,000/K and $\ln(D/a^2)$ for Arrhenius plots, the diffusion geometry assumed and equations used for calculation of $\ln(D/a^2)$ values, values of D_0/a^2 and E_a determined by linear regression through the data, as well as the criteria used in selecting data for regression and the nature of the regression algorithm. To make data more immediately useful it is also recommended to report the cumulative fraction of gas lost, f, which represents simple derived data that are essential input to diffusion calculations. In addition, as much information about the analyzed material should be reported as possible, including the grain size and known information about the sample's geological history, to allow assessment of ^{4}He concentration distributions if ^{4}He is the species being analyzed.

8.2.4. Kinetic Uncertainties and Reporting (Checklist in Table 4)

Uncertainties on kinetic data include those on the measured values (temperature and the amount of gas released at each step) as well as on the $\ln(D/a^2)$ value calculated for each step and on the linearly regressed values of D_0/a^2 and E_a. All of these uncertainties should be reported.

Uncertainties on the absolute amounts of measured gas were discussed in section 7.2. The other key measured parameters are temperature and heating duration (uncertainty in time is usually small compared to heating duration). How well these can be known is beyond the scope of this paper but is discussed briefly here. The typical heating schedule used for diffusion work consists of square pulses, but the degree to which heating and cooling ramps are short or not depends on the nature of the heating apparatus used (for modern laser systems, this will be at most a few seconds compared to heating durations of minutes). It is critical that temperature be precisely controlled and not overshot, given the exponential nature of diffusion. Since the entire point of diffusion experiments is to measure how diffusion changes with temperature, a worst-case scenario would be a broadly parabolic heating

step where the sample is never at a consistent temperature for any duration. In any case, it can be difficult to determine the precision and accuracy of the heating of any one sample, again depending on the nature of the apparatus (furnace or laser) and the measurement system (thermocouple or pyrometer). The best that can probably be done in routine operations for different samples is to apply blanket uncertainties determined from independent calibration of the heating system. The accuracy and precision of heating can be a very nonlinear function of temperature as the heating apparatus transitions from conduction- to radiation-dominated heat transfer and loss. Additional temperature uncertainty is introduced by measurement of sample temperature by a thermocouple or pyrometer that may not be exactly co-located where the grain sits in its metal packet or envelope. While measurement precisions of ± 1 °C are possible, realistic uncertainties in temperature accuracy are probably closer to 5 °C or even 10 °C. Whether inaccuracy during stepped-heating is systematic or random is debatable; both are possible.

Propagation of the analytical uncertainties for the calculation of diffusivity and then Arrhenius parameters from stepped-heating data is not difficult but rather involved numerically. The fractional loss values that are the key inputs are ratios of accumulated measured amounts of the diffusant under study; counter-intuitively, while small early steps may seem imprecise, their estimate of fractional loss is usually quite good. Additionally, in Arrhenius space, there is strong error compression of diffusivity values due to the logarithmic term. See Ginster and Reiners (2018) for additional discussion of uncertainty propagation for diffusivities and diffusion parameters. Note that the accuracy of the derived kinetic parameters is subject to the choice of data used for the linear regression to determine D_0/a^2 and E_a and to the assumptions outlined in sections 8.2.1 and 8.2.2. Thus, it is important to explain the criteria for choosing the data to regress and to discuss the relevant considerations.

8.3. ^{4}He/^{3}He

8.3.1. ^{4}He/^{3}He Fundamentals and Measurement Methods

It is possible to heat a crystal in a series of steps of varying temperature and duration to infer the distribution of ^{4}He within it (Fig. 10A; Shuster and Farley, 2004; Shuster et al., 2004); typically, this heating increases progressively in temperature, but this is not a requirement. A uniformly distributed reference isotope is required, and this is obtained via proton irradiation, which produces ^{3}He from spallation reaction with many major elements, such as Ca in apatite (Fig. 10A).

In some ways, ^{4}He/^{3}He stepped-heating analysis is similar to the ^{40}Ar/^{39}Ar method, but there are key differences, the main ones being (1) that while ^{39}Ar is produced from the parent nuclide (K), ^{3}He is not produced from U, Th, and Sm, so if there is zoning, ^{4}He and ^{3}He concentrations will not correlate in space, and (2) bulk U, Th, and Sm analysis of the outgassed grain is still required to obtain age information. The ^{4}He/^{3}He method can be used to constrain kinetics as well as to decipher a mineral's diffusion profile and therefore its thermal history. To date most ^{4}He/^{3}He studies for thermal history investigations have used apatite (e.g., Shuster et al., 2005b; Schildgen et al., 2010; Valla et al., 2011; Flowers and Farley, 2012; Christeleit et al., 2017). Early work suggests the method might also work well for zircon, although this mineral's usually significant and complex parent-nuclide zoning requires 3D characterization (Tripathy-Lang et al., 2015).

^{4}He/^{3}He stepped-heating data are typically reported as either ratio-evolution diagrams or age spectra; both of these use the cumulative fraction of the ^{3}He released as the abscissa. Ratio-evolution diagrams plot the measured ^{4}He/^{3}He ratio of each step normalized by the bulk-crystal ^{4}He/^{3}He ratio (Fig. 10B). Age spectra convert this information into apparent ages for each step using the bulk-crystal (U-Th)/He date. Different ^{4}He/^{3}He profiles may be expected for some different types of thermal histories (Shuster and Farley, 2004). In general, laboratories use various codes to invert the observed stepped-heating data for thermal history; with modern codes, it is possible to include the impact of parent nuclide zoning in the inversions (e.g., Fox et al., 2014). Beyond allowing the (U-Th)/He method to constrain thermal histories to lower temperatures (as low as ~35–40 °C for apatite), another great benefit of ^{4}He/^{3}He stepped-heating analysis is that it offers the chance to use the release of ^{3}He to gain sample-specific kinetic information for each crystal (Fig. 10D), and indeed a significant part of the diffusion kinetic data for apatite comes from ^{4}He/^{3}He analysis.

8.3.2. ^{4}He/^{3}He Data, Uncertainties, and Reporting (Checklist in Table 4)

Table 4 notes the information needed for ^{4}He/^{3}He reporting. Because date determination is typically part of ^{4}He/^{3}He analysis, all of the sample-related data required for a conventional (U-Th)/He analysis should be reported (e.g., sample information, parent and daughter absolute amounts; grain dimensions, F_T; see Tables 1–3). The facility for and conditions of irradiation should be described. Essential data measured to report include the temperature and duration of each step (to permit assessment of

gas release and kinetics) as well as the amounts of gas released at each heating step. The latter can be done in one of two ways: the ^{3}He amount released at each step and the ^{4}He/^{3}He ratios of those steps or the amounts of ^{4}He and ^{3}He released at each step. Uncertainties in amounts, ratios, and temperature must also be reported. For the convenience of users and efficiency for later data exploration, it is recommended that the cumulative fraction of gas lost also be tabulated. If ^{4}He/^{3}He data are used to derive kinetic parameters, then the additional data, uncertainties, and information for calculating diffusivities, D_0/a^2, and E_a should be reported (sections 8.2.3 and 8.2.4; Table 4).

8.4. Continuous Ramped Heating

8.4.1. Fundamentals and Measurement Methods

CRH is a variant of conventional individual aliquot (U-Th)/He analysis that involves simultaneous heating of a crystal and measurement of the gas signal (Idleman et al., 2018). The goals of this approach are to rapidly screen samples for irregularities in their gas release compared to expectations for volume diffusion and also to gain some handle on the kinetic variation among samples. At present, the method is best suited for use with more robust quadrupole mass spectrometers with internal volumes and ion sources that are able to survive high pressures because the spectrometer is exposed directly to the sample during sample heating, putting the spectrometer at risk should a vacuum accident occur. In CRH analysis, the mass spectrometer is used to monitor the growth of the ^{4}He beam as the sample is progressively heated by a tightly controlled laser, usually at rates of 20 °C/min to 30 °C/min. After heating is complete, the system has cooled, and any residual active gases have been fully gettered, a reference standard is added to determine the total ^{4}He released, as in conventional analysis. During analysis, it is important to monitor active gas species such as H and m/e = 28 to ensure that gettering is sufficient to prevent their levels from becoming too high; in large amounts, these gases can lead to significant changes in instrument sensitivity (Guo et al., 2021). To date, the CRH method has only been applied to ^{4}He release from apatite.

Because the data take the form of a cumulative fractional loss curve (Fig. 10C, top plot) and because the ramped thermal history is known, CRH data can be treated as normal stepped-heating data for the purposes of calculating diffusivities, subject to the considerations for ^{4}He diffusion data noted in section 8.2.2. Additionally, plotted against time or temperature, the first derivative of the release curve, in units

of df/°C, illustrates the progressive release pattern of gas from the sample (Fig. 10C, bottom plot). For simple volume diffusion, this should be a unimodal peak (Idleman et al., 2018). However, examination of apatite samples reveals apatite (U-Th)/He dates with variable degrees of date dispersion that in some cases correlate with different types of He release patterns (Idleman et al., 2018; McDannell et al., 2018; Guo et al., 2021). Samples with low dispersion tend to have apatite crystals that show the expected unimodal release pattern, whereas samples with more complex slow-cooling histories or those that show overdispersion in conventional (U-Th)/He dates (see companion paper for discussion of intra-sample dispersion, Flowers et al., 2022) have more grains that show complex release patterns containing some combination of sharp spikes of gas release or a second discrete peak at much higher than expected temperatures (Fig. 10C, bottom plot). Grains with anomalous He release patterns that do not conform to simple volume diffusion release may be appropriate to exclude from interpretation, because current kinetic models are founded on the expectation of volume diffusion behavior.

8.4.2. CRH Data, Uncertainties, and Reporting (Checklist in Table 4)

Table 4 notes the information needed for CRH reporting. Date determination is generally part of CRH experiments, so, as with ^{4}He/^{3}He analysis, all sample-related data should be reported as for a conventional analysis (see Tables 1–3). Because of the nature of CRH analysis, the ways in which ^{4}He blank is assessed and removed from measurements should be discussed, and because active gases such as H and m/e = 28 can poison mass spectrometer sensitivity when present in large amounts, how these gases were monitored to ensure sufficient gettering to acceptable levels needs to be described. The heating ramp rate or heating schedule should be reported as well. The core data that are required are the cumulative ^{4}He signal or amount, the time at the start of each analytical block, and the temperature at this time. Uncertainties on at least the temperatures and He beam values or amounts need to be reported, and given the continuous nature of CRH experiments and the range in signal sizes and temperatures encountered, the protocol of estimating uncertainties at any one point should be described. Finally, how the final ^{4}He signal measured by the mass spectrometer at the end of experiment was converted to an absolute amount with an uncertainty should be documented. As for kinetic and ^{4}He/^{3}He work, tabulating the cumulative fractional loss is recommended. If CRH data are used to derive ki-

netic information, then the additional relevant information should be reported (sections 8.2.3 and 8.2.4; Table 4).

9. OPPORTUNITIES AND LOOKING FORWARD

To continue pushing the spectrum of questions that can be addressed with the (U-Th)/He method and the detail that can be deciphered from the data, ongoing progress must be made on multiple fronts. These include refining He diffusion kinetic models, developing new analytical tools, and acquiring information to improve decisions about how to interpret data (see also companion paper, Flowers et al., 2022). Looking forward, we see opportunities in the following areas:

(1) *He diffusion kinetics (sections 3 and 8.2).* Continued work is needed to improve He diffusion kinetic models, because our ability to accurately interpret (U-Th)/He data is limited by how well we understand the parameters that govern He diffusion in the minerals dated. This requires better quantification of how different types of damage influence He diffusivity, the controls on how these different damage types are annealed, and if/how other factors (e.g., mineral chemistry) modify He diffusion characteristics. Materials science characterization tools (e.g., Raman spectroscopy, scanning electron microscopy, ion beam techniques, atom probe tomography), as well as several of the approaches described below, are opening new avenues in this realm. To help quantify both intralab and interlab uncertainty, it would also be useful to agree upon and develop some sort of kinetic standard that could be employed to monitor the performance of heating systems used in diffusion experiments.

(2) *Laser ablation methods.* The higher spatial resolution afforded by in situ information can enhance mineral characterization and data interpretation. The laser ablation (U-Th)/He dating approach allows for holistic integration of maps of U-Th, He, radiation damage, (U-Th)/He date, and U-Pb date in single crystals; quantification of intracrystalline heterogeneities; direct measurement of diffusion gradients in single crystals; rapid sample screening for strategic mineral selection; dating of imperfect and small crystals; and largely non-destructive analysis of high-value samples (e.g., Boyce et al., 2006, 2009; van Soest et al., 2011; Vermeesch et al., 2012; Tripathy-Lang et al., 2013; Evans et al., 2015; Tian et al., 2017; Horne et al., 2016, 2019; Danišík et al., 2017a; Anderson et al., 2020; Pickering et al., 2020). It consequently is seeing increasing adoption as a complement to the conventional whole-crystal technique. Even in the absence of in situ He data, analysis of parent iso-

tope distributions via LA-ICP-MS can improve the accuracy of F_T values for grains dated by the conventional approach, as well as enhance associated data interpretation (see companion paper for additional discussion of the influence of eU zonation on the diffusion profile and heterogeneous intracrystalline radiation damage, Flowers et al., 2022).

(3) *Atomistic descriptions of He diffusion.* Alternative strategies for characterizing He diffusion, in addition to stepped-heating diffusion experiments, would promote evaluation and refinement of He kinetic models. Theoretical studies can provide a physical understanding of He diffusion in minerals at the atomic level in a perfect crystal lattice and then investigate the role of radiation damage and chemical substitution in modifying diffusive behavior (e.g., Gautheron et al., 2020). This information provides an important complement to laboratory characterization of actual diffusive behavior in natural crystals.

(4) *$^4He/^3He$ thermochronology (section 8.3).* Broader use of the $^4He/^3He$ method has the potential to provide additional thermal history constraints in targeted studies, reduce ambiguity in the interpretation of stepped-heating diffusion experiment results, and enable more systematic diffusion studies on a wider range of minerals. Widespread adoption of this method has been hindered by the expense and logistical challenge of proton irradiations, as well as the need for magnetic sector rather than quadrupole noble gas mass spectrometer instrumentation; many (U-Th)/He labs lack magnetic sector machines owing to the greater cost associated with acquiring and maintaining this equipment. Better coordination among labs may help address some aspects of the challenges associated with proton irradiations. A newer generation of quadrupole mass spectrometers with improved resolution may also hold promise as a less expensive alternative to sector magnet machines for $^4He/^3He$ measurements (e.g., Schneider et al., 2009, for $^{40}Ar/^{39}Ar$ dating via quadrupole mass spectrometry).

(5) *CRH (section 8.4).* CRH analysis shows promise in screening He analyses for anomalous components that are likely to yield biased dates before U and Th measurements are made and the results folded into a data set. Research into what these anomalous components represent is ongoing. The argument is that if a sample should behave simply according to existing kinetic models, irregular release patterns would suggest that the sample contains artifacts that violate this expectation, and it should not be included in any modeling or interpretation (McDannell et al., 2018). Technical work is required to better control temperatures at low values, and

more research is needed to better understand the features that lead to anomalous gas release. Application to other minerals is also an obvious next step, as is applying the CRH approach to $^4He/^3He$ analysis.

(6) *Nontraditional He chronometer development.* Ongoing laboratory study is aimed at constraining He diffusion in phases that have not traditionally been used for (U-Th)/He analysis (section 4). This is further widening the scope of problems that can be addressed with the technique.

(7) *Availability of additional natural mineral standards.* Natural mineral standards analyzed with unknowns provide an important check on the quality of analyses. Additional standard materials that are widely available and well characterized would benefit the (U-Th)/He dating community. One might imagine two classes of useful natural date standards. The first class would include samples like Durango apatite and FCT zircon, aimed at minimizing complexities arising from the cooling history, morphology, alpha-ejection profile, and compositional heterogeneity. This type of standard would serve as a check on the precision and accuracy of basic parent-daughter measurements, ideally across a wide range of He/eU concentrations and dates. These could be internal fragments of large, gem-quality apatite or zircon megacrysts (e.g., Sri Lankan zircon) or possibly synthetic standards. The second class of useful standard could provide labs with opportunities to test their ability to deal with the practical complexities that characterize real "wild" samples. These materials may offer a range of sizes, morphologies, "brokenness," and inter- and intragrain compositional variation, all of which could conceivably be characterized as part of the analysis. As minerals other than apatite and zircon become more routinely analyzed, additional standards are also required for these phases (e.g., hematite).

(8) *Quantifying uncertainties.* Appropriate uncertainties must be quantified to reliably interpret (U-Th)/He data. Improved characterization of uncertainties on crystal geometric information, and thus on the F_T value, corrected (U-Th)/He date, eU, and equivalent spherical radius, is needed (section 7.3). Possible avenues include new analytical approaches to minimize uncertainties on geometric parameters (e.g., 3-D He approach, Glotzbach et al., 2019; CT study, Cooperdock et al., 2019), the use of the stoichiometric approach to improve estimates of crystal mass (Guenthner et al., 2016), and determination of "rule of thumb" values for systematic error corrections and uncertainties on geometric parameters as a function of grain size and morphology (e.g., Zeigler et al., 2021).

10. CONCLUSIONS AND SUMMARY OF RECOMMENDATIONS

This manuscript reviews the fundamentals of (U-Th)/He dating (sections 2–3), discusses the types of dateable materials (section 4), describes the workflow associated with (U-Th)/He data acquisition (section 5), and recommends more standardized reporting practices for conventional individual aliquot (U-Th)/He data and uncertainties (sections 6–7). It also reviews the fundamentals of related methods for acquiring kinetic, $^4He/^3He$, and CRH data, and makes associated reporting recommendations (sections 8). There are numerous promising avenues (section 9) for continuing to improve the quality of (U-Th)/He data and the range of materials that can be dated and interpreted, which will further expand the utility and versatility of the (U-Th)/He technique.

Reporting practices should remain an important topic of community conversation and see ongoing revision as the field continues to develop. The recommendations of this contribution are:

(1) Report essential information about the samples analyzed and experimental methods (Table 1; section 5.7).

(2) For individual aliquot data (Tables 2–3; section 6.4):

- Report crystal dimension data (and, in some cases, stoichiometric data), ^4He absolute amount, parent isotope absolute amounts, combined F_T value, R_{SV} or R_{FT}, mass, uncorrected (U-Th)/He date, and corrected (U-Th)/He date (if reporting a corrected date is considered appropriate);
- Report the methods used to compute derived data from measured data;
- Reporting concentrations (daughter, parent, eU) is recommended.

(3) For individual aliquot uncertainties (Tables 2–3; section 7.5):

- Report uncertainties on daughter and parent absolute amounts;
- Report the total analytical uncertainty and on the uncorrected and corrected (U-Th)/He dates;
- Reporting a second level of uncertainty on the corrected (U-Th)/He date that includes both the total analytical uncertainty and an estimated uncertainty on F_T is recommended;
- Reporting mineral standard averages (e.g., Durango apatite and Fish Canyon Tuff zircon) over a time frame appropriate for the samples analyzed is recommended;
- Reporting uncertainties on the F_T value, R_{SV} or R_{FT}, mass, and concentrations is

encouraged, especially as methods to quantify these improve;

- For all uncertainties, state what factors are included in the uncertainty calculation and whether given at 1σ or 2σ.

(4) For stepped-heating kinetic data and uncertainties (Table 4; sections 8.2.3 and 8.2.4):

- Report temperatures, temperature uncertainties, duration of each heating step, and how temperature uncertainty was assessed;
- Report beam values or amounts of ^{4}He and/or ^{3}He released for each heating step and uncertainties on these values;
- Report values and uncertainties for 10,000/K and $\ln(D/a^2)$ for Arrhenius plots, as well as assumed diffusion geometry used and reference to formulas used for calculating diffusivities;
- Report values and uncertainties for D_0/a^2 and E_a, discuss criteria used to select data for regression, and describe regression approach;
- Reporting values of cumulative fractional loss is recommended to allow data to be used more directly;
- For all uncertainties, state what factors are included in the uncertainty calculation and whether given at 1σ or 2σ.
- Describe sample and give as much information as possible about geologic history and characterization.

(5) For ^{4}He/^{3}He data and uncertainties (Table 4; section 8.3.2):

- Report all information needed for individual aliquot (U-Th)/He dating (Items 1, 2, and most of Item 3 above; Tables 1–3);
- Describe where and under what conditions the sample was irradiated;
- Report temperatures, temperature uncertainties, duration of each heating step, and how temperature uncertainty was assessed;
- For each step, report values and uncertainties for either ^{3}He amounts and ^{4}He/^{3}He ratio or ^{4}He and ^{3}He amounts;
- Reporting values of cumulative fractional loss is recommended to allow data to be used more directly;
- For all uncertainties, state what factors are included in the uncertainty calculation and whether given at 1σ or 2σ.
- If data are used to derive kinetic parameters, then report additional data, uncertainties, and information for calculating diffusivities, D_0/a^2, and E_a (noted in Item 4 above).

(6) For CRH data and uncertainties (Table 4; section 8.4.2):

- Report all information needed for individual aliquot (U-Th)/He dating (Items 1, 2, and most of Item 3 above; Tables 1–3);

- Describe how blanks were assessed and removed from reported data;
- Describe what active gases were monitored and gettered during heating;
- Report heating ramp rate or heating schedule;
- Report start time for each ^{4}He analytical block and temperature at that time;
- Report uncertainties in temperatures and He beam values or amounts and describe how the uncertainties were assessed across the range measured;
- Describe procedure used to determine total ^{4}He presented at the end of heating;
- Reporting values of cumulative fractional loss is recommended to allow data to be used more directly;
- For all uncertainties, state what factors are included in the uncertainty calculation and whether given at 1σ or 2σ.
- If data are used to derive kinetic parameters, then report additional data, uncertainties, and information for calculating diffusivities, D_0/a^2, and E_a (noted in Item 4 above).

ACKNOWLEDGMENTS

REFERENCES CITED

Aciego, S., Kennedy, B.M., DePaolo, D.J., Christensen, J.N., and Hutcheon, I., 2003, U-Th/He age of phenocrystic garnet from the 79 AD eruption of Mt. Vesuvius: Earth and Planetary Science Letters, v. 216, p. 209–219, https://doi.org/10.1016/S0012-821X(03)00478-3.

Allard, T., Gautheron, C.E., Bressan-Riffel, S., Balan, E., Selo, M., Fernandes, B.S., Pinna-Jamme, R., Derycke, A., Morin, G., Taitson Bueno, G., and Do Nascimento, N.R., 2018, Combined dating of goethites and kaolinites from ferruginous duricrusts. Deciphering the Late Neogene erosion history of Central Amazonia: Chemical Geology, v. 479, p. 136–150, https://doi.org/10.1016/j.chemgeo.2018.01.004.

Anderson, A.J., Hodges, K.V., and van Soest, M.C., 2017, Empirical constraints on the effects of radiation damage on helium diffusion in zircon: Geochimica et Cosmochimica Acta, v. 218, p. 308–322, https://doi.org/10.1016/j.gca.2017.09.006.

Anderson, A.J., Hodges, K.V., van Soest, M.C., and Hanchar, J.M., 2019, Helium diffusion in natural xenotime: Geochemistry, Geophysics, Geosystems, v. 20, p. 417–433, https://doi.org/10.1029/2018GC007849.

Anderson, A.J., Hanchar, J.M., Hodges, K.V., and van Soest, M.C., 2020, Mapping radiation damage zoning in zircon using Raman spectroscopy: Implications for zircon chronology: Chemical Geology, v. 538, https://doi.org/10.1016/j.chemgeo.2020.119494.

Ault, A.K., 2020, Hematite fault rock thermochronometry and textures inform fault zone processes: Journal of Structural Geology, v. 133, https://doi.org/10.1016/j.jsg.2020.104002.

Ault, A.K., Reiners, P.W., Evans, J.P., and Thomson, S.N., 2015, Linking hematite (U-Th)/He dating with the microtextural record of seismicity in the Wasatch fault damage zone, Utah, USA: Geology, v. 43, p. 771–774, https://doi.org/10.1130/G36897.1.

Ault, A.K., Guenthner, W.R., Moser, A.C., Miller, G.H., and Refsnider, K.A., 2018, Zircon grain selection reveals (de)coupled metamictization, radiation damage, and He diffusivity: Chemical Geology, v. 490, p. 1–12, https://doi.org/10.1016/j.chemgeo.2018.04.023.

Ault, A.K., Gautheron, C., and King, G.E., 2019, Innovations in (U–Th)/He, fission track, and trapped charge thermochronometry with applications to earthquakes, weathering, surface-mantle connections, and the growth and decay of mountains: Tectonics, v. 38, p. 3705–3739, https://doi.org/10.1029/2018TC005312.

Balout, H., Roques, J., Gautheron, C., Tassan-Got, L., and Mbongo-Djimbi, D., 2017, Helium diffusion in pure hematite (α-Fe2O3) for thermochronometric applications: A theoretical multi-scale study: Computational & Theoretical Chemistry, v. 1099, p. 21–28, https://doi.org/10.1016/j.comptc.2016.11.001.

Barham, M., Kirkland, C.L., and Danišík, M., 2019, Assessing volcanic origins within detrital zircon populations–A case study from the Mesozoic non-volcanic margin of southern Australia: Geoscience Frontiers, v. 10, no. 4, p. 1371–1381, https://doi.org/10.1016/j.gsf.2019.01.003.

Baughman, J.S., and Flowers, R.M., 2018, Deciphering a 2 Gyr-long thermal history from a multichronometer (U-Th)/He study of the Phalaborwa carbonatite, Kaapvaal craton, South Africa: Geochemistry, Geophysics, Geosystems, v. 19, p. 1–14, https://doi.org/10.1029/2017GC007198.

Baughman, J.S., and Flowers, R.M., 2020, Mesoproterozoic burial of the Kaapvaal craton, southern Africa during Rodinia supercontinent assembly from (U-Th)/He thermochronology: Earth and Planetary Science Letters, v. 531, https://doi.org/10.1016/j.epsl.2019.115930.

Baughman, J.S., Flowers, R.M., Metcalf, J.R., and Dhansay, T., 2017, Influence of radiation damage on titanite He diffusion kinetics: Geochimica et Cosmochimica Acta, v. 205, p. 50–64, https://doi.org/10.1016/j.gca.2017.01.049.

Baxter, E.F., 2003, Quantification of the factors controlling the presence of excess ^{40}Ar or ^{4}He: Earth and Planetary Science Letters, v. 216, p. 619–634, https://doi.org/10.1016/S0012-821X(03)00541-7.

Baxter, E.F., Asimow, P.D., and Farley, K.A., 2007, Grain boundary partitioning of Ar and He: Geochimica et Cosmochimica Acta, v. 71, p. 434–451, https://doi.org/10.1016/j.gca.2006.09.011.

Bender, M.L., 1973, Helium-uranium dating of corals: Geochimica et Cosmochimica Acta, v. 37, p. 1229–1247, https://doi.org/10.1016/0016-7037(73)90058-6.

Bengtson, A., Ewing, R.C., and Becker, U., 2012, He diffusion and closure temperatures in apatite and zircon: A density functional theory investigation: Geochimica et Cosmochimica Acta, v. 86, p. 228–238, https://doi.org/10.1016/j.gca.2012.03.004.

Bidgoli, T.S., Tyrrell, J.P., Möller, A., Douglas Walker, J., and Stockli, D.F., 2018, Conodont thermochronology of exhumed footwalls of low-angle normal faults: A pilot study in the Mormon Mountains, Tule Springs Hills, and Beaver Dam Mountains, southeastern Nevada and southwestern Utah: Chemical Geology, v. 495, p. 1–17, https://doi.org/10.1016/j.chemgeo.2018.06.026.

Biren, M.B., van Soest, M., Wartho, J.A., and Spray, J.G., 2014, Dating the cooling of exhumed central uplifts of impact structures by the (U-Th)/He method: A case study at Manicouagan: Chemical Geology, v. 377, p. 56–71, https://doi.org/10.1016/j.chemgeo.2014.03.013.

Blackburn, T.J., and Stockli, D.F., 2006, Comment on "U-Th/He age of phenocrystic garnet from the 79 AD eruption of Mt. Vesuvius" by Sarah Aciego, B.M. Kennedy, Donald J. DePaolo, John N. Christensen, and Ian Hutcheon [Earth Planet. Sci. Lett. 216 (2003) 209–219]: Earth and Planetary Science Letters, v. 250, p. 402–403, https://doi.org/10.1016/j.epsl.2006.07.026.

Blackburn, T.J., Stockli, D.F., and Walker, J.D., 2007, Magnetite (U-Th)/He dating and its application to the geochronology of intermediate to mafic volcanic rocks: Earth and Planetary Science Letters, v. 259, p. 360–371, https://doi.org/10.1016/j.epsl.2007.04.044.

Blackburn, T.J., Stockli, D.F., Carlson, R.W., and Berendsen, P., 2008, (U-Th)/He dating of kimberlites—A case

study from north-eastern Kansas: Earth and Planetary Science Letters, v. 275, p. 111–120, https://doi.org/10.1016/j.epsl.2008.08.006.

Boyce, J.W., and Hodges, K.V., 2005, U and Th zoning in Cerro de Mercado (Durango, Mexico) fluorapatite: Insights regarding the impact of recoil redistribution of radiogenic ^{4}He on (U-Th)/He thermochronology: Chemical Geology, v. 219, p. 261–274, https://doi.org/10.1016/j.chemgeo.2005.02.007.

Boyce, J.W., Hodges, K.V., Olszewski, W.J., and Jercinovic, M.J., 2005, He diffusion in monazite: Implications for (U-Th)/He thermochronometry: G-cubed, v. 6, Q12004, https://doi.org/10.1029/2005GC001058.

Boyce, J.W., Hodges, K.V., Olszewski, W.J., Jercinovic, M.J., Carpenter, B.D., and Reiners, P.W., 2006, Laser microprobe (U-Th)/He geochronology: Geochimica et Cosmochimica Acta, v. 70, p. 3031–3039, https://doi.org/10.1016/j.gca.2006.03.019.

Boyce, J.W., Hodges, K.V., King, D., Crowley, J.L., Jercinovic, M., Chatterjee, N., Bowring, S.A., and Searle, M., 2009, Improved confidence in (U-Th)/He thermochronology using the laser microprobe: An example from a Pleistocene leucogranite, Nanga Parbat, Pakistan: Geochemistry, Geophysics, Geosystems, v. 10, https://doi.org/10.1029/2009GC002497.

Braun, J., 2002, Quantifying the effect of recent relief changes on age-elevation relationships: Earth and Planetary Science Letters, v. 200, p. 331–343, https://doi.org/10.1016/S0012-821X(02)00638-6.

Braun, J., 2003, Pecube: A new finite-element code to solve the 3-D heat transport equation including the effects of a time-varying, finite amplitude surface topography: Computers & Geosciences, v. 29, p. 787–794, https://doi.org/10.1016/S0098-3004(03)00052-9.

Braun, J., van der Beek, P., Valla, P., Robert, X., Herman, F., Glotzbach, C., Pedersen, V., Perry, C., Simon-Labric, T., and Prigent, C., 2012, Quantifying rates of landscape evolution and tectonic processes by thermochronology and numerical modeling of crustal heat transport using PECUBE: Tectonophysics, v. 524–525, p. 1–28, https://doi.org/10.1016/j.tecto.2011.12.035.

Brown, R.W., Beucher, R., Roper, S., Persano, C., Stuart, F., and Fitzgerald, P., 2013, Natural age dispersion arising from the analysis of broken crystals. Part I: Theoretical basis and implications for the apatite (U-Th)/He thermochronometer: Geochimica et Cosmochimica Acta, v. 122, p. 478–497, https://doi.org/10.1016/j.gca.2013.05.041.

Calzolari, G., Ault, A.K., Hirth, G., and McDermott, R.G., 2020, Hematite (U-Th)/He thermochronometry detects asperity flash heating during laboratory earthquakes: Geology, v. 48, p. 514–518, https://doi.org/10.1130/G46965.1.

Carlson, W.D., Donelick, R.A., and Ketcham, R.A., 1999, Variability of apatite fission-track annealing kinetics I: Experimental results: The American Mineralogist, v. 84, p. 1213–1223, https://doi.org/10.2138/am-1999-0901.

Cherniak, D.J., and Watson, E.B., 2011, Helium diffusion in rutile and titanite, and consideration of the origin and implications of diffusional anisotropy: Chemical Geology, v. 288, p. 149–161, https://doi.org/10.1016/j.chemgeo.2011.07.015.

Cherniak, D.J., and Watson, E.B., 2013, Diffusion of helium in natural monazite, and preliminary results on He diffusion in synthetic light rare earth phosphates: The American Mineralogist, v. 98, p. 1407–1420, https://doi.org/10.2138/am.2013.4353.

Cherniak, D.J., Watson, E.B., and Thomas, J.B., 2009, Diffusion of helium in zircon and apatite: Chemical Geology, v. 268, p. 155–166, https://doi.org/10.1016/j.chemgeo.2009.08.011.

Cherniak, D.J., Amidon, W., Hobbs, D., and Watson, E.B., 2015, Diffusion of helium in carbonates: Effects of mineral structure and composition: Geochimica et Cosmochimica Acta, v. 165, p. 449–465, https://doi.org/10.1016/j.gca.2015.06.033.

Chew, D.M., Babechuk, M.G., Cogné, N., Mark, C., O'Sullivan, G.J., Henrichs, I.A., Doepke, D., and McKenna, C.A., 2016, (LA,Q)-ICPMS trace-element analyses of Durango and McClure Mountain apatite and implications for making natural LA-ICPMS mineral standards: Chemical Geology, v. 435, p. 35–48, https://doi.org/10.1016/j.chemgeo.2016.03.028.

Christeleit, E.C., Brandon, M.T., and Shuster, D.L., 2017, Miocene development of alpine glacial relief in the Patagonian Andes, as revealed by low-temperature thermochronometry: Earth and Planetary Science Letters, v. 460, p. 152–163, https://doi.org/10.1016/j.epsl.2016.12.019.

Cooper, F.J., Adams, B.A., Blundy, J.D., Farley, K.A., McKeon, R.E., and Ruggiero, A., 2016, Aridity-induced Miocene canyon incision in the Central Andes: Geology, v. 44, p. 675–678, https://doi.org/10.1130/G38254.1.

Cooperdock, E.H.G., and Ault, A.K., 2020, Iron oxide (U–Th)/He thermochronology: New perspectives on faults, fluids, and heat: Elements, v. 16, p. 319–324, https://doi.org/10.2138/gselements.16.5.319.

Cooperdock, E.H.G., and Stockli, D.F., 2016, Unraveling alteration histories in serpentinites and associated ultramafic rocks with magnetite (U-Th)/He geochronology: Geology, v. 44, p. 967–970, https://doi.org/10.1130/G38587.1.

Cooperdock, E.H.G., and Stockli, D.F., 2018, Dating exhumed peridotite with spinel (U–Th)/He chronometry: Earth and Planetary Science Letters, v. 489, p. 219–227, https://doi.org/10.1016/j.epsl.2018.02.041.

Cooperdock, E.H.G., Ketcham, R.A., and Stockli, D.F., 2019, Resolving the effects of 2-D versus 3-D grain measurements on (U-Th)/ He age data and reproducibility: Geochronology, v. 1, p. 17–41, https://doi.org/10.5194/gchron-1-17-2019.

Copeland, P., Watson, E.B., Urizar, S.C., Patterson, D., and Lapen, T.J., 2007, Alpha thermochronology of carbonates: Geochimica et Cosmochimica Acta, v. 71, p. 4488–4511, https://doi.org/10.1016/j.gca.2007.07.004.

Cox, S.E., Farley, K.A., and Hemming, S.R., 2012, Insights into the age of the Mono Lake Excursion and magmatic crystal residence time from (U-Th)/He and ^{230}Th dating of volcanic allanite: Earth and Planetary Science Letters, v. 319–320, p. 178–184, https://doi.org/10.1016/j.epsl.2011.12.025.

Cros, A., Gautheron, C., Pagel, M., Berthet, P., Tassan-Got, L., Douville, E., Pinna-Jamme, R., and Sarda, P., 2014, ^{4}He behavior in calcite filling viewed by (U-Th)/He dating, ^{4}He diffusion and crystallographic studies: Geochimica et Cosmochimica Acta, v. 125, p. 414–432, https://doi.org/10.1016/j.gca.2013.09.038.

Damon, P.E., and Green, W.D., 1962, Investigations of the helium age dating method by stable isotope-dilution technique, in Proceedings, Symposium on Radioactive Dating: Athens, Greece, International Atomic Energy Agency, p. 280–292.

Damon, P.E., and Kulp, J.L., 1957, Determination of radiogenic helium in zircon by stable isotope dilution technique: Eos (Transactions, American Geophysical Union), v. 38, p. 945–953, https://doi.org/10.1029/TR038i006p00945.

Danišík, M., Pfaff, K., Evans, N.J., Manoloukos, C., Staude, S., McDonald, B.J., and Markl, G., 2010, Tectono-thermal history of the Schwarzwald Ore District (Germany): An apatite triple dating approach: Chemical Geology, v. 278, p. 58–69, https://doi.org/10.1016/j.chemgeo.2010.08.022.

Danišík, M., Shane, P., Schmitt, A.K., Hogg, A., Santos, G.M., Storm, S., Evans, N.J., Keith Fifield, L., and Lindsay, J.M., 2012, Re-anchoring the late Pleistocene tephrochronology of New Zealand based on concordant radiocarbon ages and combined ^{238}U/ ^{230}Th disequilibrium and (U-Th)/He zircon ages: Earth and Planetary Science Letters, v. 349–350, p. 240–250, https://doi.org/10.1016/j.epsl.2012.06.041.

Danišík, M., Evans, N.J., Ramanaidou, E.R., McDonald, B.J., Mayers, C., and McInnes, B.I.A., 2013, (U-Th)/He chronology of the Robe River channel iron deposits, Hamersley Province, Western Australia: Chemical Geology, v. 354, p. 150–162, https://doi.org/10.1016/j.chemgeo.2013.06.012.

Danišík, M., Mcinnes, B.I.A., Kirkland, C.L., McDonald, B.J., Evans, N.J., and Becker, T., 2017a, Seeing is believing : Visualization of He distribution in zircon and implications for thermal history reconstruction on single crystals: Science Advances, v. 3, p. 1–10, https://doi.org/10.1126/sciadv.1601121.

Danišík, M., Schmitt, A.K., Stockli, D.F., Lovera, O.M., Dunkl, I., and Evans, N.J., 2017b, Application of combined U-Th-disequilibrium/U-Pb and (U-Th)/He zircon dating to tephrochronology: Quaternary Geochronology, v. 40, p. 23–32, https://doi.org/10.1016/j.quageo.2016.07.005.

Danišík, M., Lowe, D.J., Schmitt, A.K., Friedrichs, B., Hogg, A.G., and Evans, N.J., 2020, Sub-millennial eruptive recurrence in the silicic Mangaone Subgroup tephra sequence, New Zealand, from Bayesian modelling of zircon double-dating and radiocarbon ages: Quaternary Science Reviews, v. 246, https://doi.org/10.1016/j.quascirev.2020.106517.

Devanathan, R., Corrales, L.R., Weber, W.J., Chartier, A., and Meis, C., 2006, Molecular dynamics simulation of energetic uranium recoil damage in zircon: Molecular Simulation, v. 32, p. 1069–1077, https://doi.org/10.1080/08927020600959929.

Dobson, K.J., Stuart, F.M., and Dempster, T.J., 2008, U and Th zonation in Fish Canyon Tuff zircons: Implications for a zircon (U-Th)/He standard: Geochimica et Cosmochimica Acta, v. 72, p. 4745–4755, https://doi.org/10.1016/j.gca.2008.07.015.

Dodson, M.H., 1973, Closure temperatures in cooling geological and petrological systems: Contributions to Mineralogy and Petrology, v. 40, p. 259–274, https://doi.org/10.1007/BF00373790.

dos Santos Albuquerque, M.F., Horbe, A.M.C., and Danišík, M., 2020, Episodic weathering in Southwestern Amazonia based on (U-Th)/He dating of Fe and Mn lateritic duricrust: Chemical Geology, v. 553, https://doi.org/10.1016/j.chemgeo.2020.119792.

Dunai, T.J., 2005, Forward modeling and interpretation of (U-Th)/He ages: Reviews in Mineralogy and Geochemistry, v. 58, p. 259–274, https://doi.org/10.2138/rmg.2005.58.10.

Dunai, T.J., and Roselieb, K., 1996, Sorption and diffusion of helium in garnet: Implications for volatile tracing and dating: Earth and Planetary Science Letters, v. 139, no. 3–4, p. 411–421, https://doi.org/10.1016/0012-821X(96)00029-5.

Ehlers, T.A., and Farley, K.A., 2003, Apatite (U-Th)/He thermochronometry: Methods and applications to problems in tectonic and surface processes: Earth and Planetary Science Letters, v. 206, p. 1–14, https://doi.org/10.1016/S0012-821X(02)01069-5.

Evans, N.J., Wilson, N.S.F., Cline, J.S., McInnes, B.I.a., and Byrne, J., 2005a, Fluorite (U–Th)/He thermochronology: Constraints on the low temperature history of Yucca Mountain, Nevada: Applied Geochemistry, v. 20, p. 1099–1105, https://doi.org/10.1016/j.apgeochem.2005.02.008.

Evans, N.J., Byrne, J.P., Keegan, J.T., and Dotter, L.E., 2005b, Determination of uranium and thorium in zircon, apatite, and fluorite: Application to laser (UeTh)/He thermochronology: Journal of Analytical Chemistry, v. 60, no. 12, p. 1159–1165, https://doi.org/10.1007/s10809-005-0260-1.

Evans, N.J., McInnes, B.I.A., Squelch, A.P., Austin, P.J., McDonald, B.J., and Wu, Q., 2008, Application of X-ray micro-computed tomography in (U-Th)/He thermochronology: Chemical Geology, v. 257, p. 101–113, https://doi.org/10.1016/j.chemgeo.2008.08.021.

Evans, N.J., McInnes, B.I.A., McDonald, B., Danišík, M., Becker, T., Vermeesch, P., Shelley, M., Marillo-Sialer, E., and Patterson, D.B., 2015, An in situ technique for (U-Th-Sm)/He and U-Pb double dating: Journal of Analytical Atomic Spectrometry, v. 30, p. 1636–1645, https://doi.org/10.1039/C5JA00085H.

Evenson, N.S., Reiners, P.W., Spencer, J.E., and Shuster, D.L., 2014, Hematite and mn oxide (U-Th)/He dates from the buckskin-Rawhide detachment system, Western Arizona: Gaining insights into hematite (U-Th)/He systematics: American Journal of Science, v. 314, p. 1373–1435, https://doi.org/10.2475/10.2014.01.

Fanale, F.P., and Kulp, J.L., 1962, The helium method and the age of the Cornwall, Pennsylvania magnetite ore: Economic Geology, v. 57, p. 735–746, https://doi.org/10.2113/gsecongeo.57.5.735.

Farley, K.A., 2000, Helium diffusion from apatite: General behavior as illustrated by Durango fluorapatite: Journal of Geophysical Research: Solid Earth, v. 105, p. 2903–2914, https://doi.org/10.1029/1999JB900348.

Farley, K.A., 2002, (U-Th)/He dating: Techniques, calibrations, and applications, *in* Porcelli, D., Ballentine, C.J., and Wieler, R., eds., Noble Gasses in Geochemistry and Cosmochemistry: Reviews in Mineralogy and Geochemistry, v. 47, p. 819–846, https://doi.org/10.1515/9781501509056-020.

Farley, K.A., 2007, He diffusion systematics in minerals: Evidence from synthetic monazite and zircon structure phosphates: Geochimica et Cosmochimica Acta, v. 71, p. 4015–4024, https://doi.org/10.1016/j.gca.2007.05.022.

Farley, K.A., 2018, Helium diffusion parameters of hematite from a single-diffusion-domain crystal: Geochimica et Cosmochimica Acta, v. 231, p. 117–129, https://doi.org/10.1016/j.gca.2018.04.005.

Farley, K.A., and Flowers, R.M., 2012, (U-Th)/Ne and multidomain (U-Th)/He systematics of a hydrothermal hematite from eastern Grand Canyon: Earth and Planetary Science Letters, v. 359–360, p. 131–140.

Farley, K.A., and McKeon, R., 2015, Radiometric dating and temperature history of banded iron formation-associated hematite, Gogebic iron range, Michigan, USA: Geology, v. 43, p. 1083–1086, https://doi.org/10.1130/G37190.1.

Farley, K.A., and Stockli, D.F., 2002, (U-Th)/He dating of phosphates: Apatite, monazite, and xenotime: Phosphates: Geochemical, Geobiological, and Materials Importance: Reviews in Mineralogy and Geochemistry, v. 48, p. 559–577, https://doi.org/10.2138/rmg.2002.48.15.

Farley, K.A., Wolf, R.A., Silver, L.T., and Wolf, L.T., 1996, The effects of long alpha-stopping distances on (U-Th)/He ages: Geochimica et Cosmochimica Acta, v. 60, p. 4223–4229, https://doi.org/10.1016/S0016-7037(96)00193-7.

Farley, K.A., Kohn, B.P., and Pillans, B., 2002, The effects of secular disequilibrium on (U-Th)/He systematics and dating of Quaternary volcanic zircon and apatite: Earth and Planetary Science Letters, v. 201, p. 117–125, https://doi.org/10.1016/S0012-821X(02)00659-3.

Farley, K.A., Shuster, D.L., and Ketcham, R.A., 2011, U and Th zonation in apatite observed by laser ablation ICPMS, and implications for the (U–Th)/He system: Geochimica et Cosmochimica Acta, v. 75, p. 4515–4530, https://doi.org/10.1016/j.gca.2011.05.020.

Farnan, I., Cho, H., and Weber, W.J., 2007, Quantification of actinide α-radiation damage in minerals and ceramics: Nature, v. 445, p. 190–193, https://doi.org/10.1038/nature05425.

Faure, G., 1986, Principles of Isotope Geology, 2nd edition: John Wiley & Sons, Inc., 589 p.

Fechtig, H., and Kalbitzer, S., 1966, The diffusion of argon in potassium bearing solids, *in* Schaeffer, O.A., and Zahringer, J., eds., Potassium-Argon Dating: Heidelberg, Germany, Springer, p. 68–107, https://doi.org/10.1007/978-3-642-87895-4_4.

Ferreira, M.P., Macedo, R., Costa, V., Reynolds, J.H., Riley, J.E., and Rowe, M.W., 1975, Rare gas dating, II. Attempted uranium-helium dating of young volcanic rocks from the Madeira Archipelago: Earth and Planetary Science Letters, v. 25, p. 142–150, https://doi.org/10.1016/0012-821X(75)90190-9.

Flowers, R.M., and Farley, K.A., 2012, Apatite ^{4}He/^{3}He and (U-Th): He Evidence for an Ancient Grand Canyon: Science, v. 338, p. 1616–1619, https://doi.org/10.1126/science.1229390.

Flowers, R.M., and Schoene, B., 2010, (U-Th)/He thermochronometry constraints on unroofing of the eastern Kaapvaal craton and significance for uplift of the southern African Plateau: Geology, v. 38, p. 827–830, https://doi.org/10.1130/G30980.1.

Flowers, R.M., Shuster, D.L., Wernicke, B.P., and Farley, K.A., 2007, Radiation damage control on apatite (U-Th)/He dates from the Grand Canyon region, Colorado Plateau: Geology, v. 35, p. 447–450, https://doi.org/10.1130/G23471A.1.

Flowers, R.M., Ketcham, R.A., Shuster, D.L., and Farley, K.A., 2009, Apatite (U–Th)/He thermochronometry using a radiation damage accumulation and annealing model: Geochimica et Cosmochimica Acta, v. 73, p. 2347–2365, https://doi.org/10.1016/j.gca.2009.01.015.

Flowers, R.M., Ketcham, R.A., Enkelmann, E., Gautheron, C., Reiners, P.W., Metcalf, J.R., Danišík, M., Stockli, D.F., and Brown, R.W., 2022, (U-Th)/He chronology: Part 2. Considerations for evaluating, integrating, and interpreting conventional individual aliquot data: Geological Society of America Bulletin, Special Volume on Reporting and Interpretation of Geochronologic Data, v. 134, https://doi.org/10.1130/B36268.1.

Fox, M., McKeon, R., and Shuster, D.L., 2014, Incorporating 3-D parent nuclide zonation for apatite 4He/3He thermochronometry: An example from the Appalachian Mountains: Geochemistry Geophysics Geosystems, v. 15, no. 11, p. 4217–4229, https://doi.org/10.1002/2014GC005464.

Gallagher, K., 2012, Transdimensional inverse thermal history modeling for quantitative thermochronology: Journal of Geophysical Research: Solid Earth, v. 117, B02408, https://doi.org/10.1029/2011JB008825.

Gallagher, K., and Ketcham, R.A., 2018, Comment on "Thermal history modelling: HeFTy vs. QTQt" by Vermeesch and Tian, Earth-Science Reviews (2014), 139, 279–290: Earth-Science Reviews, v. 176, https://doi.org/10.1016/j.earscirev.2017.11.001.

Garver, J.I., and Kamp, P.J.J., 2002, Integration of zircon color and zircon fission-track zonation patterns in orogenic belts: Application to the Southern Alps, New Zealand: Tectonophysics, v. 349, p. 203–219.

Gautheron, C., and Tassan-Got, L., 2010, A Monte Carlo approach to diffusion applied to noble gas/helium thermochronology: Chemical Geology, v. 273, p. 212–224, https://doi.org/10.1016/j.chemgeo.2010.02.023.

Gautheron, C., and Zeitler, P.K., 2020, Noble gases deliver cool dates from hot rocks: Elements, v. 16, p. 303–309, https://doi.org/10.2138/gselements.16.5.303.

Gautheron, C., Tassan-got, L., Barbarand, J., and Pagel, M., 2009, Effect of alpha-damage annealing on apatite (U–Th)/He thermochronology: Chemical Geology, v. 266, p. 157–170, https://doi.org/10.1016/j.chemgeo.2009.06.001.

Gautheron, C., Tassan-Got, L., Ketcham, R.A., and Dobson, K.J., 2012, Accounting for long alpha-particle stopping distances in (U-Th-Sm)/He geochronology: 3-D modeling of diffusion, zoning, implantation, and abrasion: Geochimica et Cosmochimica Acta, v. 96, p. 44–56, https://doi.org/10.1016/j.gca.2012.08.016.

Gautheron, C., Barbarand, J., Ketcham, R.A., Tassan-Got, L., van der Beek, P., Pagel, M., Pinna-Jamme, R., Couffignal, F., and Fialin, M., 2013, Chemical influence on α-recoil damage annealing in apatite: Implications for (U-Th)/He dating: Chemical Geology, v. 351, p. 257–267, https://doi.org/10.1016/j.chemgeo.2013.05.027.

Gautheron, C., Djimbi, D.M., Roques, J., Balout, H., Ketcham, R.A., Simoni, E., Pik, R., Seydoux-Guillaume, A.M., and Tassan-Got, L., 2020, A multi-method, multi-scale theoretical study of He and Ne diffusion in zircon: Geochimica et Cosmochimica Acta, v. 268, p. 348–367, https://doi.org/10.1016/j.gca.2019.10.007.

Gerin, C., Gautheron, C., Oliviero, E., Bachelet, C., Mbongo Djimbi, D., Seydoux-Guillaume, A.M., Tassan-Got, L., Sarda, P., Roques, J., and Garrido, F., 2017, Influence of vacancy damage on He diffusion in apatite, investigated at atomic to mineralogical scales: Geochimica et Cosmochimica Acta, v. 197, p. 87–103, https://doi.org/10.1016/j.gca.2016.10.018.

Ginster, U., 2018, The effects of radiation damage accumulation and annealing on helium diffusion in zircon [Ph.D. thesis]: Tucson, Arizona, USA, University of Arizona, 340 p.

Ginster, U., and Reiners, P.W., 2018, Error propagation in the derivation of noble gas diffusion parameters for minerals from step heating experiments: Geochemistry, Geophysics Geosystems, v. 19, p. 3706–3720, https://doi.org/10.1029/2018GC007531.

Ginster, U., Reiners, P.W., Nasdala, L., and Chanmuang, N.C., 2019, Annealing kinetics of radiation damage in zircon: Geochimica et Cosmochimica Acta, v. 249, p. 225–246, https://doi.org/10.1016/j.gca.2019.01.033.

Gleadow, A., Harrison, M., Kohn, B., Lugo-Zazueta, R., and Phillips, D., 2015, The Fish Canyon Tuff: A new look at an old low-temperature thermochronology standard: Earth and Planetary Science Letters, v. 424, p. 95–108, https://doi.org/10.1016/j.epsl.2015.05.003.

Glotzbach, C., Lang, K.A., Avdievitch, N.N., and Ehlers, T.A., 2019, Increasing the accuracy of (U-Th(-Sm))/He dating with 3-D grain modelling: Chemical Geology, v. 506, p. 113–125, https://doi.org/10.1016/j.chemgeo.2018.12.032.

Goldsmith, A.S., Ketcham, R.A., and Stockli, D.F., 2020, Simulating effects of heterogeneous ^{4}He concentration profiles and radiation damage annealing on whole-grain zircon diffusivity analyses: Geochimica et Cosmochimica Acta, v. 284, p. 239–253, https://doi.org/10.1016/j.gca.2020.05.033.

Grabowski, D., Enkelmann, E., and Ehlers, T.A., 2013, Evaluation of the spatial extent of rapid exhumation in the St. Elias syntaxis region, SE Alaska: Journal of Geophyscial Research: Earth Surface, v. 118, p. 1–18, https://doi.org/10.1002/jgrf.20136.

Guenthner, W.R., 2021, Implementation of an alpha damage annealing model for zircon (U-Th)/He thermochronology with comparison to a zircon fission track annealing model: Geochemistry, Geophysics, Geosystems, v. 22, p. 1–16, https://doi.org/10.1029/2019GC008757.

Guenthner, W.R., Reiners, P.W., Ketcham, R.A., Nasdala, L., and Giester, G., 2013, Helium diffusion in natural zircon: Radiation damage, anisotropy, and the interpretation of zircon (U-Th)/He thermochronology: American Journal of Science, v. 313, p. 145–198, https://doi.org/10.2475/03.2013.01.

Guenthner, W.R., Reiners, P.W., and Chowdhury, U., 2016, Isotope dilution analysis of Ca and Zr in apatite and zircon (U-Th)/He chronometry: Geochemistry, Geophysics, Geosystems, v. 17, p. 1623–1640, https://doi.org/10.1002/2016GC006311.

Guo, H., Zeitler, P.K., Idleman, B.D., Fayon, A.K., Fitzgerald, P.G., and McDannell, K.T., 2021, Helium diffusion systematics inferred from continuous ramped heating analysis of Transantarctic Mountains apatites showing age overdispersion: Geochimica et Cosmochimica Acta, v. 310, p. 113–130, https://doi.org/10.1016/j.gca.2021.07.015.

Hardie, R.A., Schneider, D.A., and Garver, J.I., 2017, (U-Th)/He thermochronology of the Ottawa embayment, eastern Canada: The temperature-time history of an ancient, intracratonic rift basin: The Journal of Geology, v. 125, p. 659–680, https://doi.org/10.1086/693859.

Herman, F., Braun, J., Senden, T.J., and Dunlap, W.J., 2007, (U-Th)/He thermochronometry: Mapping 3-D geometry using micro-X-ray tomography and solving the associated production-diffusion equation: Chemical Geology, v. 242, p. 126–136, https://doi.org/10.1016/j.chemgeo.2007.03.009.

Hiess, J., Condon, D.J., McLean, N., and Noble, S.R., 2012, ^{238}U/^{235}U systematics in terrestrial uranium-bearing minerals: Science, v. 335, p. 1610–1615, https://doi.org/10.1126/science.1215507.

Hofmann, F., Treffkorn, J., and Farley, K.A., 2020, U-loss associated with laser-heating of hematite and goethite in vacuum during (U-Th)/He dating and prevention using high O2 partial pressure: Chemical Geology, v. 532, https://doi.org/10.1016/j.chemgeo.2019.119350.

Holland, H., and Gottfried, D., 1955, The effect of nuclear radiation on the structure of zircon: Acta Crystallographica, v. 8, p. 291–300, https://doi.org/10.1107/S0365110X55000947.

Holmes, A., and Paneth, F., 1936, Helium-ratios of rocks and minerals from the diamond pipes of South Africa: Proceedings of the Royal Society of London, Series A: Mathematical, Physical and Engineering Sciences, v. 154, p. 385–413.

Horne, A.M., van Soest, M.C., Hodges, K.V., Tripathy-Lang, A., and Hourigan, J.K., 2016, Integrated single crystal laser ablation U/Pb and (U-Th)/He dating of detrital accessory minerals—Proof-of-concept studies of titanites and zircons from the Fish Canyon tuff: Geochimica et Cosmochimica Acta, v. 178, p. 106–123, https://doi.org/10.1016/j.gca.2015.11.044.

Horne, A.M., van Soest, M.C., and Hodges, K.V., 2019, U/Pb and (U-Th-Sm)/He "double" dating of detrital apatite by laser ablation: A critical evaluation: Chemical Geology, v. 506, p. 40–50, https://doi.org/10.1016/j.chemgeo.2018.12.004.

Horstwood, M.S.A., Košler, J., Gehrels, G., Jackson, S.E., McLean, N.M., Paton, C., Pearson, N.J., Sircombe, K., Sylvester, P., Vermeesch, P., Bowring, J.F., Condon, D.J., and Schoene, B., 2016, Community-derived

standards for LA-ICP-MS U-(Th-)Pb geochronology—uncertainty propagation, age interpretation and data reporting: Geostandards and Geoanalytical Research, v. 40, p. 311–332, https://doi.org/10.1111/j.1751-908X.2016.00379.x.

Hourigan, J.K., Reiners, P.W., and Brandon, M.T., 2005, U-Th zonation-dependent alpha-ejection in (U-Th)/He chronometry: Geochimica et Cosmochimica Acta, v. 69, p. 3349–3365, https://doi.org/10.1016/j.gca.2005.01.024.

House, M.A., Farley, K.A., and Stockli, D.F., 2000, Helium chronometry of apatite and titanite using Nd-YAG laser heating: Earth and Planetary Science Letters, v. 183, p. 365–368, https://doi.org/10.1016/S0012-821X(00)00286-7.

Hurley, P.M., 1954, The helium age method and the distribution and migration of helium in rocks, *in* Faul, H. ed., Nuclear Geology: New York, John Wiley & Sons, p. 301–329.

Idleman, B.D., Zeitler, P.K., and McDannell, K.T., 2018, Characterization of helium release from apatite by continuous ramped heating: Chemical Geology, v. 476, p. 223–232, https://doi.org/10.1016/j.chemgeo.2017.11.019.

Ito, H., and Danišík, M., 2020, Dating late Quaternary events by the combined U-Pb LA-ICP-MS and (U-Th)/He dating of zircon: A case study on Omachi Tephra suite (central Japan): Terra Nova, v. 32, p. 134–140, https://doi.org/10.1111/ter.12452.

JCGM, 2012, International Vocabulary of Metrology—Basic and General Concepts and Associated Terms (VIM): Technical Report, Joint Committee for Guides in Metrology.

Jensen, J.L., Siddoway, C.S., Reiners, P.W., Ault, A.K., Thomson, S.N., and Steele-MacInnis, M., 2018, Single-crystal hematite (U–Th)/He dates and fluid inclusions document widespread Cryogenian sand injection in crystalline basement: Earth and Planetary Science Letters, v. 500, p. 145–155, https://doi.org/10.1016/j.epsl.2018.08.021.

Johnson, J.E., Flowers, R.M., Baird, G.B., and Mahan, K.H., 2017, "Inverted" zircon and apatite (U–Th)/ He dates from the Front Range, Colorado: High-damage zircon as a low-temperature (<50 °C) thermochronometer: Earth and Planetary Science Letters, v. 466, p. 80–90, https://doi.org/10.1016/j.epsl.2017.03.002.

Johnstone, S., Hourigan, J., and Gallagher, C., 2013, LA-ICP-MS depth profile analysis of apatite: Protocol and implications for (U–Th)/He thermochronometry: Geochimica et Cosmochimica Acta, v. 109, p. 143–161, https://doi.org/10.1016/j.gca.2013.01.004.

Kelly, N.M., Flowers, R.M., Metcalf, J.R., and Mojzsis, S.J., 2018, Late accretion to the Moon recorded in zircon (U–Th)/He thermochronometry: Earth and Planetary Science Letters, v. 482, p. 222–235, https://doi.org/10.1016/j.epsl.2017.11.009.

Ketcham, R.A., 2005, Forward and inverse modeling of low temperature thermochronometry data, *in* Reiners, P.W., and Ehlers, T.A. eds., Low-Temperature Thermochronology: Techniques, Interpretations, and Applications: Reviews in Mineralogy and Geochemistry, v. 58, p. 275–314, https://doi.org/10.2138/rmg.2005.58.11.

Ketcham, R.A., Gautheron, C., and Tassan-Got, L., 2011, Accounting for long alpha-particle stopping distances in (U-Th-Sm)/He geochronology: Refinement of the baseline case: Geochimica et Cosmochimica Acta, v. 75, p. 7779–7791, https://doi.org/10.1016/j.gca.2011.10.011.

Ketcham, R.A., Guenthner, W.R., and Reiners, P.W., 2013, Geometric analysis of radiation damage connectivity in zircon, and its implications for helium diffusion: The American Mineralogist, v. 98, p. 350–360, https://doi.org/10.2138/am.2013.4249.

Kraml, M., Pik, R., Rahn, M., Selbekk, R., Carignan, J., and Keller, J., 2006, A new multi-mineral age reference material for $^{40}Ar/^{39}Ar$, (U-Th)/He and fission track dating methods: The Limberg t3 tuff: Geostandards and Geoanalytical Research, v. 30, p. 73–86, https://doi.org/10.1111/j.1751-908X.2006.tb00914.x.

Kuiper, K.F., Deino, A., Hilgen, F.J., Krijgsman, W., Renne, P.R., and Wijbrans, J.R., 2008, Synchronizing rock clocks of Earth history: Science, v. 320, p. 500–504, https://doi.org/10.1126/science.1154339.

Landman, R.L., Flowers, R.M., Rosenau, N.A., and Powell, J., 2016, Conodont (U–Th)/He thermochronology: A

case study from the Illinois Basin: Earth and Planetary Science Letters, v. 456, p. 55–65, https://doi.org/10.1016/j.epsl.2016.10.003.

Leventhal, J.S., 1975, An evaluation of the uranium-thorium helium method for dating young basalts: Journal of Geophysical Research: Solid Earth and Planets, v. 80, p. 1911–1914, https://doi.org/10.1029/JB080i014p01911.

Li, Y., Zheng, D., Wu, Y., Wang, Y., He, H., Pang, J., Wang, Y., and Yu, J., 2017, A potential (U-Th)/He reference material from Penglai zircon megacrysts: Geostandards and Geoanalytical Research, v. 41, p. 359–365, https://doi.org/10.1111/ggr.12168.

Lippolt, H.J., and Weigel, E., 1988, ^{4}He diffusion in ^{40}Ar-retentive minerals: Geochimica et Cosmochimica Acta, v. 52, p. 1449–1458, https://doi.org/10.1016/0016-7037(88)90215-3.

Lippolt, H.J., Wernicke, R.S., and Boschmann, W., 1993, ^{4}He diffusion in specular hematite: Physics and Chemistry of Minerals, v. 20, p. 415–418, https://doi.org/10.1007/BF00203111.

Lippolt, H.J., Leitz, M., Wernicke, R.S., and Hagedorn, B., 1994, (Uranium + thorium)/helium dating of apatite: Experience with samples from different geochemical environments: Chemical Geology, v. 112, p. 179–191, https://doi.org/10.1016/0009-2541(94)90113-9.

Lippolt, H.J., Wernicke, R.S., and Bähr, R., 1995, Paragenetic specularite and adularia (Elba, Italy): Concordant (U + Th)-He and K-Ar ages: Earth and Planetary Science Letters, v. 132, p. 43–51, https://doi.org/10.1016/0012-821X(95)00046-H.

Marsden, R.C., Danišík, M., Ahn, U.S., Friedrichs, B., Schmitt, A.K., Kirkland, C.L., McDonald, B.J., and Evans, N.J., 2021a, Zircon double-dating of Quaternary eruptions on Jeju Island, South Korea: Journal of Volcanology and Geothermal Research, v. 410, https://doi.org/10.1016/j.jvolgeores.2020.107171.

Marsden, R.C., Danišík, M., Ito, H., Kirkland, C.L., Evans, N.J., Miura, D., Friedrichs, B., Schmitt, A.K., Uesawa, S., and Daggitt, M.L., 2021b, Considerations for double dating zircon in secular disequilibrium with protracted crystallisation histories: Chemical Geology, v. 581, https://doi.org/10.1016/j.chemgeo.2021.120408.

Martin, P., 2021, HeCalc: https://doi.org/10.5281/zenodo.5672830 (accessed 12 November 2021).

Mbongo-Djimbi, D., Gautheron, C., Roques, J., Tassan-Got, L., Gerin, C., and Simoni, E., 2015, Impact of apatite chemical composition on (U-Th)/He thermochronometry: An atomistic point of view: Geochimica et Cosmochimica Acta, v. 167, p. 162–176, https://doi.org/10.1016/j.gca.2015.06.017.

McDannell, K.T., and Issler, D.R., 2021, Simulating sedimentary burial cycles—Part 1: Investigating the role of apatite fission track annealing kinetics using synthetic data: Geochronology, v. 3, p. 321–335, https://doi.org/10.5194/gchron-3-321-2021.

McDannell, K.T., Zeitler, P.K., Janes, D.G., Idleman, B.D., and Fayon, A.K., 2018, Screening apatites for (U-Th)/He thermochronometry via continuous ramped heating: He age components and implications for age dispersion: Geochimica et Cosmochimica Acta, v. 223, p. 90–106, https://doi.org/10.1016/j.gca.2017.11.031.

McDougall, I., and Harrison, T.M., 1999, Geochronology and Thermochronology by the $^{40}Ar/^{39}Ar$ Method: New York, Oxford University Press, 269 p.

McDowell, F.W., McIntosh, W.C., and Farley, K.A., 2005, A precise ^{40}Ar-^{39}Ar reference age for the Durango apatite (U-Th)/He and fission-track dating standard: Chemical Geology, v. 214, p. 249–263, https://doi.org/10.1016/j.chemgeo.2004.10.002.

Meesters, A.G.C.A., and Dunai, T.J., 2002a, Solving the production–diffusion equation for finite diffusion domains of various shapes: Chemical Geology, v. 186, p. 347–363, https://doi.org/10.1016/S0009-2541(02)00073-6.

Meesters, A.G.C.A., and Dunai, T.J., 2002b, Solving the production-diffusion equation for finite diffusion domains of various shapes part II. Application to cases with α-ejection and nonhomogeneous distribution of the source: Chemical Geology, v. 186, p. 57–73, https://doi.org/10.1016/S0009-2541(01)00423-5.

Meesters, A.G.C.A., and Dunai, T.J., 2005, A noniterative solution of the (U-Th)/He age equation: Geochemistry,

Geophysics, Geosystems, v. 6, p. 4–6, https://doi.org/10.1029/2004GC000834.

Metcalf, J.R., and Flowers, R.M., 2013, Initial development of baddeleyite (U-Th)/He thermochronology: Denver, Colorado, presented at 2013 Annual Geological Society of America Meeting.

Min, K., Farley, K.A., Renne, P.R., and Marti, K., 2003, Single grain (U-Th)/He ages from phosphates in Acapulco meteorite and implications for thermal history: Earth and Planetary Science Letters, v. 209, p. 323–336, https://doi.org/10.1016/S0012-821X(03)00080-3.

Min, K., Reiners, P.W., and Shuster, D.L., 2013, (U-Th)/He ages of phosphates from St. Séverin LL6 chondrite: Geochimica et Cosmochimica Acta, v. 100, p. 282–296, https://doi.org/10.1016/j.gca.2012.09.042.

Miro, S., Studer, F., Costantini, J.-M., Haussy, J., Trouslard, P., and Grob, J.-J., 2006, Effect of composition on helium diffusion in fluoroapatites investigated with nuclear reaction analysis: Journal of Nuclear Materials, v. 355, p. 1–9, https://doi.org/10.1016/j.jnucmat.2006.04.004.

Monteiro, H.S., Vasconcelos, P.M., Farley, K.A., Spier, C.A., and Mello, C.L., 2014, (U-Th)/He geochronology of goethite and the origin and evolution of cangas: Geochimica et Cosmochimica Acta, v. 131, p. 267–289, https://doi.org/10.1016/j.gca.2014.01.036.

Monteiro, H.S., Vasconcelos, P.M.P., and Farley, K.A., 2018, A combined (U-Th)/He and cosmogenic ^{3}He record of landscape armoring by biogeochemical iron cycling: Journal of Geophysical Research: Earth Surface, v. 123, p. 298–323, https://doi.org/10.1002/2017JF004282.

Murray, K.E., Orme, D.A., and Reiners, P.W., 2014, Effects of U–Th-rich grain boundary phases on apatite helium ages: Chemical Geology, v. 390, p. 135–151, https://doi.org/10.1016/j.chemgeo.2014.09.023.

Nasdala, L., Wenzel, M., Vavra, G., Irmer, G., Wenzel, T., and Kober, B., 2001, Metamictisation of natural zircon: Accumulation versus thermal annealing of radioactivity-induced damage: Contributions to Mineralogy and Petrology, v. 141, p. 125–144, https://doi.org/10.1007/s004100000235.

Ouchani, S., Dran, J.C., and Chaumont, J., 1998, Exfoliation and diffusion following helium ion implantation in fluorapatite: Implications for radiochronology and radioactive waste disposal: Applied Geochemistry, v. 13, p. 707–714, https://doi.org/10.1016/S0883-2927(97)00078-4.

Peppe, D.J., and Reiners, P.W., 2007, Conodont (U–Th)/He thermochronology: Initial results, potential, and problems: Earth and Planetary Science Letters, v. 258, p. 569–580, https://doi.org/10.1016/j.epsl.2007.04.022.

Peterman, E.M., Hourigan, J.K., and Grove, M., 2014, Experimental and geologic evaluation of monazite (U–Th)/He thermochronometry: Catnip Sill, Catalina Core Complex, Tucson, AZ: Earth and Planetary Science Letters, v. 403, p. 48–55, https://doi.org/10.1016/j.epsl.2014.06.020.

Pi, T., Solé, J., and Taran, Y., 2005, (U-Th)/He dating of fluorite: Application to the La Azul fluorspar deposit in the Taxco mining district, Mexico: Mineralium Deposita, v. 39, p. 976–982, https://doi.org/10.1007/s00126-004-0443-y.

Pickering, J., Matthews, W., Enkelmann, E., Guest, B., Sykes, C., and Koblinger, B.M., 2020, Laser ablation (U-Th-Sm)/He dating of detrital apatite: Chemical Geology, v. 548, https://doi.org/10.1016/j.chemgeo.2020.119683.

Pidgeon, R.T., Brander, T., and Lippolt, H.J., 2004, Late Miocene (U+Th)-^{4}He ages of ferruginous nodules from lateritic duricrust, Darling Range, Western Australia: Australian Journal of Earth Sciences, v. 51, p. 901–909, https://doi.org/10.1111/j.1400-0952.2004.01094.x.

Pik, R., Marty, B., Carignan, J., and Lavé, J., 2003, Stability of the Upper Nile drainage network (Ethiopia) deduced from (U–Th)/He thermochronometry: Implications for uplift and erosion of the Afar plume dome: Earth and Planetary Science Letters, v. 215, p. 73–88, https://doi.org/10.1016/S0012-821X(03)00457-6.

Powell, J.W., Schneider, D.A., Desrochers, A., Flowers, R.M., Metcalf, J.R., Gaidies, F., and Stockli, D.F., 2018, Low-temperature thermochronology of Anticosti Island: A case study on the application of conodont (U-Th)/He thermochronology to carbonate basin analy-

sis: Marine and Petroleum Geology, v. 96, p. 441–456, https://doi.org/10.1016/j.marpetgeo.2018.05.018.

Rahl, J.M., Reiners, P.W., Campbell, I.H., Nicolescu, S., and Allen, C.M., 2003, Combined single-grain (U-Th)/He and U/Pb dating of detrital zircons from the Navajo Sandstone, Utah: Geology, v. 31, p. 761–764, https://doi.org/10.1130/G19653.1.

Recanati, A., Gautheron, C., Barbarand, J., Missenard, Y., Pinna-Jamme, R., Tassan-Got, L., Carter, A., Douville, E., Bordier, L., Pagel, M., and Gallagher, K., 2017, Helium trapping in apatite damage: Insights from (U-Th-Sm)/He dating of different granitoid lithologies: Chemical Geology, v. 470, p. 116–131, https://doi.org/10.1016/j.chemgeo.2017.09.002.

Reich, M., Ewing, R.C., Ehlers, T.A., and Becker, U., 2007, Low-temperature anisotropic diffusion of helium in zircon: Implications for zircon (U–Th)/He thermochronology: Geochimica et Cosmochimica Acta, v. 71, p. 3119–3130, https://doi.org/10.1016/j.gca.2007.03.033.

Reiners, P.W., and Farley, K.A., 1999, Helium diffusion and (U-Th)/He thermochronometry of titanite: Geochimica et Cosmochimica Acta, v. 63, p. 3845–3859, https://doi.org/10.1016/S0016-7037(99)00170-2.

Reiners, P.W., and Farley, K.A., 2001, Influence of crystal size on apatite (U-Th)/He thermochronology: An example from the Bighorn Mountains, Wyoming: Earth and Planetary Science Letters, v. 188, p. 413–420, https://doi.org/10.1016/S0012-821X(01)00341-7.

Reiners, P.W., Brady, R., Farley, K.A., Fryxell, J.E., Wernicke, B., and Lux, D., 2000, Helium and argon thermochronometry of the Gold Butte block, south Virgin Mountains, Nevada: Earth and Planetary Science Letters, v. 178, p. 315–326, https://doi.org/10.1016/S0012-821X(00)00080-7.

Reiners, P.W., Farley, K.A., and Hickes, H.J., 2002, He diffusion and (U-Th)/He thermochronometry of zircon: Initial results from Fish Canyon Tuff and Gold Butte: Tectonophysics, v. 349, p. 297–308, https://doi.org/10.1016/S0040-1951(02)00058-6.

Reiners, P.W., Spell, T.L., Nicolescu, S., and Zanetti, K.A., 2004, Zircon (U-Th)/He thermochronometry: He diffusion and comparisons with ⁴⁰Ar/³⁹Ar dating: Geochimica et Cosmochimica Acta, v. 68, p. 1857–1887, https://doi.org/10.1016/j.gca.2003.10.021.

Reiners, P.W., Thomson, S.N., McPhillips, D., Donelick, R.A., and Roering, J.J., 2007, Wildfire thermochronology and the fate and transport of apatite in hillslope and fluvial environments: Journal of Geophysical Research: Earth Surface, v. 112, https://doi.org/10.1029/2007JF000759.

Reiners, P.W., Chan, M.A., and Evenson, N.S., 2014, (U-Th)/He geochronology and chemical compositions of diagenetic cement, concretions, and fracture-filling oxide minerals in Mesozoic sandstones of the Colorado Plateau: Geological Society of America Bulletin, v. 126, p. 1363–1383, https://doi.org/10.1130/B30983.1.

Reiners, P.W., Carlson, R.W., Renne, P.R., Cooper, K.M., Granger, D.E., McLean, N.M., and Schoene, B., 2018, The (U-Th)/He system, *in* Reiners, P.W., Carlson, R.W., Renne, P.R., Cooper, K.M., Granger, D.E., McLean, N.M., and Schoene, B., eds., Geochronology and Thermochronology: Hoboken, New Jersey, USA, John Wiley & Sons Ltd., p. 291–356.

Robinson, K.H., Flowers, R.M., and Metcalf, J.R., 2019, Rutile (U-Th)/He thermochronology: Temperature sensitivity and radiation damage effects: Geochemistry, Geophysics Geosystems, v. 20, p. 4737–4755, https://doi.org/10.1029/2019GC008484.

Rutherford, E., 1905, Present problems in radioactivity: Popular Science Monthly, v. 67, p. 1–11.

Schaen, A.J., et al., 2020, Interpreting and reporting ⁴⁰Ar/³⁹Ar geochronologic data: Geological Society of America Bulletin, v. 133, p. 461–487, https://doi.org/10.1130/B35560.1.

Schildgen, T.F., Balco, G., and Shuster, D.L., 2010, Canyon incision and knickpoint propagation recorded by apatite ⁴He/³He thermochronometry: Earth and Planetary Science Letters, v. 293, p. 377–387, https://doi.org/10.1016/j.epsl.2010.03.009.

Schmitt, A.K., Stockli, D.F., and Hausback, B.P., 2006, Eruption and magma crystallization ages of Las Tres

Vírgenes (Baja California) constrained by combined ²³⁰Th/²³⁸U and (U-Th)/He dating of zircon: Journal of Volcanology and Geothermal Research, v. 158, p. 281–295, https://doi.org/10.1016/j.jvolgeores.2006.07.005.

Schmitt, A.K., Stockli, D.F., Niedermann, S., Lovera, O.M., and Hausback, B.P., 2010, Eruption ages of Las Tres Vírgenes volcano (Baja California): A tale of two helium isotopes: Quaternary Geochronology, v. 5, p. 503–511, https://doi.org/10.1016/j.quageo.2010.02.004.

Schmitt, A.K., Martin, A., Stockli, D.F., Farley, K.A., and Lovera, O.M., 2013, (U-Th)/He zircon and archaeological ages for a late prehistoric eruption int he Salton Trough (California, USA): Geology, v. 41, no. 1, p. 7–10, https://doi.org/10.1130/G33634.1.

Schmitt, A.K., Danišík, M., Siebel, W., Elitok, Ö., Chang, Y.W., and Shen, C.C., 2014, Late Pleistocene zircon ages for intracaldera domes at Gölcük (Isparta, Turkey): Journal of Volcanology and Geothermal Research, v. 286, p. 24–29, https://doi.org/10.1016/j.jvolgeores.2014.08.027.

Schneider, B., Kuiper, K., Postma, O., and Wijbrans, J., 2009, ⁴⁰Ar/³⁹Ar geochronology using a quadrupole mass spectrometer: Quaternary Geochronology, v. 4, p. 508–516, https://doi.org/10.1016/j.quageo.2009.08.003.

Schoene, B., Crowley, J.L., Condon, D.J., Schmitz, M.D., and Bowring, S.A., 2006, Reassessing the uranium decay constants for geochronology using ID-TIMS U-Pb data: Geochimica et Cosmochimica Acta, v. 70, p. 426–445, https://doi.org/10.1016/j.gca.2005.09.007.

Schoene, B., Condon, D.J., Morgan, L., and McLean, N., 2013, Precision and accuracy in geochronology: Elements, v. 9, p. 19–24, https://doi.org/10.2113/gselements.9.1.19.

Schwartz, S., Gautheron, C., Ketcham, R.A., Brunet, F., Corre, M., Agranier, A., Pinna-Jamme, R., Haurine, F., Monvoin, G., and Riel, N., 2020, Unraveling the exhumation history of high-pressure ophiolites using magnetite (U-Th-Sm)/He thermochronometry: Earth and Planetary Science Letters, v. 543, https://doi.org/10.1016/j.epsl.2020.116359.

Shuster, D.L., and Farley, K.A., 2004, ⁴He/³He thermochronometry: Earth and Planetary Science Letters, v. 217, p. 1–17, https://doi.org/10.1016/S0012-821X(03)00595-8.

Shuster, D.L., and Farley, K.A., 2009, The influence of artificial radiation damage and thermal annealing on helium diffusion kinetics in apatite: Geochimica et Cosmochimica Acta, v. 73, p. 183–196, https://doi.org/10.1016/j.gca.2008.10.013.

Shuster, D.L., Farley, K.A., Sisterson, J.M., and Burnett, D.S., 2003, Quantifying the diffusion kinetics and spatial distributions of radiogenic ⁴He in minerals containing proton-induced ³He: Earth and Planetary Science Letters, v. 217, p. 19–32, https://doi.org/10.1016/S0012-821X(03)00594-6.

Shuster, D.L., Farley, K.A., Sisterson, J.M., and Burnett, D.S., 2004, Quantifying the diffusion kinetics and spatial distributions of radiogenic ⁴He in minerals containing proton-induced ³He: Earth and Planetary Science Letters, v. 217, no. 1–2, p. 19–32, https://doi.org/10.1016/S0012-821X(03)00594-6.

Shuster, D.L., Vasconcelos, P.M., Heim, J.A., and Farley, K.A., 2005a, Weathering geochronology by (U-Th)/He dating of goethite: Geochimica et Cosmochimica Acta, v. 69, p. 659–673, https://doi.org/10.1016/j.gca.2004.07.028.

Shuster, D.L., Ehlers, T.A., Rusmore, M.E., and Farley, K.A., 2005b, Rapid glacial erosion at 1.8 Ma revealed by 4He/3He thermochronometry: Science, v. 310, p. 1668–1670, https://doi.org/10.1126/science.1118519.

Shuster, D.L., Flowers, R.M., and Farley, K.A., 2006, The influence of natural radiation damage on helium diffusion kinetics in apatite: Earth and Planetary Science Letters, v. 249, p. 148–161, https://doi.org/10.1016/j.epsl.2006.07.028.

Siebel, W., Hann, H.P., Danišík, M., Shang, C.K., Berthold, C., Rohrmüller, J., Wemmer, K., and Evans, N.J., 2010, Age constraints on faulting and fault reactivation: A multi-chronological approach: International Journal of Earth Sciences, v. 99, p. 1187–1197, https://doi.org/10.1007/s00531-009-0474-9.

Spiegel, C., Kohn, B., Belton, D., Berner, Z., and Gleadow, A., 2009, Apatite (U–Th–Sm)/He thermochronology of rapidly cooled samples: The effect of He implantation: Earth and Planetary Science Letters, v. 285, p. 105–114, https://doi.org/10.1016/j.epsl.2009.05.045.

Stanley, J.R., and Flowers, R.M., 2016, Dating kimberlite emplacement with zircon and perovskite (U-Th)/He geochronology: Geochemistry, Geophysics, Geosystems, v. 17, p. 4517–4533, https://doi.org/10.1002/2016GC006519.

Stockli, D.F., and Farley, K.A., 2004, Empirical constraints on the titanite (U-Th)/He partial retention zone from the KTB drill hole: Chemical Geology, v. 207, p. 223–236, https://doi.org/10.1016/j.chemgeo.2004.03.002.

Stockli, D.F., Wolfe, M.R., Blackburn, T.J., Zack, T., Walker, J.D., and Luvizotto, G.L., 2007, He diffusion and (U-Th)/He thermochronometry of rutile: Abstract V23C–1548 presented at 2007 Fall Meeting, American Geophysical Union, San Francisco, California, 10–14 December.

Strutt, R., 1908a, Helium and radio-activity in rare and common minerals: Proceedings of the Royal Society of London. Series A, Containing Papers of a Mathematical and Physical Character, v. 80, p. 572–594.

Strutt, R., 1908b, On the accumulation of Helium in geological time: Proceedings of the Royal Society of London. Series A, Containing Papers of a Mathematical and Physical Character, v. 83, p. 272–277.

Strutt, R., 1910a, Measurements of the rate at which Helium is produced in Thorianite and Pitchblende, with a minimum estimate of their antiquity: Proceedings of the Royal Society of London. Series A, Containing Papers of a Mathematical and Physical Character, v. 84, p. 379–388.

Strutt, R., 1910b, The accumulation of Helium in geological time. II: Proceedings of the Royal Society of London. Series A, Containing Papers of a Mathematical and Physical Character, v. 83, p. 96–99.

Strutt, R., 1910c, The accumulation of He in geological time. III: Proceedings of the Royal Society of London. Series A, Containing Papers of a Mathematical and Physical Character, v. 83, p. 298–301.

Strutt, R., 1910d, The accumulation of Helium in geological time. IV: Proceedings of the Royal Society of London. Series A, Containing Papers of a Mathematical and Physical Character, v. 84, p. 194–196.

Taylor, J.R., 1997, An introduction to error analysis. The study of uncertainties in physical measurements: Sausalito, California, USA, University Science Books, 317 p.

Thompson, A., and Taylor, B.N., 2008, Guide for the Use of the International System of Units (SI): National Institute of Standards and Technology Special Publication, v. 811, p. 90 p., https://10.1097/00005768-199901000-00046.

Thomson, S.N., Reiners, P.W., Hemming, S.R., and Gehrels, G.E., 2013, The contribution of glacial erosion to shaping the hidden landscape of East Antarctica: Nature Geoscience, v. 6, p. 203–207, https://doi.org/10.1038/ngeo1722.

Tian, Y., Vermeesch, P., Danišík, M., Condon, D.J., Chen, W., Kohn, B., Schwanethal, J., and Rittner, M., 2017, LGC-1: A zircon reference material for in-situ (U-Th)/He dating: Chemical Geology, v. 454, p. 80–92, https://doi.org/10.1016/j.chemgeo.2017.02.026.

Tincher, C.R., and Stockli, D.F., 2009, Cenozoic volcanism and tectonics in the Queen Valley area, Esmeralda County, western Nevada, in Oldow, J.S., and Cashman, P.H., Late Cenozoic Structure and Evolution of the Great Basin—Sierra Nevada Transition: Geological Society of America Special Paper 447, p. 255–274, https://doi.org/10.1130/2009.2447(13).

Tremblay, M.M., Cooperdock, E.H.G., and Zeitler, P.K., eds., 2020, Noble Gas Thermochronology: Elements, v. 16, no. 5, p. 331–336, https://doi.org/10.2138/gselements.16.5.331.

Tripathy-Lang, A., Hodges, K.V., Monteleone, B.D., and van Soest, M.C., 2013, Laser (U-Th)/He thermochronology of detrital zircons as a tool for studying surface processes in modern catchments: Journal of Geophysical Research: Earth Surface, v. 118, p. 1333–1341, https://doi.org/10.1002/jgrf.20091.

Tripathy-Lang, A., Fox, M., and Shuster, D.L., 2015, Zircon 4He/3He thermochronometry: Geochimica et Cosmochimica Acta, v. 166, p. 1–14, https://doi.org/10.1016/j.gca.2015.05.027.

Turekian, K.K., Kharkar, D.P., Funkhouser, J., and Schaeffer, O.A., 1970, An evaluation of the uranium-helium method of dating of fossil bones: Earth and Planetary Science Letters, v. 7, p. 420–424, https://doi.org/10.1016/0012-821X(70)90084-1.

Ulusoy, İ., Sarıkaya, M.A., Schmitt, A.K., Şen, E., Danišík, M., and Gümüş, E., 2019, Volcanic eruption eye-witnessed and recorded by prehistoric humans: Quaternary Science Reviews, v. 212, p. 187–198, https://doi.org/10.1016/j.quascirev.2019.03.030.

Valla, P.G., Shuster, D.L., and Van Der Beek, P.A., 2011, Significant increase in relief of the European Alps during mid-Pleistocene glaciations: Nature Geoscience, v. 4, p. 688–692, https://doi.org/10.1038/ngeo1242.

van Soest, M.C., Monteleone, B.D., Hodges, K.V., and Boyce, J.W., 2011, Laser depth profiling studies of helium diffusion in Durango fluorapatite: Geochimica et Cosmochimica Acta, v. 75, p. 2409–2419, https://doi.org/10.1016/j.gca.2011.02.008.

Vasconcelos, P.M., Heim, J.A., Farley, K.A., Monteiro, H., and Waltenberg, K., 2013, $^{40}Ar/^{39}Ar$ and (U-Th)/He - $^4He/^3He$ geochronology of landscape evolution and channel iron deposit genesis at Lynn Peak, Western Australia: Geochimica et Cosmochimica Acta, v. 117, p. 283–312, https://doi.org/10.1016/j.gca.2013.03.037.

Vermeesch, P., Sherlock, S.C., Roberts, N.M.W., and Carter, A., 2012, A simple method for in-situ U-Th-He dating: Geochimica et Cosmochimica Acta, v. 79, p. 140–147, https://doi.org/10.1016/j.gca.2011.11.042.

Warnock, A.C., Zeitler, P.K., Wolf, R.A., and Bergman, S.C., 1997, An evaluation of low-temperature apatite U-Th/He thermochronometry: Geochimica et Cosmochimica Acta, v. 61, p. 5371–5377, https://doi.org/10.1016/S0016-7037(97)00302-5.

Weisberg, W.R., Metcalf, J.R., and Flowers, R.M., 2018, Distinguishing slow cooling versus multiphase cooling and heating in zircon and apatite (U-Th)/He datasets: The case of the McClure Mountain syenite standard: Chemical Geology, v. 485, p. 90–99, https://doi.org/10.1016/j.chemgeo.2018.03.038.

Wells, M.A., Danišík, M., McInnes, B.I.A., and Morris, P.A., 2019, (U-Th)/He-dating of ferruginous duricrust: Insight into laterite formation at Boddington, WA: Chemical Geology, v. 522, p. 148–161, https://doi.org/10.1016/j.chemgeo.2019.05.030.

Wernicke, R.S., and Lippolt, H.J., 1993, Botryoidal hematite from the Schwarzwald (Germany): Heterogeneous uranium distributions and their bearing on the helium dating method: Earth and Planetary Science Letters, v. 114, p. 287–300, https://doi.org/10.1016/0012-821X(93)90031-4.

Wernicke, R.S., and Lippolt, H.J., 1994a, Dating of vein Specularite using internal (U+Th)/^{4}He isochrons: Geophysical Research Letters, v. 21, p. 345–347, https://doi.org/10.1029/94GL00014.

Wernicke, R.S., and Lippolt, H.J., 1994b, ^{4}He age discordance and release behavior of a double shell botryoidal hematite from the Schwarzwald, Germany: Geochimica et Cosmochimica Acta, v. 58, p. 421–429, https://doi.org/10.1016/0016-7037(94)90474-X.

Willett, C.D., Fox, M., and Shuster, D.L., 2017, A helium-based model for the effects of radiation damage annealing on helium diffusion kinetics in apatite: Earth and Planetary Science Letters, v. 477, p. 195–204, https://doi.org/10.1016/j.epsl.2017.07.047.

Wolf, R.A., Farley, K.A., and Silver, L.T., 1996, Helium diffusion and low temperature thermochronometry of apatite: Geochimica et Cosmochimica Acta, v. 60, p. 4231–4240, https://doi.org/10.1016/S0016-7037(96)00192-5.

Wolf, R.A., Farley, K.A., and Kass, D.M., 1998, Modeling of the temperature sensitivity of the apatite (U-Th)/He thermochronometer: Chemical Geology, v. 148, p. 105–114, https://doi.org/10.1016/S0009-2541(98)00024-2.

Wolff, R., Dunkl, I., Kempe, U., and Von Eynatten, H., 2015, The age of the latest thermal overprint of tin and polymetallic deposits in the Erzgebirge, Germany: Constraints from fluorite (U-Th-Sm)/He thermochronology: Economic Geology, v. 110, p. 2025–2040, https://doi.org/10.2113/econgeo.110.8.2025.

Wolff, R., Dunkl, I., Kempe, U., Stockli, D., Wiedenbeck, M., and von Eynatten, H., 2016, Variable helium diffusion characteristics in fluorite: Geochimica et Cosmochimica Acta, v. 188, p. 21–34, https://doi.org/10.1016/j.gca.2016.05.029.

Wu, L.Y., Stuart, F.M., Di Nicola, L., Heizler, M., Benvenuti, M., and Hu, R.Z., 2019, Multi-aliquot method for determining (U + Th)/He ages of hydrothermal hematite: Returning to Elba: Chemical Geology, v. 504, p. 151–157, https://doi.org/10.1016/j.chemgeo.2018.11.005.

Yakubovich, O.V., Vikentyev, I.V., Zarubina, O.V., Bryanskiy, N.V., Gorokhovskii, B.M., Kotov, A.B., Dril, S.I., and Bortnikov, N.S., 2019, U–Th–He dating of pyrite from the Uzelga copper-zinc massive sulfide deposit (South Urals, Russia): First application of a new geochronometer: Doklady Earth Sciences, v. 485, no. 2, p. 368–371, https://doi.org/10.1134/S1028334X19040263.

Yu, S., Sun, J., Evans, N.J., Danišík, M., Wu, L., Tian, Y., and Shen, Z., 2020, Further evaluation of Penglai zircon megacrysts as a reference material for (U-Th)/He dating: Geostandards and Geoanalytical Research, v. 44, no. 4, p. 763–783, https://doi.org/10.1111/ggr.12331.

Zeigler, S.K.D., Metcalf, J.R., Flowers, R.M., and Coulombe, J.C., 2021, Quantifying uncertainty and correcting for systematic error on alpha-ejection and eU in apatite (U-Th)/He chronology based on realistic grain sizes and shapes: Abstract presented at 17th International Conference on Thermochronology, Santa Fe, New Mexico, 12–17 September, https://doi.org/10.1002/essoar.10507962.1.

Zeitler, P.K., Herczeg, A.L., McDougall, I., and Honda, M., 1987, U-Th-He dating of apatite: A potential thermochronometer: Geochimica et Cosmochimica Acta, v. 51, p. 2865–2868, https://doi.org/10.1016/0016-7037(87)90164-5.

Zeitler, P.K., Enkelmann, E., Thomas, J.B., Watson, E.B., Ancuta, L.D., and Idleman, B.D., 2017, Solubility and trapping of helium in apatite: Geochimica et Cosmochimica Acta, v. 209, p. 1–8, https://doi.org/10.1016/j.gca.2017.03.041.